UDP-D-galactose-dependent organization of the *trans*-Golgi network
&
Mechanisms for polar localization of boric acid channels in *Arabidopsis thaliana*
(シロイヌナズナにおける UDP-D-ガラクトースに依存したトランスゴルジ網の構造維持およびホウ酸チャネルの細胞膜内偏在機構)

Hokkaido University Graduate School of Agriculture
Division of Agrobiology Doctor Course

Sheliang Wang

Table of contents

Part I

UDP-D-galactose synthesis by UDP-glucose 4-epimerase 4 is required for organization of the *trans*-Golgi network/early endosome in *Arabidopsis thaliana* root epidermal cells

Abstract

Endomembrane organization is essential for cell physiology. A previous study identified an *Arabidopsis thaliana* mutant in which a plasma membrane (PM) marker GFP-NIP5;1 and *trans*-Golgi network/early endosome (TGN/EE) markers were accumulated in intracellular aggregates in epidermal cells of the root elongation zone. The mutant was identified as an allele of *UDP-glucose epimerase 4 (UGE4)/root hair defective 1/root epidermal bulgar 1*, which was previously described as a mutant with swollen root epidermal cells and has an altered sugar composition in cell wall polysaccharides. Importantly, these defects including aggregate formation were restored by supplementation of D-galactose in the medium. These results suggested that UDP-D-galactose synthesis by UGE4 is important for endomembrane organization in addition to cell wall structure. Here, I further investigated the nature of the aggregates using various markers of endomembrane compartments and BOR1-GFP, which traffics from PM to vacuole in response to high-B supply. The markers of multi-vesicular bodies/late endosomes (MVB/LEs) and BOR1-GFP were

strongly accumulated in the intracellular aggregates, while those of the endoplasmic reticulum (ER), the vacuolar membrane, and the Golgi were only slightly affected in the *uge4* mutant. The abnormal localizations of these markers in the *uge4* mutant differed from the effects of inhibitors of actin and microtubule polymerization, although they also affected endomembrane organization. Furthermore, electron microscopy analysis revealed accumulation of abnormal high-electron-density vesicles in elongating epidermal cells. The abnormal vesicles were often associated or interconnected with TGN/EEs and contained ADP-ribosylation factor 1, which is usually localized to the Golgi and the TGN/EEs. On the other hand, structures of the ER, Golgi apparatus, and MVB/LEs were apparently normal in *uge4* cells. Together, these data indicate the importance of UDP-D-galactose synthesis by UGE4 for the organization and function of endomembranes, especially TGN/EEs, which are a sorting station of the secretory and vacuolar pathways.

Keywords: *Arabidopsis thaliana* UDP-D-galactose UDP-D-glucose 4-epimerase endomembrane organization TGN/EEs

Abbreviations

UGE4: UDP-D-glucose-4 epimerase 4

rhd1: Root hair defective (rhd) 1

reb1: Root epidermal bulgar

PM: Plasma membrane

TGN: *Trans*-Golgi network

MVB: Multi-vesicular body

ER: Endoplasmic reticulum

GFP/YFP: Green/Yellow fluorescence protein

NIP: Nodulin 26-like intrinsic protein

EE: Early endosome

LE: Late endosome

HDVs: High-electron-density vesicles

BFA: Brefeldin A

ARF-GEF: ADP-ribosylation factor-Guanine nucleotide exchange factors

DIC: Differential interference contrast

FM4-64: N-(3-Triethylammoniumpropyl)-4-(6-(4-(Diethylamino) Phenyl) Hexatrienyl) Pyridinium Dibromide

Introduction

UDP-D-galactose is synthesized in the cytosol by UDP-D-glucose-4 epimerase isoforms (UGEs) and transported into the Golgi apparatus to serve as a nucleotide sugar donor for the biosynthesis of cell wall polysaccharides (Reiter and Vanzin, 2001; Yin et al., 2011). The Arabidopsis genome encodes five *UGE* genes, and their expression has been detected in every plant organ (Seifert et al. 2002). Among these genes, *UGE4* is most highly expressed in epidermal cells of the root elongation zone, followed by *UGE1* (Barber et al. 2006; Rösti et al. 2007). Mutants of *UGE4* are known as *root hair defective (rhd) 1/root epidermal bulgar (reb) 1*, which exhibit defects in root hair development, root morphology, and susceptibility to nematodes (Schiefelbein and Somerville, 1990; Baskin et al., 1992; Baum et al., 2000). The trichoblasts (root hair-forming cells) of the mutants become swollen and the base of the root hair shows a widened (bulbous) morphology (Schiefelbein and Somerville 1990). In the swollen cells, microtubules were disordered or absent entirely (Andeme-Onzighi et al., 2002). UGE4 is located close to the Golgi stacks and was shown to be

specifically required for the galactosylation of xyloglucan and type II arabinogalactan, but was not thought to be involved in galactolipid biosynthesis (Seifert et al., 2002; Barber et al., 2006; Rösti et al., 2007).

Based on fluorescence imaging-based screening using a plasma-membrane (PM) localized boric acid channel fused with green fluorescence protein (GFP-NIP5;1), a novel allele of *UDP-D-glucose 4-epimerase 4* was identified (line 20-2, Uehara et al. 2014). The epidermal cells in both the elongation zone and root hair zone, but not meristem zone, of the mutant line 20-2 showed intracellular aggregates containing GFP-NIP5;1. The aggregates were stained by FM4-64, a lipophilic styryl dye that stains vesicles in the endocytic pathway, and contained the *trans*-Golgi network (TGN) markers YFP-RabA1e and YFP-VTI12 (Uehara et al. 2014). TGN functions as a major sorting hub for the secretory and endocytic pathways, and is thus referred to as TGN/early endosome (EE) in plant cells (Viotti et al., 2010; Uemura et al., 2012). Importantly, the addition of D-galactose to the medium decreased endomembrane aggregates and rescued growth defects of *uge4* mutants. Pharmacological analysis using oryzalin and latruncurin B on GFP-NIP5;1 localization showed that disruption of microtubules and the actin cytoskeleton caused endomembrane

disorganization, but the effects were distinct from those observed in the *uge4* mutants. Furthermore, analysis of several mutants with reduced accumulation of cell wall polysaccharides such as xyloglucan, arabinogalactan proteins (AGPs), and pectin, combined with the use of β-D-glucosyl Yariv reagent which binds to AGPs did not show endomembrane disorganization or abnormal intracellular aggregates (Uehara et al. 2014). These results suggested that the intracellular aggregates containing TGN/EEs were not caused by disruption of the cell wall structure or cytoskeleton.

In this study, to verify the nature of the aggregates in *uge4* mutants, I performed fluorescence imaging of various endosome markers and electron microscopy analysis of the elongating epidermal cells of the *uge4* mutant. These results show the accumulation of abnormal vesicles derived from TGN/EEs in *uge4* mutant cells, and suggest the importance of UDP-D-galactose for the organization and function of TGN/EEs.

Material and Methods

Plant materials and growth conditions

Arabidopsis thaliana (L.) Heynh. ecotype Col-0 was used as the wild-type strain in this study and was from our laboratory stock. Transgenic Arabidopsis plants expressing BOR1-GFP (Takano et al. 2010), ER-GFP, Vac-GFP (Nelson et al., 2007), YFP-Got1 (Geldner et al. 2009), and GFP-VAMP727 (Ebine et al., 2008) were described previously. SALK_080766, a T-DNA insertion allele of *uge4*, was provided by the Arabidopsis Biological Resource Center (ABRC, Alonso et al., 2003) and the homozygous line was established (Uehara et al. 2014). SALK_080766 expressing GFP-VAMP727 was selected from the F2 progeny of a cross between a GFP-VAMP727 line and SALK_080766. Other markers were introduced into the SALK_080766 line using the *Agrobacterium*-mediated *in planta* transformation method (Clough and Bent, 1998) by Mr. Uehara. Plants were grown on solid media (Takano et al. 2005) containing 1 % (w/v) sucrose, 1.5 % (w/v) gellan gum (Wako Pure Chemical Industries), and 10 μM boric acid for 4-5 days in a growth chamber at 22 °C under a light/dark

cycle of 16 h/8 h.

Laser scanning confocal microscopy

Laser scanning confocal microscopy was performed using a Leica TCS-SP8 equipped with HCX PL APO CS ×40 water immersion lens. Excitation and detection wavelengths were 488 nm and 500-530 nm for GFP, and 488 nm and 500–540 nm for YFP, 488 nm and 500-530 nm for Venus, and 488 nm and >640 nm for FM4-64, respectively. FM4-64 (Molecular Probes) was prepared as a 10 mM stock solution in water and used at 4 μM. Plants grown for 4 days were treated with 10 μM latrunculin B or 10 μM oryzalin (Wako Pure Chemicals Industries) in liquid medium for 2 days. The liquid medium was replaced every day. Control experiments were performed with 0.1 % DMSO. Image analysis was performed using the Image J software (Abràmoff et al. 2004). The fluorescence intensity profiles were quantified along a line drawn through the region of interest. For calculation of Pearson and Spearman correlation coefficients, a PSC colocalization plug-in (French et al., 2008) for ImageJ was used to quantify the linear Pearson's value (*rp*) and the nonlinear Spearman's value (*rs*) of

GFP and FM4-64 fluorescent signals in selected regions. The values ranged from +1 (perfect positive correlation) to -1 (perfect negative correlation).

Electron microscopy

Root tips containing the elongation zone were obtained from 4-day-old plants of wild type and *uge4* mutant (SALK_080766). A high-pressure freezing system (Leica EM PACT2) was used to freeze samples, followed by incubation with 2 % osmium tetroxide-acetone solution. Gradually thawed samples were washed with acetone at room temperature and then suspended in Epon (Nisshin EM Corporation)-acetone solution series with 25, 50, 75 and 100 % Epon. Samples embedded in the Epon resin were polymerized at 60 °C for 48 h. Ultrathin sections (120 nm) were cut using grass knives or a diamond knife (Sumi Knife 45°, Sumitomo Electric Industries) on an ultramicrotome (Reichert-Nissei ULTRACUT N) and mounted on copper slot grids coated with Formvar film (Nisshin EM Corporation). The cut sections were then stained with 2 % uranyl acetate and Reynold's lead citrate and dried at 60 °C for 30 min. Electron micrographs were obtained with a transmission electron microscope

(JEM-2100, JEOL). To perform electron tomography, specimens prepared for transmission electron microscopy were used and the side of the grid carrying the section was coated with Formvar. The grid was coated with carbon on both sides using a Carbon Coater vacuum device (Nisshin EM Corporation). The specimens were hydrophilized by an ion spatter (E101, Hitachi), after which 1 μl of 15-nm colloidal gold solution was applied to each side and dried at 60 °C for 2 min. Electron tomography was performed using a JEM-3200FS transmission electron microscope (JEOL), and the images were processed using the 3dmod program of the IMOD package (Kremer et al., 1996; Chanoca and Otegui, 2014).

Immunoelectron microscopy

High-pressure freeze substitution was performed for immunoelectron microscopy following the method of Chanoca and Otegui (2014) with slight modifications. The frozen samples were incubated in 0.2% glutaraldehyde with 0.2% uranyl acetate solution at −80 °C for 3 days and warmed to −20 °C for 20 h. Then, the samples were washed three times with acetone at −20 °C followed by infiltration in a LR white resin-acetone solution series

of 33, 66, and 100% with 24-h intervals. Polymerization was accelerated by adding LR white accelerator at −20°C under UV light for 72 h. Ultrathin sections (80 nm) were cut using a diamond knife (Sumi Knife 45°, Sumitomo Electric Industries) on an ultramicrotome (Reichert-Nissei ULTRACUT N). Sections were mounted on Formvar-coated nickel grids and blocked for 20 min with 5% (w/v) skim milk (Difco) in phosphate-buffered saline (PBS, pH 7.2) containing 0.1% Tween 20 and 0.1% NaN_3. The samples were incubated in a blocking buffer containing 1:100 anti-ADP-ribosylation factor 1 (ARF1) antibody (Agrisera) overnight at 4°C. After rinsing three times for 1 min in PBS buffer containing 0.5% Tween 20, the sections were incubated in a blocking buffer containing 1:40 goat anti-rabbit IgG conjugated 10 nm gold (BBI Solutions) for 1.5 h. Then, the sections were washed in PBS buffer containing 0.5% Tween 20 twice and distilled water twice for 1 min each. The sections were stained with 2% uranyl acetate for 5 min and dried at 60°C for 30 min. Electron micrographs of the gold particles were obtained using a transmission electron microscope (JEM-2100, JEOL).

Results and Discussion

Intracellular aggregates in the *uge4* mutant contained endomembrane markers in the secretory and vacuolar pathways

In this study, to investigate the effects of the *uge4* mutation on endomembrane organization, I employed several markers of the secretory and vacuolar pathways. Uehara previously showed that the abnormal aggregates that accumulated in root epidermal cells of *uge4* mutant contained TGN/EEs markers and were stained by FM4-64, a tracer for endocytosis, as well as the ER-staining dye ER-Tracker Red (Uehara et al. 2014). To verify whether the ER membrane is contained in the aggregates, I analyzed the localization of an ER marker that contains the signal peptide of AtWAK2 (Wall-Associated Kinase 2) at the N-terminus of the GFP and the ER retention signal His-Asp-Glu-Leu at its C-terminus (Nelson et al. 2007). In the wild-type plants, the ER-GFP marker showed network-like structure and brightly fluorescent fusiform bodies (ER bodies) in the elongating epidermal cells (Figs. 1.1a, Fig. S1a) (Nelson et al. 2007). In an *uge4* mutant

line (SALK_080766), ER-GFP was mainly observed in the bright fusiform bodies (ER bodies), as was the case in the wild type, and also in the aggregates stained by FM4-64 (Figs. 1.1b-d, Fig. S1b-d). To quantify the level of colocalization of ER-GFP and FM4-64 in the aggregates, I calculated the linear Pearson (r_p) and the nonlinear Spearman's (r_s) correlation (PSC) coefficients for the pixels in the selected region (Fig. 1.1e). These values ranged from +1 (perfect positive correlation) to -1 (perfect negative correlation) (French et al. 2008). The PSC coefficients of $r_p = 0.77$ and $r_s = 0.85$ confirmed that the ER marker is present in the aggregates stained by FM4-64. Furthermore, a plot profile analysis supported the partial colocalization of the ER marker and FM4-64 (Fig. 1.1e, f). These data suggested that the lack of UGE4 function affected the structure of the ER or trafficking of the ER marker. Although C-terminal HDEL signal effectively retains secretory proteins in ER, protein that escapes from the ER can be secreted or transported into the vacuole (Gomord et al., 1997; Petruccelli et al., 2006). The presence of ER marker signals in the intracellular aggregates may indicate proteins that escaped from ER and were trapped in the abnormal endosomes. Then, the localization of a Golgi marker YFP-Got1p homolog (Geldner et al. 2009) was investigated. Similar

to the wild type, the marker in the *uge4* mutant showed punctate structures often associated with the aggregates labeled by FM4-64 (Figs. 1.1g-k, Fig. S1e-h). The PSC coefficients of r_p = 0.29 and r_s = 0.45 and the plot profile of GFP and FM4-64 signal intensity in the selected region containing the aggregates supported the association or partial colocalization (Fig. 1.1k, l). These results suggest that the structure of the Golgi apparatus was not largely affected, while the localization was slightly affected.

I then investigated the localization of markers in the vacuolar pathway in the *uge4* mutant. VAMP727 is a component of SNARE complex located on the multi-vesicular bodies/late endosomes (MVB/LEs) (Uemura and Ueda, 2014). Compared to wild-type cells (Figs. 1.2a, Fig. S1i), the number of punctate structures labeled by GFP-VAMP727 decreased in the epidermal cells as the intracellular aggregates appeared (Figs. 1.2b, Fig. S1j), and GFP-VAMP727 was accumulated in these aggregates together with FM4-64 (Figs. 1.2b-d, Fig. S1j-l). The PSC coefficients of r_p = 0.97 and r_s = 0.97 in the selected region containing aggregates (Fig. 1.2e) strongly supported the colocalization of GFP-VAMP727 and FM4-64. Similar plot profile patterns of GFP and FM4-64 also supported the strong colocalization (Fig. 1.2e,f). These results suggested that either MVB/LEs accumulated in

the aggregates or GFP-VAMP727 miss-localized to the abnormal endosomes. I then observed a marker for vacuolar membrane, g-TIP-GFP (vac-GFP) (Nelson et al. 2007) in the *uge4* mutant. The shape of the vacuole was apparently normal in the cells with the aggregates, but was not yet swollen (Figs. 1.2g, h, Fig. S1 m, n) (Uehara et al. 2014). The aggregates stained by FM4-64 contained weak GFP signals and were surrounded by stronger GFP signal (Figs. 1.2h-l, Fig. S1n-p). The PSC coefficients in the selected regions (Fig. 1.2k) were r_p value = -0.28 and r_s value = -0.27. The normal localization of g-TIP-GFP on the vacuolar membrane and the abnormal accumulation in the aggregates were probably dependent on the timing of protein synthesis. The g-TIP-GFP present on the vacuolar membrane was thought to represent those synthesized during the younger cell stages. As trafficking of g-TIP/TIP1;1 to the vacuolar membrane is dependent on Golgi and TGN (Rivera-Serrano et al., 2012), the newly synthesized g-TIP-GFP was likely trapped in the abnormal endosomes during trafficking to the vacuolar membrane.

As a PM marker that traffics through secretory and vacuolar pathways, a borate transporter BOR1 fused with GFP (BOR1-GFP) (Takano et al. 2010) was expressed in the *uge4* mutant. Compared with the exclusive PM

localization of BOR1-GFP in wild-type plants under low boron conditions (Figs. 1.3a, Fig. S1q), BOR1-GFP was also accumulated in intracellular aggregates stained with FM4-64 in the *uge4* mutant (Figs. 1.3b-e, Fig. S1r-t), which is similar to the case of GFP-NIP5;1 (Uehara et al., 2014). The PSC coefficients of r_p value = 0.79 and r_s value = 0.83 and plot profiles of GFP and FM4-64 signal intensity (Fig. 1.3e, f) supported the colocalization of BOR1-GFP and FM4-64 in the aggregates. This may be due to accumulation of BOR1-GFP in the endomembranes of the secretary pathway or vacuolar pathway. I then performed a time-course analysis of BOR1-GFP trafficking from the PM to MVB/LE after high-boron supply (Takano et al. 2005, 2010). The BOR1-GFP signal decreased gradually from the PM of the wild-type and *uge4* cells without aggregate and appeared in punctate structures within 40 min (Fig. 1.3g-k), which was previously identified as MVB/LEs (Takano et al. 2010). In contrast, the BOR1-GFP signal less frequently appeared in punctate structures in the *uge4* mutant cells containing aggregates (Fig. 1.3l-p). These results suggest that either the endocytic pathway from the PM to the MVB/LE is defective or the MVB/LEs accumulated in the aggregates in the *uge4* mutant.

Disruption of the cytoskeleton is not a primary cause of the endomembrane aggregates in the *uge4* mutant

It has been shown that microtubules in the swollen cells were disordered or absent entirely in the *uge4* mutants (Andeme-Onzighi et al. 2002). Pharmacological analysis using latruncurin B and oryzalin showed that disruption of actin and microtubule cytoskeleton, respectively, caused accumulation of GFP-NIP5;1 in spherical structures (Uehara et al. 2014). This indicated that the cytoskeletal disruption causes endomembrane disorganization, but the effect was distinct from that in the *uge4* mutants. To further compare the consequence of cytoskeletal disruption and lack of UDP-D-galactose synthesis in the *uge4* mutant, I investigated the effects of latrunculin B and oryzalin on localization of protein markers in the secretary and vacuolar pathways. Compared with the control (Figs. 1.4a and 1.5a), 48 hr treatment with 10 μM latruncurin B or oryzalin significantly disrupted the organization of actin and microtubules, respectively, in the root epidermal cells (Figs. 1.4b and 1.5b). Under this condition, the large intracellular aggregates typical in the *uge4* mutant were not visualized by FM4-64 or any marker used in this study, although significant effects were observed in the

localization of some markers (Figs. 1.4c-n and 1.5c-n). The Golgi marker YFP-Got1p homolog and the TGN marker YFP-VTI12 showed larger structures after latruncurin B treatment (Fig. 1.4f, h), and BOR1-GFP showed punctate structures in the cells after latruncurin B and oryzalin treatment (Figs. 1.4n and 1.5n). These effects can be attributed to the requirement of actin and microtubules for movement of organelle and organization of the endomembranes (Tamura et al., 2005; Brandizzi and Wasteneys, 2013). These data suggest that cytoskeletal disruption is not the primary cause of intracellular aggregates in root epidermal cells of the *uge4* mutant.

Ultrastructure analysis of the aggregates in the *uge4* mutant revealed the presence of high-electron-density vesicles derived from TGN/EEs

To further address the nature of the aggregates in the *uge4* mutants, I analyzed the ultrastructure using transmission electron microscopy. The structures including ER, Golgi stacks, TGN, MVB, vacuole, and mitochondria in elongating epidermal cells of wild-type plants are shown in

Fig. 1.6a-c. In the *uge4* cells, the structures of ER, Golgi, MVB, and vacuole were not apparently different from those of the wild-type cells (Fig. 1.6f, g). However, I noticed that the cytosol contained many large vesicles typically 150 to 250 nm in diameter and filled with high-electron-density materials (Fig. 1.6d, indicated by white triangles). The high-electron-density vesicles (HDVs) were observed in epidermal cells, but not in cortical cells of the mutant roots (Fig. 1.6d). I assume that the HDVs represent abnormally enlarged TGNs because (i) the mean size was greater than that of TGNs (diameter, 60–100 nm), (ii) they are closely associated with TGNs and some were interconnected (Fig. 1.6g), similar to the characteristics of TGN (Fig. 1.6b, c) (Otegui et al., 2006). I also found ER tubules in the region of HDVs accumulation (Fig. 1.6g, h) and Golgi around the region of HDVs (Fig. 1.6h). These results are consistent with the localization of the fluorescent ER marker in the aggregates (Fig. 1.1b-e) and the Golgi marker associated with the aggregates (Fig. 1.1h-k). I then investigated the spatial structure of HDVs in more detail using electron tomography. The three-dimensional analysis clearly illustrated that HDVs were interconnected with each other and occasionally also to TGNs (Fig. 1.7).

This observation strongly supports the assumption that the HDVs represent abnormally enlarged TGNs.

To further characterize the nature of the HDVs, I performed immunogold analysis of the ARF1 protein, which is localized to the Golgi and the TGN (Stierhof and El Kasmi, 2010; Robinson et al., 2011). The ARF1 antibody specifically labeled the Golgi apparatus and TGN/EEs in wild-type cells (Fig. 1.8a). The Golgi, the TGN/EEs, and the large vesicles were labeled in the *uge4* mutant cells (Fig. 1.8b). The large vesicles were observed only in *uge4* cells and thus most likely corresponded to the HDVs, although electron-dense materials were hardly observed without use of osmium acetate for the structural analysis (Fig. 1.6). These findings further suggest that the HDVs in the *uge4* mutant cells represent abnormally enlarged TGNs.

As the MVB/LE structures were not affected in *uge4* mutant cells, accumulation of FM4-64, the MVB/LEs marker GFP-VAMP727, the vacuolar membrane marker g-TIP-GFP and BOR1-GFP in the aggregates (Figs. 1.2b-e, h-k, 1.3b-e, l-p, Fig. S1j-l, n-p, r-t) would probably have been trapped in the abnormal TGN/EEs before being transported to MVB/LEs and the vacuole.

Previously, accumulation of such HDVs was observed in an electron micrograph of brefeldin A (BFA)-treated elongating epidermal cells of Arabidopsis roots (Grebe et al., 2003). BFA is an inhibitor of a subset of guanine-nucleotide exchange factors for ADP-ribosylation factors (ARF-GEFs) and induces agglomeration of TGN/EEs in Arabidopsis roots (Geldner et al., 2003; Dettmer et al., 2006). These results suggest that the defect in membrane trafficking causes accumulation of HDVs derived from TGN/EEs in the elongating epidermal cells of Arabidopsis roots. The lack of UDP-D-galactose in *uge4* cells may cause insufficient glycosylation of some membrane glycoproteins in Golgi cisternae and TGN, which have essential functions during membrane trafficking from TGNs. Alternatively, insufficient glycosylation of some cargo proteins could cause aggregation of protein in the TGNs and affect proper TGN function.

Conclusions

This analysis showed that the intracellular aggregates in elongating epidermal cells of the *uge4* mutant were mainly composed of abnormal TGN/EEs, and at a lower frequency ER tubules, and were associated with

the Golgi apparatus. The abnormal TGN/EEs exhibited larger sizes and spatial interconnections, and contain high-electron-density materials, likely to be proteins, membrane components, and cell wall polysaccharides. The disorganization of TGN/EEs is not likely a consequence of the defect of cytoskeleton in the *uge4* cells. Although the mechanism requires further elucidation, this analysis established the requirement for UDP-D-galactose synthesis by UGE4 for the organization and function of TGN/EEs.

Part II

Polar localization of a boric acid channel is mediated by phosphorylation and plays a crucial role in growth of *Arabidopsis thaliana* under low boron conditions.

Abstract

Boron (B) is essential for plant development but toxic in excess. In *Arabidopsis thaliana*, a boric acid channel, NIP5;1 plays an important role in B uptake under B limitation. NIP5;1 is expressed at the outermost cell layers of roots and shows polar localization toward the soil-side in the plasma membrane (PM). The polar localization is assumed to be important for the efficient uptake of boric acid from soil solution. However, the molecular mechanism generating polar localization of NIP5;1 and its physiological importance for boric acid uptake are not yet established.

To elucidate the mechanism of polar localization, I compared the localization of NIP5;1 and its homologs by the expression of GFP-NIP fusions under control of the *NIP5;1* promoter in transgenic *Arabidopsis thaliana* plants. In root epidermal cells, distinct localization patterns of members of NIPs family were observed. Among 8 homologs, NIP6;1, another boric acid channel and the closest homolog of NIP5;1 showed similar polar localization to NIP5;1, while NIP1;2 showed non-polar localization at the PM. Chimera analysis between NIP5;1 and NIP1;2 indicated a requirement of the N-terminal region of NIP5;1 for the polar localization of NIP5;1. Moreover, the N-terminal region of NIP5;1 was found to target aquaporin proteins to the polar domain.

To identify the sorting signal of the polar localization, I further investigated contributions of amino acid residues in the N-terminal region of NIP5;1 and NIP6;1. Deletion analysis of the N-terminal region of NIP5;1 revealed that the conserved "TPG" repeat sequences are important for the polar localization. Furthermore, GFP-NIP5;1 T18A/T21A/T24A (3T/3A) substituted mutant showed non-polar localization and GFP-NIP5;1 T18D/T21D/T24D (3T/3D) phosphomimic mutant showed polar localization at the PM of epidermal and endodermal cells. Similar non-polar localization was observed for GFP-NIP6;1 T15A/T16A/T19A at the PM of epidermal cells. In addition, immuno-blotting analysis using a specific antibody targeting phosphorylated NIP5;1 and Phos-tag gel, a phosphorylated protein separation tool, indicated that these threonine residues were phosphorylated *in vivo*. These results suggested the important role of phosphorylation in polar localization of boric acid channels.

To investigate the physiological role of the polar localization of NIP5;1 in plant growth, transport activity of GFP-NIP5;1 wild type and 3T/3A mutant was analyzed in *Xenopus* oocytes and transgenic Arabidopsis plants. Comparable B transport activity was observed for GFP-NIP5;1 wild-type and 3T/3A mutant in *Xenopus* oocytes. However, in transgenic plants, the induction of GFP-NIP5;1 wild-type into the *nip5;1-1* mutant showed favorable performance of plant growth than that of GFP-NIP5;1 3T/3A under low B conditions. These results suggest that polar

localization of NIP5;1 plays a crucial role in plant growth, probably increasing the efficiency of B uptake.

These evidences show that the polar localization of boric acid channel on the PM is mediated by phosphorylation and plays a crucial role in the growth of *Arabidopsis thaliana* under low B conditions.

Keywords: Boric acid NIP5;1 Polar localization Threonine residues Phosphorylation Plant nutrition

Abbreviation

PM: Plasma membrane

TGN: Trans-Golgi network

MVB: Multi-vesicular body

ER: Endoplasmic reticulum

GFP/YFP: Green/Yellow fluorescence protein

NIP: Nodulin 26-like intrinsic protein

FM4-64: N-(3-Triethylammoniumpropyl)-4-(6-(4-(Diethylamino) Phenyl) Hexatrienyl) Pyridinium Dibromide

BFA: Brefeldin A

TMD: Transmembrane domain

TBST: Tris-buffered saline–Tween 20

PID: One AGCVIIIa kinase, PINOID

ICP-MS: Inductively coupled plasma mass spectrometry

PIN: PIN-formed protein

5`UTR: Five prime untranslated region

CIAP: Calf intestine Alkaline phosphatase

DTT: Dithiothreitol

ORF: Open read frame

RG-II: Rhamnogalacturonan II

FRAP: Fluorescence recovery after complete bleaching

ERAD: ER-associated protein degradation

ESCRT: Endosomal sorting complex required for transport

Introduction

Boron and transporters in plants

Function of boron

Boron (B) was established as an essential trace element for higher plants. Warington (1923) observed the B-deficiency symptoms of broad bean plants. The effect of B deficiency includes swelling and elongation of cells, reduced root growth and leaf expansion, and loss of fertility and crops production (Kouchi and Kumazawa, 1976; Loomis and Durst, 1992; Dell and Huang, 1997; Shorrocks, 1997). Furthermore, numerous reports suggested B plays direct or indirect roles in very diverse processes in vascular plants (reviewed in Camacho-Cristóbal et al., 2008).

In tabacco cultured cells, majority of B were found to be distributed in the cell wall when supplied at limited concentrations (Matoh et al., 1992). The B-polysaccharide complexes of different plants were isolated from cell walls and identified as rhamnogalacturonan II (RG-II), one of pectic polysaccharides present in the primary cells walls (Matoh et al., 1993; Ishii and Matsunaga, 1996; Kobayashi et al., 1996). The biosynthesis of dimeric RG-II was also established *in vitro* when boric acid and isolated monomeric RG-II were incubated together (O'Neill et al., 1996). Dimeric RG-II is formed by borate cross-linking of monomeric RG-II at

identical apiosyl residues in the apiofuranosyl residues of the 2-O-methyl D-xylose (2Me-Xyl)-containing side chains (Ishii et al., 1999). These results demonstrated the structural role of B in the RG-II dimerization process while the physiological function of dRG-II-B remained unknown. A glucuronyltransferase 1 gene from tabacco, *NpGUT1,* was shown to be responsible for the synthesis of pectin in RG-II and essential for the formation of RG-II-B complex (Iwai et al., 2002). The *NpGUT1* was specifically expressed in shoot and root apical meristems and reproductive tissues. Loss-of-function of NpGUT1 caused defects in reproductive tissue development and fertilization, and reduced B and RG-II pectin in the pollen tube tip (Iwai et al., 2002; Iwai et al., 2006). Two allelic Arabidopsis mutants (*mur1-1* and *mur1-2*) showed defects in the formation of GDP–L-Fucose in RG-II resulting in altered structure of RG-II (O'Neill et al., 2001). Most importantly, this altered RG-II significantly reduced the rate of formation and stability of RG-II-B, and reduced shoot growth of Arabidopsis (O'Neill et al., 2001). An Arabidopsis CTP:3-deoxy-D-manno-2-octulosonate cytidylyltransferase (CMP-KDO synthetase, CKS) is responsible for the activation of 3-deoxy-D-manno-2-octulosonic acid (KDO), a specific component monosaccharide of RG-II before it incorporates into RG-II (Kobayashi et al., 2011). Loss-of-function *cks* mutant showed impaired pollen tube elongation leading to the failure of pollen fertilization. These studies indicated the important function of RG-II-B complex in plant growth and reproductive tissue

development. Recently, the RG-II-B complex formation was shown to be facilitated by the addition of glycosylinositol phosphorylceramides (GIPCs), major components of lipid rafts in membrane (Voxeur and Fry, 2014). Moreover, GIPC-B-RG-II could be formed *in vitro* suggesting the possible attachment site between the cell wall and the plasma membrane (PM) (Voxeur and Fry, 2014).

Boric acid channels

Boron usually remains as uncharged boric acid [$B(OH)_3$] in soil solution. Plant root takes up boric acid via three distinct molecular mechanisms: 1) passive diffusion across lipid bilayer; 2) channel proteins; 3) secondary active transporters (Takano et al., 2008).

It was suggested that passive diffusion would be sufficient to fullfill B requirement for plants grown under normal B condition (Brown et al., 2002). The involvement of channel proteins in B transport was first indicated by the finding that channel blockers partially inhibited the B permeation across PM vesicles from squash roots (Dordas et al., 2000). Later on, a boric acid channel was identified from *Arabidopsis thaliana* (Takano et al., 2006). As a gene strongly induced in response to low B treatment, NIP5;1, a member of major intrinsic protein (MIP) family was identified (Takano et al., 2006). Two independent mutants of *NIP5;1* showed reduced root and shoot growth and defects in B uptake from medium to roots under limited B conditions. The B uptake activity of NIP5;1 was shown in *Xenopus* oocyte. These results suggested that the NIP5;1 is essential for efficient boron uptake and plant development under B limitaiton. Later on, the 5' untranslated region (UTR) was

identified to be responsible for the B-dependent regulation of *NIP5;1* transcript level in cells (Tanaka et al., 2011).

NIP6;1, the closed homolog of *NIP5;1* in Arabidopsis, is specifically expressed in the node region of the stem, the base of flowers, and the petioles of immature rosette leaves but absent in mature leaves (Tanaka et al., 2008). NIP6;1 showed high boric acid transport activity in oocytes. The T-DNA insertion lines of *NIP6;1* showed reduced expansion and B concentration in young rosette leaves grown in low-B conditions. These data strongly supported that NIP6;1 is a boric acid channel required for preferential distribution of boric acid to young developing shoot tissues.

Another NIP5;1 homolog in NIPs family, NIP7;1, was also identified as a boric acid channel (Li et al., 2011), however its physiological role in boron transport remains to be elucidated. NIP7;1 is expressed in pollen and in anthers, and showed relatively low boric acid transport activity compared to NIP5;1 in oocytes. This is because a conserved tyrosine residue (Tyr81) stabilizes the closed pore conformation by interacting with the canonical Arg220 in ar/R region. Substitution of Tyr81 with cysteine or phenylalanine established open conformational channels with robust transport activity for boric acid as well as other uncharged solutes. *NIP5;1*-like genes were also identified in rice and maize, and were shown to encode boric acid channels essential for plant development under B-deficient conditions (Durbak et al., 2014; Hanaoka et al., 2014; Leonard et al., 2014).

Recently, a new subfamily of MIP named X Intrinsic Proteins (XIPs) has been identified in several eudicot plants and fungi and a protozoan species (Danielson and Johanson, 2008; Gupta and Sankararamakrishnan, 2009; Sade et al., 2009; Park et al.,

2010). Among them, *Solanaceae* XIPs were revealed to facilitate transport of uncharged substrates glycerol and urea, and increase the sensitivity of yeast cells to externally supplied hydrogen peroxide and boric acid, suggesting XIP isoforms are permeable to hydrogen peroxide and boric acid (Bienert et al., 2011).

Mechanisms of polar localization of membrane proteins in plant cells

Apical/basal localization of PM proteins mediated by phosphorylation

Polar localization of membrane protein can be established either by polar secretion after *de novo* synthesis and/or by polar recycling after non-polar secretion. In plants, the cell-to-cell unidirectional flow of auxin is dependent on the function of PIN-FORMED (PINs), auxin efflux carries. The Arabidopsis genome encodes eight PIN proteins, and five of them showed polar localization in the PM toward apical/basal/lateral-sides depending on cell type and developmental stage. For example: PIN1 is basally localized at the PM of embryos and at vascular tissues of leaves and roots, but apically localized at the epidermal cells of embryos and shoot apices; PIN2 is apically localized at the epidermal cells and basally localized in cortical cells (Gälweiler et al., 1998; Friml et al., 2003; Bennett et al., 2006).

Studies on PINs revealed an important role of phosphorylation in polar sorting. A PINOID (PID) serine/threonine kinase was identified as a regulator of PIN

apical-basal localization (Benjamins et al., 2001; Friml et al., 2004). The importance of phosphorylation of PINs by PID was indicated by the genetic evidences where overexpression of PID led to transcytosis of PIN1, PIN2 and PIN4 from basal PM to apical PM, while loss-of function *pid* mutants showed opposite switch of PIN1 from apical to basal PM in embryos, root cells and inflorescence apices (Friml et al., 2004). Furthermore, it was suggested that PID directly phosphorylates the central hydrophilic loop (HL) of PIN proteins in PM because of their colocalization in PM (Friml et al., 2004; Michniewicz et al., 2007).

Mass spectrometry analysis and point mutagenesis of PINs identified three evolutionarily conserved TPRXS(N/S) motifs within the PINHL, in which the central serine residue is phosphorylated by PID (Nuhse et al., 2004; Michniewicz et al., 2007; Huang et al., 2010). PID belongs to the plant AGCIII kinase subfamily, (cAMP-dependent protein kinase A, cGMP-dependent protein kinase G, and protein kinase C) and was grouped into AGC3 subclade together with WAG1, WAG2 and AGC3-4 (Galván-Ampudia and Offringa, 2007). Studies on the function of WAG1 and WAG2 indicated that both kinases are able to phosphorylate the conserved motif within PINHL *in vitro* and induce basal-to-apical localization shift of PIN *in vivo* (Galván-Ampudia and Offringa, 2007; Cheng et al., 2008; Dhonukshe et al., 2010). Importantly, the protein phosphatase 2A (PP2A) antagonistically acts upon phosphorylated PIN proteins in these central hydrophilic loop resulting in down-regulated phosphorylation level of PINs (Michniewicz et al., 2007). Loss-of-function mutant of PP2A showed basal-to-apical shift of PIN1, PIN2 and PIN4 in embryos and roots.

The polar localization of PINs at the PM is a dynamic process maintained by vesicle trafficking pathways. These trafficking pathways directing PINs to distinct polar domain require different factors. Basally localized PINs need ADP-ribosylation factor-guanine nucleotide exchange factor (ARF-GEF) GNOM for endocytic recycling (Geldner et al., 2003; Kleine-Vehn et al., 2008). Short time brefeldin A (BFA) treatment inhibits GNOM function and interferes with the normal recycling and induces intracellular accumulation of basally localized PM proteins (Geldner et al., 2003; Kleine-Vehn et al., 2008). In contrast, apically localized PIN proteins such as PIN2 in root epidermal cells showed only weak sensitivity to BFA treatment (Kleine-Vehn et al., 2008).

Mechanisms of soil-side/stele-side polar localization of PM proteins

Increasing number of membrane proteins has been reported to be localized toward the soil /stele-side PM in root cells. The boric acid channel, NIP5;1 (Takano et al., 2010), the exporter of the plant hormone precursor indole-3-buryric acid PIS1/PDR9/ABCG37 (Ruzicka et al., 2010), the pathogen-defense-related transporter PEN3/PDR8/ABCG36 (Strader and Bartel, 2009), the silicic acid channel OsLsi1 (Ma et al., 2006) and iron-regulated transporter IRT1 (Barberon et al., 2014) are localized toward the soil-side PM. The boric acid/borate transporter BOR1 (Takano et al., 2010), the efflux transporter of silicic acid OsLsi2 (Ma et al., 2007) are localized toward the stele-side PM.

AtBOR1 is localized toward the stele-side PM and acts as a boric acid/borate exporter mediating B loading toward xylem (Takano et al., 2002). BOR1 has two or

three conserved tyrosine-based signals in a large loop between the predicted 8th and 9th transmembrane domains (Takano et al., 2010). The BOR1 (Y373A/Y398A/Y405A)-GFP mutant showed non-polar localization at epidermal cells, but yet to be polar at the differentiated zone endodermal cells. BFA made BOR1 localization to be non-polar at epidermal cells (Takano et al., 2010) but not at endodermal cell (Alassimone et al., 2010). In the cell wall of endodermal cells, there are Casparian strips which functions as a apoplastic diffusion barrier and also as a membrane diffusion barrier (Alassimone et al., 2010). These results suggested that the mechanism of polar localization is not only dependent on the tyrosine-based signals but also on another trafficking mechanism.

To explore the cellular mechanism of polar localization in the PM toward soil-side, Langowski et al (2010) analyzed the localization of ABCG36, ABCG37 and borate efflux transporter BOR4 in Arabidopsis. GFP-ABCG37 showed polar localization at the three outermost cell layers including epidermal, cortical and endodermal cells but showed non-polar localization at further interior root cells (Langowski et al., 2010). The fluorescence recovery after complete bleaching (FRAP) analysis of these proteins revealed that the newly synthesized proteins appeared at the soil-side PM. Differences in trafficking of the apical/basal proteins versus these proteins were further investigated by the pharmacological analysis. In contrast to the fact that BFA inhibits endocytic recycling of PINs, little effect of BFA was observed for the proteins localized toward the soil-side of the PM. Disruption of microtubules by oryzalin and depolymerization of actin by Latrunculin B (LatB) did not largely affect the polar localization toward soil-side (Langowski et al., 2010). However, the

trafficking of apical/basal cargos was dependent on the organization of actin cytoskeleton (Rahman et al., 2007). Moreover, the soil-side localization of PM proteins did not change when expressed in *gnom* mutants, PID overexpressing line, and *pp2a* mutants suggesting neither the GNOM-mediated trafficking pathway nor PID/PP2A-depedent phosphorylation status involved in polar targeting toward soil-side (Langowski et al., 2010). So far, neither sorting signal nor regulatory machinery was identified for the polar localization toward the soil-side PM.

As a boric acid channel, NIP5;1 plays an important role in B uptake under B deficiency. NIP5;1 is expressed in the outermost cell layers of roots and shows a polar localization toward the soil-side of the PM (Takano et al. 2010). The polar localization is assumed to be an important feature for the efficient uptake of boric acid from soil solution. In this study, I focus on the mechanisms underlying polar localization of NIP5;1 and its physiological role in plant growth.

Materials and Methods

Plant materials and growth conditions

Arabidopsis thaliana Col-0 was from our laboratory stock. The T-DNA insertion mutant *nip5;1-1* was obtained from the Arabidopsis Biological Resource Center (ABRC, Ohio State University) and homozygous line was established (Takano et al., 2006). Transgenic Arabidopsis plants expressing EYFP-NPSN12 (Geldner et al., 2009), EGFP-Lti6a (Cutler et al., 2000) were obtained from Niko Geldner (University of Lausanne) and ABRC, respectively. T1 lines expressing GFP fused proteins were selected on half strength MS medium supplemented with 20 μM hygromycin B. T3 homozygous lines harboring pNIP5;1 (without 5' UTR): GFP-NIP5;1 (Tanaka et al., 2011) were provided by Dr. Mayuki Tanaka (University of Tokyo). For imaging, plants were grown on solid media (Takano et al., 2005) containing 1% (w/v) sucrose, 1.5% (w/v) gellan gum (Wako Pure Chemical Industries, Osaka), and 10 μM boric acid for 4-5 days in a growth chamber at 22 °C under a light/dark cycle of 16 h/8 h. Solid media used for growth analysis were supplemented with 0.1, 0.3, 1.0 and 3.0 μM boric acid. Highly purified water was produced using the MILLI-Q ADVANTAGE A10 purification system (Millipore, Tokyo).

Plasmid construction

The open reading frame (ORF) of *NIP7;1* was amplified from RNA of Col-0 flowers, and other NIPs and PIP2;1 were amplified from RNA of Col-0 roots using the One-step RT-PCR kit (Qiangen, Tokyo) with specific primers (Table 1). Then ORFs of interest were subcloned into pENTR/D-TOPO vector (Lifetechnologies, CA) that is compatible with Gateway destination vectors. A series of truncated GFP-NIP5;1 (ΔN17, 26, 40, 60, 75, 78, and ΔC11) and mutated GFP-NIP5;1 (L76A, S75AT77A, R78Q, SLTR/AAAA and L76F), mutated GFP-NIP6;1 (L78A, L78F) were generated from the templates pShw6 (pENTR/D-TOPO NIP5;1) and pShw15 (pENTR/D-TOPO NIP6;1) using specific primers. To generate chimera constructs (GFP-Nter1;2-NIP5;1, GFP-Nter5;1-TMD1;2-Cter5;1, GFP-NIP5;1-Cter1;2, GFP-Nter5;1-NIP1;2 and GFP-Nter5;1-PIP2;1), PCR fragments of NIP1;2, NIP5;1 and PIP2;1 and a pENTR/D-TOPO backbone were amplified from entry vector [pShw2 (pENTR/D-TOPO NIP1;2), pShw6 and pShw116 (pENTR/D-TOPO PIP2;1)] using specific primers. The amplified PCR fragments were then fused using an In-Fusion HD Cloning kit (Takara Clontech, Tokyo). A gateway destination vector containing *NIP5;1* promoter without 5' UTR and sGFP was constructed as follows. A Gateway vector pGWB506 containing the cauliflower mosaic virus 35S (CaMV35S) promoter and sGFP for N-terminal fusion (Nakagawa et al., 2007) was digested with restriction enzyme *Hind* III and *Xba* I (Takara-bio, Tokyo) to remove

the promoter sequence. A PCR fragment containing 2180 bp NIP5;1 promoter sequence was digested with restriction enzyme *Hind* III and *Xba* I and then ligated with the digested pGWB506 to construct pShw18 in which CaMV35S promoter was replaced with NIP5;1 promoter without 5' UTR (Tanaka et al., 2011). Gateway LR reaction was performed between NIPs containing entry vectors and pShw18 destination vector to obtain expression constructs.

The constructs pNIP5;1 (w/o 5' UTR): sGFP-NIP5;1 (T18A/T21A/T24A, T18A, T21A, T24A) were generated by PCR using specific primers including point mutations (Table 1) and the pNIP5;1 (w/o 5' UTR): sGFP-NIP5;1 (Tanaka et al., 2011) as a template. To construct the pNIP5;1(w/o 5' UTR): sGFP-NIP6;1, the backbone sequence pNIP5;1 (w/o 5' UTR): sGFP was amplified from the plasmid pNIP5;1 (w/o 5' UTR): sGFP-NIP5;1 by PCR with specific primers. Then NIP6;1 sequence amplified by PCR with specific primers (Table 1) and pNIP5;1(w/o 5' UTR): sGFP backbone sequence were fused using an In-Fusion HD Cloning kit (Takara Clontech, Tokyo). pNIP5;1(w/o UTR): GFP-NIP6;1 (T15A/T16A/T19A, T16A, T19A) mutants were generated by PCR using specific primers including point mutations (Table 1) and pNIP5;1(w/o UTR): GFP-NIP6;1 as a template. To construct pCASP1:sGFP-NIP5;1 wild-type and 3T/3A vectors, an endodermis-expressing promoter, *CASP1*, was amplified from the plasmid pCASP1:CASP1-GFP (Roppolo et al., 2011) and a vector backbone including

sGFP-NIP5;1 was from pNIP5;1 (w/o 5' UTR): sGFP-NIP5;1 (Tanaka et al., 2011) as a template by PCR using specific primers (Table 1). These fragments were fused using In-Fusion HD Cloning kit (Takara Clontech, Tokyo).

Transformation of plant

Binary plasmids were transformed into *Agrobacterium tumefaciens* GV3101::pMP90. The *nip5;1-1* mutant was used for transformation by the *Agrobacterium*-mediated *in planta* transformation method (Clough and Bent, 1998).

Microscopy imaging

Laser scanning confocal microscopy Leica TCS-SP8 system equipped with an HC PL APO CS x40 water immersion lens was used for imaging with the following set of excitation and detection wavelengths: GFP/YFP (488 nm and 500–540 nm); FM4-64 (488 nm and >640 nm). For xzy view, galvanometric driven z-stage (SuperZ) was used in laser scanning confocal microscopy Leica TCS-SP5 system. The 3-5 days-old plants grown on vertically placed solid medium were used. The working solution of FM4-64 (Lifetechnologies, Tokyo) was applied at a concentration of 4 μM in liquid medium for 30 minutes prior to imaging.

Isolation of membrane fractions and immunoprecipitation

Microsomal fraction was prepared using the method (Takano et al., 2010) with

modifications. Roots of plants grown on liquid medium (Takano et al., 2005) containing 10 μM boric acid were harvested and homogenized by Multi Beads Shocker (YASUI KIKAI, Osaka) with buffer (250 mM Tris, pH 8.5, 290 mM sucrose, 5 mM DTT) supplemented with protease inhibitors cOmplete Mini EDTA-free (Roche) and 0.5 mg/L Pefabloc SC (Roche, Mannheim) on ice. The extract was centrifuged two times at 10,000 xg for 15 min at 4 °C to remove cell debris and the resultant supernatant was pelleted by a centrifugation at 100,000 xg for 30 min at 4 °C using Beckman Coulter OptimaTM TLX Ultracentrifuge.

For treatment with alkaline phosphatase, the membrane pellets were dissolved in 1x Calf intestinal alkaline phosphatase (CIAP) buffer (50 mM Tris-HCl, pH 9.0, 10 mM $MgCl_2$) supplemented with 1x protease inhibitor (for plant cell and tissue extracts, Sigma-Aldrich, Tokyo) and 0.5 mg/ml pefabloc SC (Roche, Mannheim).

To prepare IP samples, the pellets were resuspended in lysis buffer (50 mM Tris-HCl, pH8.0, 150 mM NaCl, 1% (v/v) Triton X-100) with 0.2% (v/v) 3-[(3-Cholamidopropyl)dimethylammonio]-1-propanesulfonate (CHAPS), 1x protease inhibitor (for plant cell and tissue extracts, Sigma-aldrich), and 0.5 mg/ml Pefabloc SC (Roche, Mannheim). Resuspended samples were centrifuged for 10 min at 100,000 xg and supernatant was used for immunoprecipitation. Immunoprecipitation was done using the μMACS GFP tagged protein isolation kit (Miltenyl Biotec, Tokyo) following the supplier's protocol with a following

modification. After rinsing columns with 1x 100 µl wash buffer 2 (20 mM Tris HCl, pH 7.5), the IP samples conjugated with microbeads were collected in ~50 µl of CIAP buffer.

Generation of anti-phospho-threonine antibody

The anti-phospho-threonine antibody of NIP5;1 (anti-pTNIP5;1) was generated by SCRUM Inc. (Tokyo) as follows. A phosphorylated peptide [Cys-MAPP(pT)PG(pT)PG(pT)PG] with >80% purity was synthesized and used to immunize rabbits. After 6 weeks immunization, 20 ml serum was collected and affinity purified with the phosphorylated peptide in an affinity column. To remove antibodies recognizing non-phosphoryltaed peptide, the eluted fraction was absorbed with a non-phosphorylated peptide (Cys-MAPPTPGTPGTPG) in an affinity column. The flow-through fraction contained anti-phospho-threonine antibody.

Alkaline phosphatase treatment

A tube with 9.2 µl sample including microbeads (IP sample) or membrane fraction was added with 0.8 µl CIAP (Takara-bio, Tokyo) and incubated at 37 °C for 2 hour. Then samples were added with 4 µl 4x SDS-sample buffer or 4x LDS buffer containing 200 mM DTT and incubated for another 1 hour. Finally, samples were denatured for 5 min at 85 °C.

Analysis of phosphorylation by immuno-blotting

For the analysis of phosphorylation status of NIP5;1, samples were either ran in 10% Supersep Phos-tag gel (Wako Pure Chemical Industries, Osaka) or in 4-12% Tris-Bis NuPAGE gel (Invitrogen, Tokyo). After electrophoresis, Phos-tag gel was washed for 10 min x 3 times with transfer buffer (25 mM Tris, 190 mM glycine, 20% methanol, 0.1% SDS) containing 5 mM EDTA to improve transfer membrane efficiency. The transferred-membrane was immediately blocked with 0.3% (w/v) skim milk (Difco) in TBST at room temperature. The immuno-blotting process was performed by SNAP i.d. Protein detection system (Millipore, Tokyo). 1/4000 diluted anti-GFP monoclonal antibody [anti-GFP (Mouse IgG1-k), Nacalai tesque. inc] or 1/1000 diluted Rabbit anti-pTNIP5;1 polyclonal antibody was used as first antibody in Can Get Signal Solution 1 (Toyobo, Tokyo). 1/20,000 diluted Mouse anti-horseradish peroxidase (HRP)-conjugated anti-mouse IgG antibody (GE Healthcare, Tokyo) or 1/20,000 diluted Rabbit anti-HRP-conjugated anti-mouse IgG antibody (GE Healthcare, Tokyo) was used as second antibody in Can Get Signal Solution 2 (Toyobo, Tokyo). The membrane was washed three times with 30 mL of 1xTBST after antibody incubation for 10 min. Two ml of Luminata Forte Western HRP substrate (Millipore, Tokyo) was added onto membrane followed by imaging by LAS-3000 imaging system (Fujifilm, Tokyo).

Boron uptake assay in *Xenopus* oocyte

The ORFs of NIPs N-terminally fused to GFP tag were amplified by PCR using the specific primers (Table 1), which contain *Bam* HI restriction sites at both 5' end. The PCR products were digested with *Bam* HI and were subcloned into the pXβG-ev1 oocyte expression vector (Preston et al., 1992; Mitani-Ueno et al., 2011) which was digested with *Bgl* II. Capped cRNA was transcribed *in vitro* from *Xba* I linearized vector using the mMESSAGE mMACHINE kit (Ambion, Tokyo). Oocytes injected with cRNA of interest using a injector (Drummond Nanoject II Auto-Nanoliter, Broomall, PA, USA) were kept in MBS buffer [88.0 mM NaCl, 1.0 mM KCl, 2.4 mM $NaHCO_3$, 15.0 mM Tris-HCl (pH7.6), 0.3 mM $Ca(NO_3)_2\,4H_2O$, 0.41mM $CaCl_2\,4H_2O$, 0.82 mM $MgSO_4\,7H_2O$, 10 ug/ml sodium penicillin, 10 ug/ml streptomycin sulfate] for 48 h. Then oocytes with GFP signal were selected under Olympus MVX10 fluorescence microscopy and incubated in medium supplemented with 5 mM boric acid for 30 min. B contents in oocytes were determined by inductively coupled plasma mass spectrometry (ICP-MS).

Root length measurement

T3 homozygous seeds harboring GFP-NIP5;1 wild type and T18A/T21A/T24A mutant in *nip5;1-1* background, Col-0, and *nip5;1-1* were sown on solid medium (Takano et al., 2005) with 1% (w/v) sucrose, and 1.5% (w/v) Gellan Gum and

various boron concentrations. The plates were vertically placed in growth chambers at 22 °C under a cycle of 18-h light and 6-h dark. The photos of one-week-old plants were taken and root lengths were measured by RootNav software (Pound et al., 2013).

ICP-MS

The samples were digested for 24 hours in Digi TUBEs (GL sciences, Tokyo) with 6 mL concentrated nitric acid [For B determination (60-61%), Wako Pure Chemical Industries, Osaka] at 110 °C with DigiPREP Jr. equipment (GL sciences, Tokyo). After the solution was evaporated, 10 mL of 2% nitric aicd was added to dissolve the samples. Solution was filtered with DigiFILTER 0.45 μm (GL sciences, Tokyo) to remove solid materials. ICP-MS was performed using ICP-MS ELAN DRC-e and ESI Autosamplers (PerkinElmer, Waltham, Massachusetts, USA). Highly purified water was produced using the MILLI-Q ADVANTAGE A10 purification system (Millipore, Tokyo).

Results

Distinct localization of NIPs in epidermal cells

Several studies reported that NIP5;1 (Takano et al., 2006), NIP6;1 (Tanaka et al., 2008) and NIP2;1 (Choi and Roberts, 2007) were localized mainly in the PM whereas

NIP1;1 (Geldner et al., 2009) were localized in the PM but also in intracellular membranes and NIP2;1 in the ER (Mizutani et al., 2006). To date, AtNIP5;1 was a only NIP that showed polar localization in the PM toward soil-side in root cells (Fig. 2.3 A) (Takano et al., 2006). Considering the high sequence similarity of the central region from first transmembrane domain to sixth transmembrane domain and high divergence of cytosolic N- and C-terminal regions of NIPs (Fig. 2.1), I hypothesized that the N- or C-terminal region of NIP5;1 is responsible for the polar localization. Therefore, I intended to identify a homolog having distinct localization in the PM, which would allow me to explore the sorting signal for polar localization.

To identify such a non-polar NIP, I generated a set of constructs which have the protein sequence of NIPs fused with sGFP tag at the N-terminus under the control of the NIP5;1 promoter w/o 5' UTR (Tanaka et al., 2011) (Fig. 2.2). They were introduced by Agrobacterium-infiltration procedure into the *nip5;1-1* mutant. GFP-NIP1;1, GFP-NIP2;1, and GFP-NIP4;1 showed both PM and intracellular localization, presumably in the ER, in root epidermal cells (Fig. 2.3 B). Similar localization was previously reported for NIP1;1 (Geldner et al., 2009). GFP-NIP1;2 and GFP-NIP5;1 exclusively accumulated in the PM. As previously reported (Tanaka et al., 2008), GFP-NIP6;1 was mainly localized in the PM. The GFP derived from GFP-NIP7;1 and GFP-NIP3;1 were localized in intracellular membranes (Fig. 2.3 B). These results represented the distinct localization pattern of NIP homologs in root

epidermal cells.

Identification of non-polar localization of NIP1;2

To identify a non-polar NIP, I further compared the localization patterns of NIP1;2, NIP5;1, and NIP6;1 in the PM of epidermal cells. For comparison, FM4-64, a lipophilic styryl dye was used to stain PM in a non-polar manner. Both GFP signals of NIP5;1 and NIP6;1 showed gradual increase of intensity toward soil-side when compared to FM4-64 fluorescence signals (Fig. 2.4), indicating polar localization. In contrast, the GFP-NIP1;2 showed only little increase in intensity toward soil-side compared to FM4-64. Similarly, little gradient was observed for PM markers EYFP-NPSN12 (Geldner et al., 2009) and EGFP-Lti6a (Cutler et al., 2000) (Fig. 2.4). I assume EYFP-NPSN12 and EGFP-Lti6a localize to the PM in a non-polar manner because EYFP-NPSN12 was localized both in the stele and soil-side PM of endodermal cells (Alassimone et al. 2010) and Lti6 homologs showed fast diffusion rates in the PM by FRAP analyses (Kleine-Vehn et al., 2011; Luu et al., 2012). It is likely that the cell thickness affected the transmission efficiency of green light (GFP) to greater extent than that of the red light (FM 4-64) in the longitudinal optical section of root. Therefore, I judged that NIP1;2 localization is non-polar in the PM.

To confirm the distinct localization of NIP1;2 and NIP5;1, cross-sectional images were taken by a xzy scanning mode of confocal microscopy equipped with

galvanometric driven z-stage (SuperZ) (Fig. 2.5, left). Then, a plot profile was employed for quantitative analysis of polar localization (Fig. 2.5, right). The GFP-NIP5;1 showed strong intensity in the soil-side but little signal in the stele-side PM, which is consistent with the xyz view (Fig. 2.4). In contrast, the GFP-NIP1;2 was similarly observed both in the soil- and stele-side PM. Stronger YFP/GFP intensity were observed at the stele-side of epidermal cells for YFP-NPSN12 and EGFP-Lti6a due to the fluorescence also coming from the PM of cortical cells. Therefore, NIP1;2 was confirmed to be a non-polar localized NIP.

N-terminal region of NIP5;1 is required for its polar localization

Non-polar localized NIP1;2 is a good tool to identify the polar sorting signal in NIP5;1. I first generated 3 chimera constructs by swapping the corresponding N-terminal region, C-terminal region, and central region from the first transmembrane domain (TMD) to the sixth TMD between NIP1;2 and NIP5;1 (Fig.2.6).

A chimera protein GFP-NIP5;1-Cter1;2 expressed in *nip5;1-1* background showed polar localization in the PM with strong intracellular signal in elongating epidermal cells (Fig. 2.6). I also generated GFP-NIP5;1 ΔC11 by deleting 11 amino acid residues from C-terminal region of NIP5;1 because the 11 amino acid residues are well conserved in NIP5;1 and NIP6;1. Consistent with the result of GFP-NIP5;1-Cter1;2, GFP-NIP5;1 ΔC11 showed polar localization (Fig. 2.6). These

results indicate that the C-terminal region of NIP5;1 is not involved in polar localization. Similarly, a chimera protein GFP-Nter5;1-TMD1;2-Cter5;1, which was generated by substitution of the region from first TMD to sixth TMD of NIP5;1 with NIP1;2 showed polar localization in the PM (Fig. 2.6), suggesting that the central region of NIP5;1 is not required for polar localization. However, a N-terminal substituted chimera protein GFP-Nter1;2-NIP5;1 showed non-polar localization (Fig. 2.6). Thus, these results demonstrate that the N-terminal region of NIP5;1 is required for the polar localization in the PM.

N-terminal region of NIP5;1 sufficiently directs polar localization of aquaporins

I further investigated whether the N-terminal region of NIP5;1 would confer polar localization on other non-polar aquaporins, such as NIP1;2 and PIP2;1. For this purpose, I expressed the chimera constructs GFP-Nter5;1-NIP1;2 and GFP-Nter5;1-PIP2;1 in *nip5;1-1* mutant (Fig. 2.7). The chimera protein GFP-Nter5;1-NIP1;2 showed polar localization in the PM although the signal simultaneously occurred in cytoplasm (Fig. 2.7). PIP2;1 was usually localized in the PM in a non-polar manner, however the GFP-Nter5;1-PIP2;1 chimera showed polar localization toward the soil-side PM (Fig. 2.7). These findings demonstrate that the N-terminal region of NIP5;1 is sufficient to target non-polar PM proteins toward

soil-side.

Conserved "TPG" repeats in the N-terminal region is important for the polar localization of NIP5;1

The amino acid sequence of the N-terminal regions of Arabidopsis NIPs subfamily are very diverse and both NIP5;1 and NIP6;1 possess an obviously longer sequence than others (Fig. 2.8). A conserved sequence was found in both N-terminal regions: TPGTPGTPG from the position of 18 to 26 of NIP5;1 and TPGTPG from the position of 16 to 21 of NIP6;1 (Fig 2.8). To identify a sorting signal for the polar localization, I performed deletion analysis of NIP5;1 by deleting 17 and 26 amino acid residues from the N-terminal region of NIP5;1. Like the wild-type GFP-NIP5;1, the ΔN17 mutant showed polar localization in the PM, whereas ΔN26 mutant showed little polar localization (Fig. 2.9), suggesting the important function of the "TPG" repeats in polar localization.

The whole N-terminal region of NIP5;1 contains 78 amino acid residues based on predication by PHDhtm (Rost et al., 1995). I further performed the deletion analysis by expressing four truncated mutants GFP-NIP5;1 ΔN40, ΔN60, ΔN75, and ΔN78 in the *nip5;1-1* mutant. The GFP signal of ΔN40 version was hardly detectable for unknown reason (Fig. 2.9). The GFP-NIP5;1 ΔN60 and ΔN75 were localized to the PM with a weak or non-polar manner (Fig. 2.9). Interestingly, the ΔN78 mutant

showed little GFP signal suggesting the importance of residues from 76 to 78 for protein stability (Fig. 2.9). Additionally, ΔN17 and ΔN26 mutants showed significant dotty structures (Fig. 2.9). To investigate whether deletion of the N-terminal region triggers targeting of NIP5;1 variants to the vacuole for degradation, I observed the GFP signal after dark treatment for 8h. Compared to the exclusive PM-localization of GFP-NIP5;1 wild-type, ΔN17, and ΔN26 mutants showed vacuolar accumulation after the dark treatment (Fig. 2.10). These findings suggest that the deletion of N-terminal region of NIP5;1 induced protein sorting to the vacuolar pathway (Fig. 2.10). Nonetheless, these results suggest that the conserved "TPG" repeats in the N-terminal region of NIP5;1 is required for the polar localization of NIP5;1 although other region of the N-terminal region contribute to PM localization.

A conserved leucine residue is important for the PM localization but not for polar localization of NIP5;1 and NIP6;1

To clarify the reason of the disappearance of GFP signal caused by the deletion of N-terminal region of NIP5;1, I further explored the potential signal residues involved in this process. The deletion of the whole N-terminal region including three residues "leucine-threonine-arginine (LTR)" from 76 to 78 (ΔN78) but not ΔN75 caused undetectable expression of GFP-NIP5;1 in epidermal cells (Fig. 2.9). Alignment of NIPs sequences showed that, except in NIP7;1, leucine/phenylalanine

(L/F) residue is conserved and at the end of the N-terminus of NIP5;1 and NIP6;1, a arginine residue (R) is present where others have a glutamine residue (Q) (Fig. 2.8). In addition, the serine residue prior to leucine residue is conserved between NIP5;1 and NIP6;1. Based on this comparison, four mutants GFP-NIP5;1 SLTR/AAAA, L76A, S75A/T77A, R78Q were generated and expressed under the control of *NIP5;1* promoter without 5' UTR.

The localization and expression level of GFP-NIP5;1 S75AT77A and R78Q were indistinguishable from wild-type GFP-NIP5;1 in the epidermal cells when observed under confocal microscopy with the same setting (Fig. 2.11). However, the GFP-NIP5;1 SLTR/AAAA as well as L76A showed little signal (Fig.2.11), which were similar to the case of GFP-NIP5;1 ΔN78 (Fig. 2.9). Interestingly, the substitution of leucine 76 with phenylalanine (L76F) kept the PM localization of GFP-NIP5;1 in a polar manner (Fig. 2.11) suggesting the compatible function of phenylalanine and leucine residues .

Next, I tested the possibility that the conserved leucine plays a common role in maintaining PM localization of NIP5;1 and NIP6;1. Indeed, GFP-NIP6;1 L78A was hardly detectable in the epidermal cells (Fig. 2.11), whereas GFP-NIP6;1 L78F showed PM localization in a polar manner (Fig. 2.11). The instability of L to A mutants might be a result of ER-associated protein degradation (ERAD). To test this speculation, I treated the plants expressing GFP-NIP5;1 L76A and GFP-NIP6;1 L78A

with MG132, an inhibitor of the 26S proteasome for 4 h. After the treatment with 50 μM MG132, both mutants showed cytosolic accumulation of GFP signal while they were undetectable under control condition (Fig. 2.12). In contrast, the wild-type controls did not show significant change after the MG132 treatment.

Conserved threonine resides contributes to polar localization of NIP5;1 and NIP6;1

In rice and maize, two orthologs of AtNIP5;1 have been recently reported as boric acid channels (Chatterjee et al., 2014; Durbak et al., 2014; Leonard et al., 2014). Alignment of their N terminal regions showed that they also share the conserved "TPGTPG" sequence (Fig. 2.13). Therefore, I speculated that these conserved sequence commonly determine the polar localization of boric acid channels, although the localization of these two orthologs were not yet known. I first focus on the threonine residues in this conserved sequence because of the potential modification by phosphorylation. I found the vector pNIP5;1 (w/o 5' UTR): sGFP-NIP5;1 (Tanaka et al., 2008) produces stronger level of protein expression than the destination vector pShw18 in root cells (data not shown). Therefore, I utilized the vector (Tanaka et al., 2008) to generate the stronger expression lines for the analysis of contribution of the threonine residues in epidermal and endodermal cells. The phosphomimic mutant GFP-NIP5;1 T18D/T21D/T24D (3T/3D) did not show significant difference from

wild-type GFP-NIP5;1 in root epidermal and endodermal cells (Fig. 2.14 A and B). In contrast, the GFP-NIP5;1 T18A/T21A/T24A (3T/3A) showed non-polar localization at the PM of the epidermal cells (Fig. 2.14 A). This result illustrates the importance of the threonine residues on the polar localization and implies that the phosphorylation status acts as a switch for the localization pattern. Similary, non-polar localization of GFP-NIP5;1 3T/3A was observed in the endodermal cells under control of the native promoter or endodermis-specific promoter from CASP1 (Roppolo et al., 2011) (Fig.2.14 B and C). These results suggest the common mechanism controlling polar localization of NIP5;1 in both epidermal and endodermal cells. Then, the single alanine-substituted mutants were established and their contributions on polar localization of NIP5;1 were investigated. As shown in fig. 2.14 A, each alanine substitution seemed to affect polar localization to different extents. Among these threonine residues, the second (at the position of 21) most likely has a major contribution on polar localization of GFP-NIP5;1. These results suggest that the threonine residues play a role in determining the polar localization at the PM.

Given the importance of conserved threonine residues in polar localization of NIP5;1, I then tested whether the mechanism is common to NIP6;1. GFP-NIP6;1 3T/3A (T15A/T16A/T19A) showed non-polar localization at the PM (Fig. 2.15) as well as GFP-NIP5;1 3T/3A mutant (Fig. 2.14 A). Single point mutations of three conserved threonine residues (at position of 15, 16 and 19) showed polar localization

of GFP-NIP6;1 variants at the PM, although the level of polar localization needs to be analyzed more carefully (Fig. 2.15). These results suggest that they redundantly contribute to polar localization of NIP6;1 and a common mechanism for polar localization of boric acid channels toward soil-side PM.

Phosphorylation of conserved threonine mediates polar localization of NIP5;1

Having shown the remarkable importance of the conserved threonine residues in the polar localization of NIP5;1 and NIP6;1, I postulated that phosphorylation controls polar localization of NIP5;1 and NIP6;1. According to PhosPhAt database (Heazlewood et al., 2008; Durek et al., 2010; Zulawski et al., 2013), these threonine residues are predicted to be phosphorylation sites. To verify the phosphorylation of threonine residues, I first performed immuno-blotting analysis [using NuPAGE gel (Invitrogen, Tokyo)] with a mouse anti-GFP monoclonal antibody and a rabbit anti-pTNIP5;1 polyclonal antibody. The anti-pTNIP5;1 antibody were generated against the artificial NIP5;1 peptide containing the phosphothreonine residues. By the anti-pTNIP5;1 antibody wild-type GFP-NIP5;1 was detected but not after treatment with Calf intestinal alkaline phosphatase (CIAP) (Fig. 2.16 A). Furthermore, GFP-NIP5;1 3T/3A protein was detected by an anti-GFP antibody but not by the anti-pTNIP5;1 antibody. These results suggest that the GFP-NIP5;1 was

phosphorylated at the conserved threonine residues *in vivo*.

Phos-tag gel (Wako Pure Chemical Industries, Osaka) is useful for separating proteins with different phosphorylation status. To confirm the phosphorylation status of GFP-NIP5;1 *in vivo,* I ran the microsomal fraction containing wild-type GFP-NIP5;1 with or without CIAP treatment on the Phos-tag gel and blotted with an anti-GFP antibody. The band of GFP-NIP5;1 was shifted downwards by the CIAP treatment (Fig. 2.16 B). This result indicates NIP5;1 undergoes phosphorylation *in vivo*. In addition, GFP-NIP5;1 3T/3A showed higher mobility than GFP-NIP5;1 wild-type (Fig. 2.16 C), directly support the notion that the PM-localized NIP5;1 is phosphorylated at these conserved threonine residues.

Boron uptake assay of wild type and non-polar version of GFP-NIP5;1 in *Xenopus* oocytes

As a subfamily of plant MIPs, NIP proteins transport a wide range of substrates such as water, glycerol (Dean et al., 1999), lactic acid (Choi and Roberts, 2007), urea (Wallace and Roberts, 2005), and boric acid (Takano et al., 2006). These characteristics of NIPs have been explained based on the sequence similarity of the aromatic/arginine (ar/R) constriction regions (Wallace et al., 2006; Verdoucq et al., 2014). To current understanding, the aromatic/arginine selectivity filter, Asn-Pro-Ala (NPA) motif, and other specificity-determining residues are located in neither N- and

C-terminal region of MIPs (Fu et al., 2000; Sui et al., 2001; Hove and Bhave, 2011; Mitani-Ueno et al., 2011).

The boric acid transport activity of NIP5;1 had been shown in Arabidopsis plant and *Xenopus* oocytes (Takano et al., 2006). To examine whether conservation of threonine residues is important for the B-transport activity of NIP5;1, I performed the boric acid uptake assay in *Xenopus* oocytes by injecting cRNA of GFP-NIP1;2, GFP-NIP5;1, and GFP-NIP5;1 3T/3A. The GFP-tag was used to validate the expression and localization of these proteins in the PM of the oocytes. Identical amount of cRNAs were injected and similar expression levels were observed on the PM of the oocytes. Equal amount of water was injected as a negative control and showed scarcely detectable fluorescence (Fig. 2.17 A).

The injected oocytes were incubated in 5 mM boric acid containing MBS buffer for 30 min and subsequently digested in HNO_3 solution for ICP-MS analysis. GFP-NIP5;1 expressing oocytes accumulated higher B content (0.81 ± 0.11 nmol/oocyte) compared to water injected control and GFP-NIP1;2 expressing oocytes (0.30 ± 0.18 and 0.42 ± 0.15 nmol/oocyte) (Fig. 2.17 B). However, the transport rate by GFP-NIP5;1 was significantly lower than that of previous report (Takano, 2006), possibly because of addition of GFP tag leading to reduced efficiency of activity. As expected, the comparable B accumulation by GFP-NIP5;1 wild-type and 3T/3A was observed (0.81 ± 0.11 versus 0.97 ± 0.03 nmol/oocyte) confirming that no or little

effect of conserved threonine residues on B transport activity of GFP-NIP5;1 in *Xenopus* oocytes (Fig. 2.17 B).

Polar localization of NIP5;1 plays a crucial role in plant growth under low boron conditions

As comparable B-transport activity of GFP-NIP5;1 3T/3A to GFP-NIP5;1 wild-type was observed, I asked whether the polar localization of NIP5;1 plays a crucial role in plant growth under B limitation. I hypothesize that the boric acid uptake activity in stele-side PM by GFP-NIP5;1 3T/3A might play an antagonistic role to BOR1, which export boric acid/borate against concentration gradient toward the center of roots. Thus, non-polar localization of GFP-NIP5;1 will exhibit unfavorable plant growth under low boron conditions.

I investigated the phenotype of transgenic Arabidopsis expressing GFP-NIP5;1 wild-type and 3T/3A mutant in *nip5;1-1* background under B-deficient conditions (Fig. 2.18). Col-0 and *nip5;1-1* were used as controls. At 0.1 μM B condition, 7-day-old *nip5;1-1* plants showed only about 32 (± 6) % of root length relative to Col-0 because of the defect in boric acid uptake (Takano et al., 2006). However, GFP-NIP5;1 wild-type expressing *nip5;1-1* lines showed similar but slightly shorter root length relative to Col-0 [77 (± 8) - 83 (± 8) %] and GFP-NIP5;1 3T/3A expressing lines showed significant reduction of root length relative to Col-0 [43(± 12)

- 59 (± 6) %] (Figs. 2.18, 2.19). At 0.3 µM B, the GFP-NIP5;1 wild-type expressing lines showed similar root length relative to Col-0 [83 (± 14) - 93(± 16) %], which was again longer than that of GFP-NIP5;1 3T/3A expressing lines [57 (± 6) - 74 (± 13) %] (Figs. 2.18, 2.19). At 1.0 µM B condition both GFP-NIP5;1 wild-type and 3T/3A expressing lines showed comparable root length relative to Col-0 [86 (± 19) - 98 (± 6) % and 85 (± 16) - 106 (± 15) %], whereas *nip5;1-1* mutant developed about 54 (± 17) % root length relative to Col-0 (Figs. 2.18, 2.19). Similarly, when grown at 3.0 µM B condition, no significant difference were observed in the root length of GFP-NIP5;1 wild-type and 3T/3A expressing lines compared to Col-0 [99 (± 12) - 101(± 10) % and 98 (± 17) - 110 (± 9) %]. However, the root length of *nip5;1-1* mutant relative to Col-0 remained shorter under the 3.0 µM condition [68 (± 12) %] (Figs. 2.18, 2.19). Taken together, these findings confirmed that the polar localization of NIP5;1 plays a crucial role in plant growth under low B conditions.

Discussion

The N-terminal region of NIP5;1 is involved in protein quality control

In mammalian cells, the N- and C- terminal regions of AQPs play multiple roles in its localization to the apical PM and shuttling between the apical PM and

intracellular vesicles (van Balkom et al., 2004; Noda and Sasaki, 2005). In plant cells, a N-terminal diacidic motif (DIE) was demonstrated to be required for the trafficking of ZmPIP2;4 and ZmPIP2;5 to the PM (Zelazny et al., 2009). ZmPIP1s were shown to be targeted to PM by physical interaction to ZmPIP2s. However, the sorting signal for the PM localization of boric acid channels is not yet known. NIP5;1 and NIP6;1 have similar diacidic signals (D/EXE) in their N-terminal regions (Fig. 2.8), whereas in our transgenic plants, the deleted 17 amino acid residues of the N-terminal region of NIP5;1 did not cause ER retention (Fig. 2.9). To date, there is no evidence indicating that NIP5;1 assembles heterotetramers with other aquaporin proteins. Furthermore, ZmPIP2;1/2;2 do not contain diacidic motif in the similar position, but are able to target to the PM (Hachez et al., 2006). These results point to different ER export mechanisms for aquaporin proteins.

In this study, a leucine (L76) residue at the end of the N-terminal region of NIP5;1 was revealed to be important for PM localization of NIP5;1 and NIP6;1 (Figs. 2.11, 2.12). Alanine substitutions of L76 of NIP5;1 and L78 of NIP6;1 resulted in undetectable level of the GFP fusions. ERAD is an important quality control system, which causes transport of misfolded proteins from ER to cytosol and degradation in the proteasome by an ubiquitination-mediated manner (Meusser et al., 2005; Römisch, 2005). The significant reduction of GFP-NIP5;1 L76A and GFP-NIP6;1 L78A in cells and the appearance of cytosolic fluorescence signal after MG132 treatment (Fig.

2.12) suggested that the reduction was the consequence of ERAD. Similarly, a conserved leucine residue at the center of the first intracellular loop (ICL1) of human G protein-coupled receptors (GPCRs) was previously identified to be required for the export of GPCRs from ER (Duvernay et al., 2009). Importantly, the substitution of the leucine to phenylalaine but not any others were tolerated in the case of GPCRs, this compatible function of phenylalanine was verified in the cases of L76F of NIP5;1 and L78F of NIP6;1 (Fig. 2.11). Considering the conservation of L/F at the end of the N-terminal region of NIP proteins (Fig. 2.8), these results reveal the significance of the L/F residue in NIP proteins to the ER quality control system.

Besides the ERAD quality control system, the defective PM proteins can be monitored by so-called PM quality control to maintain the PM homeostasis (Apaja and Lukacs, 2014). These proteins were downregulated via endocytosis and vacuolar-sorting pathway that is dependent on the ubiquitination. This modification acts as a sorting signal for proteins into multivescicular body (MVB) prior to reaching the vacuole. Deletion of 17 residues from the N-terminus of NIP5;1 induced the dotty signals in the cell, presumably MVBs, and vacuolar GFP accumulation under the dark treatment (Fig. 2.10). These results suggest that the PM-protein quality control system is operating. It needs to be clarified whether the GFP-NIP5;1 ΔN17 is ubiquitinated and transported to MVBs. It can be analyzed by immuno-blotting using anti-ubiquitin antibody and coexpression with MVB marker. Taken together, these

findings support that the N-terminal region of NIP5;1 is involved in two different protein-quality control systems in the ER and in the PM.

The N-terminal region of NIP5;1 is involved in the polar localization in PM

Among most Arabidopsis NIPs, (GFP-) NIP6;1 also showed polar localization toward the soil-side PM in the root epidermal cells (Fig. 2.4). This results is consistent with the evolutional relationship that NIP6;1 is the most similar paralog to NIP5;1 (Maurel, 2007; Tanaka et al ., 2008). In contrast, NIP1;2 was identified as an non-polar NIP in root epidermal cell (Fig. 2.4). NIP1;2 is evolutionally distant from NIP5;1 and NIP6;1, especially in the N- and C-terminal region. Subsequently, the replacement of the N-terminal, C-terminal and central region of NIP5;1 with the corresponding region of NIP1;2 identified the requirement of the N-terminal region of NIP5;1 for the polar localization in the PM (Fig. 2.6). Similar to the case of NIPs family, PINs have highly conserved transmembrane domains and have a diverged hydrophilic loop (HL) of varying lengths (Křeček et al., 2009; Ganguly et al., 2012). The long HL-type PINs (PIN1-4, 6 and 7) consistently localize at the PM in various tissues and showed distinct apical/basal polar localization (Grunewald and Friml, 2010; Ganguly et al., 2012), while shorter HL-type PINs (PIN5 and 8) localize at internal compartment, mainly the ER (Mravec et al., 2009; Ganguly et al., 2010;

Bosco et al., 2012; Ding et al., 2012). The intracellular retention of shorter HL-type PINs might be attributed to the lack of molecular cue that mediates trafficking to the PM. Indeed, a chimera construct PIN5:PIN2-HL resulted in the PM targeting although it failed to localize in a polar manner in the PM (Ganguly et al., 2014). In contrast, the N-terminal region of NIP5;1 was able to sort other non-polar aquaporin proteins such as NIP1;2 and PIP2;1 to the soil-side PM (Fig. 2.7). I propose that the N-terminal region of NIP5;1 is a useful tool to genetically modify the localization pattern of PM proteins toward the soil-side PM.

Phosphorylation mediates the polar localization of boric acid channels

Phosphorylation is critical for the polar localization of many PM proteins in various organisms (Offringa and Huang, 2013; Tejos et al., 2014). The "TPG" repeat sequence is highly conserved in the long N-terminal region of NIP5;1 and NIP6;1 and their homologs in rice and maize. Phosphomimic and dephosphorylating mutation of NIP5;1 resulted in distinct localization in the epidermal and endodermal cells (Figs. 2.14), highlighting the crucial role of phosphorylation on the polar localization of NIP5;1. In agreement with this, polar localization of NIP6;1 also requires the conserved threonine residues evidenced by the non-polar localization of GFP-NIP6;1 3T/3A in the epidermal cells (Fig. 2.15). Immuno-blotting using Phos-tag gel and an

antibody specific to phosphorylated NIP5;1 verified that NIP5;1 is phosphorylated *in vivo* at the threonine residues (Fig. 2.16). These findings revealed the fact that phosphorylation mediates the polar localization of NIP5;1.

In the case of PINs, the polar localization in the PM is a dynamic process, which is dependent on the phosphorylation level of proteins. The kinases, PID and WAGs coordinately phosphorylate the PIN proteins to mediate apical polar localization, whereas the protein phosphatase 2A (PP2A) antagonistically acts on phosphorylated PIN proteins to mediate basal polar localization (Friml et al., 2004; Nuhse et al., 2004; Galván-Ampudia and Offringa, 2007; Michniewicz et al., 2007; Cheng et al., 2008; Dhonukshe et al., 2010). In order to redirect auxin flow during phototropism or gravitropism, PIN3 can switch its localization in the PM toward the stele-side or gravisensing-side in different cell types (Kleine-Vehn et al., 2010; Ding et al., 2011). The phosphorylation of NIP5;1 seems to be independent of B conditions since the polar localization of NIP5;1 was not affected in response to high-B conditions (Takano et al., 2010). A question arising is why aspartate was not evolutionally selected instead of threonine. One possible explanation is that the localization pattern is regulated in different tissues. NIP6;1 was localized in the phloem companion cells, phloem parenchyma cells, and sieve elements in stem nodes (Tanaka et al., 2008). Although it needs further elucidation, the localization of GFP-NIP6;1 in these cells seems to be non-polar. An important role of NIP6;1 have been revealed to be in

preferential transport of B to sink tissues in shoots. NIP6;1 in stem nodes was suggested to be involved in xylem-phloem transfer of B by taking up B into the phloem companion/parenchyma cells and directly into sieve elements. Polar localization of NIP6;1 might not be required for these processes. The threonine residues might provide flexibility to control of polar/non-polar localization of boric acid channels by phosphorylation levels in various tissues.

Since localization patterns of the rice ortholog OsNIP3;1 and maize ortholog ZmNIP3;1 are at present not known, further studies are needed to examine whether this phosphorylation of conserved threonine residues extends to their orthologs. In addition to the conserved "TPG" repeats sequence, other similar sequence is present in N-terminal region of NIP6;1 ("STPSTPA"), OsNIP3;1 ("SSPxxxxSAP"), and ZmNIP3;1 ("STPxxxSAP") (Fig. 2.13). The roles of these sequences in phosphorylation-mediated polar localization remain to be examined.

Mechanisms for the polar localization of boric acid channels

I revealed that the phosphorylation mediates polar localization of boric acid channels. However, the mechanisms in which phosphorylation affect polar localization remain unclear. In epidermal cells upon BFA treatment, BOR1 accumulated in intracellular aggregation and lost its polar localization, while NIP5;1 as well as other soil-side PM localized proteins showed only little accumulation in the

intracellular aggregation and normal polar localization (Langowski et al., 2010; Takano et al., 2010). BFA has been used as an inhibitor for recycling of PM localized proteins by inhibiting ARF-GEFs including GNOM (Steinmann et al., 1999, Geldner et al., 2003). Recent study indicated that GNOM is localized mainly to Golgi and indirectly acts on the basal recycling pathway (Naramoto et al., 2014). A proposed model for the localization of PINs is that the phosphorylation level plays a key role in entering into the GNOM-dependent basal recycling pathway or the GNOM-independent apical targeting pathway (Offringa and Huang, 2013; Luschnig and Vert, 2014). Similar to the apically localized PINs, the soil-side PM localized proteins did not change their localization in the PM in the *gnom* mutants (Langowski et al., 2010). Despite lack of direct evidence that polar localization of NIP5;1 is independent of GNOM activity, I presume that the polar localization of NIP5;1 can be established by at least two possible pathways. One possibility is that NIP5;1 follows a GNOM-independent recycling pathway which establishes its polar localization. The phosphorylation may enhance the affinity of NIP5;1 to a specific recycling pathway from other PM domains to the soil-side domain (transcytosis) or between the soil-side PM domain and endosomes closely located (localized recycling). The other possibility is polar secretion of NIP5;1 which is phosphorylated at the secretory pathway. To test this hypothesis, the phosphorylation level of NIP5;1 in different membrane compartments needs to be examined. Immunochemical approaches using

the anti-phospho-threonine antibody would be suitable for this purpose.

The next direction of my research is the identification of the gene encoding kinase that specifically modify the threonine residues in NIP5;1 and NIP6;1. It is a challenge since enormous number of genes encoding kinases presents in *Arabidopsis thaliana* genome. Although the "TPX" sequence were found in the "TPRXS(N/S)" motif of PINs, it is unlikely that the PID kinase is responsible for phosphorylation of NIP5;1 since the serine but not the threonine in "TPRXS(N/S)" motif is the phosphorylation site by PID (Michniewicz et al., 2007; Huang et al., 2010). A mitogen-activated protein kinase (MAPKs) preferably phosphorylates substrate with serine/threonine residues prior to proline residue within the substrate recognition consensus motif "ΨXS/TP", where Ψ represents proline or an aliphatic amino acid (Clark-Lewis et al., 1991; Pearson et al., 2001; Liu and Zhang, 2004). The "TPG" repeat sequences in NIP5;1 and NIP6;1 is consistent with the target motif of MAPKs pointing to the potential candidate in this MAPKs family. Considering the functional redundancy of homologs, RNA interference of multiple genes encoding kinases including MAPKs would help in the identification. The identification and characterization of responsible kinases should extend the basis of mechanisms of polar localization toward soli-side in plant cells.

Polar localization of NIP5;1 is crucial for plant growth

Boron uptake and transport are dependent on the boric acid channels and exporters (Takano et al., 2008). Although the NIP5;1 promoter is preferentially expressed in epidermal cells, it also expressed the GFP fusions in the endodermal cells (Fig. 2.14B). The data in this thesis support that NIP5;1 takes up boric acid from the soil-side PM of epidermal and endodermal cells. Because the presence of the apoplastic barrier Casparian strip, the polar uptake of B by NIP5;1 in endodermis is supposed important for plant B loading into the stele under B limitation. In this study, I found that polar localization of NIP5;1 is altered both in epidermal and endodermal cells by substituting threonine residues to alanine. These GFP-NIP5;1 3T/3A expressing lines showed reduced growth compared to GFP-NIP5;1 wild-type expressing lines in *nip5;1-1* background under low B conditions (Figs. 2.18, 2.19). These results indicated the crucial role played by the polar localization of NIP5;1 in plant growth. It remains unclear how non-polar localization of the NIP5;1 mutant affected boron accumulation and root growth under low boron conditions. One possibility is that non-polar NIP5;1 also forms channel toward the stele-side PM which results in antagonistic action with BOR1 exporter under B limitation. Consequently, non-polar GFP-NIP5;1 expressing lines could transport fewer B toward center of roots.

The polar localization of an iron transporter IRT1 toward the soil-side PM was observed under metal-depleted conditions (Barberon et al., 2014). The plants overexpressing FYVE1, a phosphatidylinositol-3-phosphate-binding protein caused non-polar localization of IRT1 in the epidermal cells and were hypersensitive to low iron conditions (Barberon et al., 2014). These results suggested that the polar localization of IRT1 plays a crucial role in metal homeostasis. However, in this experiment, the side effect of FYVE1 overexpression was not excluded. FYVE1 can directly bind to ubiquitin and become a component of the endosomal sorting complex for transport (ESCRT) which capture ubiquitinated cargos in the endosomal membrane (Gao et al., 2014). To my knowledge, my work highlights the role of polar localization of transport proteins in plant growth for the first time by directly modifying the transport protein itself. This work will be a foundation for understanding the mechanisms of polar localization of PM proteins and the application in improvement of plant tolerance to mineral stresses.

Reference

Alassimone J, Naseer S, Geldner N (2010) A developmental framework for endodermal differentiation and polarity. Proc Natl Acad Sci U S A **107**: 5214–5219

Alonso JM, Stepanova AN, Leisse TJ, Kim CJ, Chen H, Shinn P, Stevenson DK, Zimmerman J, Barajas P, Cheuk R, et al (2003) Genome-wide insertional mutagenesis of Arabidopsis thaliana. Science (80-) **301**: 653–657

Andeme-Onzighi C, Sivaguru M, Judy-March J, Baskin TI, Driouich A (2002) The reb1-1 mutation of Arabidopsis alters the morphology of trichoblasts, the expression of arabinogalactan-proteins and the organization of cortical microtubules. Planta **215**: 949–958

Apaja PM, Lukacs GL (2014) Protein homeostasis at the plasma membrane. Physiology (Bethesda) **29**: 265–277

Van Balkom BWM, Graat MPJ, van Raak M, Hofman E, van der Sluijs P, Deen PMT (2004) Role of cytoplasmic termini in sorting and shuttling of the aquaporin-2 water channel. Am J Physiol Cell Physiol **286**: C372–C379

Barber C, Rosti J, Rawat A, Findlay K, Roberts K, Seifert GJ, Rösti J, Rawat A, Findlay K, Roberts K, et al (2006) Distinct properties of the five UDP-D-glucose/UDP-D-galactose 4-epimerase isoforms of Arabidopsis thaliana. J Biol Chem **281**: 17276–17285

Barberon M, Dubeaux G, Kolb C, Isono E, Zelazny E, Vert G (2014) Polarization of IRON-REGULATED TRANSPORTER 1 (IRT1) to the plant-soil interface plays crucial role in metal homeostasis. Proc Natl Acad Sci U S A **111**: 8293–8298

Baskin TI, Betzner AS, Hoggart R, Cork A, Williamson RE (1992) Root morphology mutants in Arabidopsis thaliana. Funct Plant Biol **19**: 427–437

Baum TJ, Wubben MJ, Hardyy KA, Su H, Rodermel SR (2000) A Screen for Arabidopsis thaliana Mutants with Altered Susceptibility to Heterodera schachtii. J Nematol **32**: 166–173

Benjamins R, Quint A, Weijers D, Hooykaas P, Offringa R (2001) The PINOID protein kinase regulates organ development in Arabidopsis by enhancing polar auxin transport. Development **128**: 4057–4067

Bennett M, Berleth T, Benfey P, Benkova E, Ju G, Geldner N, Grebe M, Heisler M, Heja J (2006) Apical – basal polarity : why plant cells don ' t stand on their heads. Trends Plant Sci **11**: 12–14

Bienert GP, Bienert MD, Jahn TP, Boutry M, Chaumont F (2011) Solanaceae XIPs are plasma membrane aquaporins that facilitate the transport of many uncharged substrates. Plant J **66**: 306–317

Bosco CD, Dovzhenko A, Liu X, Woerner N, Rensch T, Eismann M, Eimer S, Hegermann J, Paponov I a., Ruperti B, et al (2012) The endoplasmic reticulum localized PIN8 is a pollen-specific auxin carrier involved in intracellular auxin homeostasis. Plant J **71**: 860–870

Brandizzi F, Wasteneys GO (2013) Cytoskeleton-dependent endomembrane organization in plant cells: An emerging role for microtubules. Plant J **75**: 339–349

Brown PH, Bellaloui N, Wimmer MA, Bassil ES, Ruiz J, Hu H, Pfeffer H, Dannel F, Römheld V (2002) Boron in plant biology. Plant Biol **4**: 205–223

Camacho-Cristóbal JJ, Rexach J, González-Fontes A (2008) Boron in Plants: Deficiency and Toxicity. J Integr Plant Biol **50**: 1247–1255

Cárdenas L, Lovy-Wheeler A, Kunkel JG, Hepler PK (2008) Pollen tube growth oscillations and intracellular calcium levels are reversibly modulated by actin polymerization. Plant Physiol **146**: 1611–1621

Chanoca A, Otegui MS (2014) Immunogold labeling and electron tomography of plant endosomes. Methods Mol Biol **1209**: 63–80

Chatterjee M, Tabi Z, Galli M, Malcomber S, Buck A, Muszynski M, Gallavotti A (2014) The Boron Efflux Transporter ROTTEN EAR Is Required for Maize Inflorescence Development and Fertility. Plant Cell **26**: 2962–2977

Cheng Y, Qin G, Dai X, Zhao Y (2008) NPY genes and AGC kinases define two key steps in auxin-mediated organogenesis in Arabidopsis. Proc Natl Acad Sci **105**: 21017–21022

Choi WG, Roberts DM (2007) Arabidopsis NIP2;1, a Major Intrinsic Protein Transporter of Lactic Acid Induced by Anoxic Stress. J Biol Chem **282**: 24209–24218

Clark-Lewis I, Sanghera JS, Pelech SL (1991) Definition of a consensus sequence for peptide substrate recognition by p44mpk, the meiosis-activated myelin basic protein kinase. J Biol Chem **266**: 15180–15184

Clough SJ, Bent AF (1998) Floral dip: a simplified method for Agrobacterium-mediated transformation of Arabidopsis thaliana. Plant J **16**: 735–743

Cutler SR, Ehrhardt DW, Griffitts JS, Somerville CR (2000) Random GFP::cDNA fusions enable visualization of subcellular structures in cells of Arabidopsis at a high frequency. Proc Natl Acad Sci **97**: 3718–3723

Danielson JÅH, Johanson U (2008) Unexpected complexity of the aquaporin gene family in the moss Physcomitrella patens. BMC Plant Biol **8**: 45

Dean RM, Rivers RL, Zeidel ML, Roberts DM (1999) Purification and functional reconstitution of soybean nodulin 26. An aquaporin with water and glycerol transport properties. Biochemistry **38**: 347–353

Dell B, Huang LB (1997) Physiological response of plants to low boron. Plant Soil **193**: 103–120

Dettmer J, Hong-Hermesdorf A, Stierhof Y-D, Schumacher K (2006) Vacuolar H+-ATPase activity is required for endocytic and secretory trafficking in Arabidopsis. Plant Cell **18**: 715–730

Dhonukshe P, Grigoriev I, Fischer R, Tominaga M, Robinson DG, Hasek J, Paciorek T, Petrásek J, Seifertová D, Tejos R, et al (2008) Auxin transport inhibitors impair vesicle motility and actin cytoskeleton dynamics in diverse eukaryotes. Proc Natl Acad Sci U S A **105**: 4489–4494

Dhonukshe P, Huang F, Galvan-Ampudia CS, Mähönen AP, Kleine-Vehn J, Xu J, Quint A, Prasad K, Friml J, Scheres B (2010) Plasma membrane-bound AGC3 kinases phosphorylate PIN auxin carriers at TPRXS (N/S) motifs to direct apical PIN recycling. Development **137**: 3245–3255

Ding Z, Galván-Ampudia CS, Demarsy E, Łangowski Ł, Kleine-Vehn J, Fan Y, Morita MT, Tasaka M, Fankhauser C, Offringa R (2011) Light-mediated polarization of the PIN3 auxin transporter for the phototropic response in Arabidopsis. Nat Cell Biol **13**: 447–452

Ding Z, Wang B, Moreno I, Duplakova N, Simon S, Carraro N, Reemmer J, Pencik A, Chen X, Tejos R, et al (2012) ER-localized auxin transporter PIN8 regulates auxin homeostasis and male gametophyte development in Arabidopsis. Nat Commun **3**: 941

Dordas C, Chrispeels MJ, Brown PH (2000) Permeability and channel-mediated transport of boric acid across membrane vesicles isolated from squash roots. Plant Physiol **124**: 1349

Durbak AR, Phillips KA, Pike S, O'Neill MA, Mares J, Gallavotti A, Malcomber ST, Gassmann W, McSteen P (2014) Transport of Boron by the tassel-less1 Aquaporin Is Critical for Vegetative and Reproductive Development in Maize. Plant Cell **26**: 2978–2995

Durek P, Schmidt R, Heazlewood JL, Jones A, MacLean D, Nagel A, Kersten B, Schulze WX (2010) PhosPhAt: the Arabidopsis thaliana phosphorylation site database. An update. Nucleic Acids Res **38**: D828–D834

Duvernay MT, Dong C, Zhang X, Robitaille M, Hébert TE, Wu G (2009) A single conserved leucine residue on the first intracellular loop regulates ER export of G protein-coupled receptors. Traffic **10**: 552–566

Ebine K, Okatani Y, Uemura T, Goh T, Shoda K, Niihama M, Morita MT, Spitzer C, Otegui MS, Nakano A, et al (2008) A SNARE complex unique to seed plants is required for protein storage vacuole biogenesis and seed development of Arabidopsis thaliana. Plant Cell **20**: 3006–3021

Fleischer A, O'Neill MA, Ehwald R (1999) The pore size of non-graminaceous plant cell walls is rapidly decreased by borate ester cross-linking of the pectic polysaccharide rhamnogalacturonan II. Plant Physiol **121**: 829–838

French AP, Mills S, Swarup R, Bennett MJ, Pridmore TP (2008) Colocalization of fluorescent markers in confocal microscope images of plant cells. Nat Protoc **3**: 619–628

Friml J, Vieten A, Sauer M, Weijers D, Schwarz H, Hamann T, Offringa R, Jurgens G (2003) Efflux-dependent auxin gradients establish the apical-basal axis of Arabidopsis. Nature 426:

Friml J, Yang X, Michniewicz M, Weijers D, Quint A, Tietz O, Benjamins R, Ouwerkerk PBF, Ljung K, Sandberg G, et al (2004) A PINOID-dependent binary switch in apical-basal PIN polar targeting directs auxin efflux. Science **306**: 862–865

Fu D, Libson A, Miercke LJW, Weitzman C, Nollert P, Krucinski J, Stroud RM (2000) Structure of a Glycerol-Conducting Channel and the Basis for Its Selectivity. Science (80-) **290**: 481–486

Galván-Ampudia CS, Offringa R (2007) Plant evolution: AGC kinases tell the auxin tale. Trends Plant Sci **12**: 541–547

Gälweiler L, Guan C, Müller A, Wisman E, Mendgen K, Yephremov A, Palme K (1998) Regulation of polar auxin transport by AtPIN1 in Arabidopsis vascular tissue. Science (80-) **282**: 2226

Ganguly A, Lee SH, Cho M, Lee OR, Yoo H, Cho H-T (2010) Differential auxin-transporting activities of PIN-FORMED proteins in Arabidopsis root hair cells. Plant Physiol **153**: 1046–1061

Ganguly A, Park M, Kesawat MS, Cho HT (2014) Functional Analysis of the Hydrophilic Loop in Intracellular Trafficking of Arabidopsis PIN-FORMED Proteins. Plant Cell **26**: 1570–1585

Ganguly A, Sasayama D, Cho HT (2012) Regulation of the polarity of protein trafficking by phosphorylation. Mol Cells **33**: 423–430

Gao C, Luo M, Zhao Q, Yang R, Cui Y, Zeng Y, Xia J, Jiang L (2014) A unique plant ESCRT component, FREE1, regulates multivesicular body protein sorting and plant growth. Curr Biol **24**: 2556–2563

Geldner N, Anders N, Wolters H, Keicher J, Kornberger W, Muller P, Delbarre A, Ueda T, Nakano A, Jürgens G (2003) The Arabidopsis GNOM ARF-GEF mediates endosomal recycling, auxin transport, and auxin-dependent plant growth. Cell **112**: 219–230

Geldner N, Dénervaud-Tendon V, Hyman DL, Mayer U, Stierhof YD, Chory J (2009) Rapid, combinatorial analysis of membrane compartments in intact plants with a multicolor marker set. Plant J **59**: 169–178

Gomord V, Denmat L-AA, Fitchette-Lainé A-CC, Satiat-Jeunemaitre B, Hawes C, Faye L (1997) The C-terminal HDEL sequence is sufficient for retention of secretory proteins in the endoplasmic reticulum (ER) but promotes vacuolar targeting of proteins that escape the ER. Plant J **11**: 313–325

Grebe M, Xu J, Möbius W, Ueda T, Nakano A, Geuze HJ, Rook MB, Scheres B (2003) Arabidopsis Sterol Endocytosis Involves Actin-Mediated Trafficking via ARA6-Positive Early Endosomes. Curr Biol **13**: 1378–1387

Grunewald W, Friml J (2010) The march of the PINs: developmental plasticity by dynamic polar targeting in plant cells. EMBO J **29**: 2700–2714

Gupta AB, Sankararamakrishnan R (2009) Genome-wide analysis of major intrinsic proteins in the tree plant Populus trichocarpa: characterization of XIP subfamily of aquaporins from evolutionary perspective. BMC Plant Biol **9**: 134

Hachez C, Moshelion M, Zelazny E, Cavez D, Chaumont F (2006) Localization and quantification of plasma membrane aquaporin expression in maize primary root: a clue to understanding their role as cellular plumbers. Plant Mol Biol **62**: 305–323

Hanaoka H, Uraguchi S, Takano J, Tanaka M, Fujiwara T (2014) OsNIP3;1, a rice boric acid channel, regulates boron distribution and is essential for growth under boron-deficient conditions. Plant J **78**: 890–902

Heazlewood JL, Durek P, Hummel J, Selbig J, Weckwerth W, Walther D, Schulze WX (2008) PhosPhAt: a database of phosphorylation sites in Arabidopsis thaliana and a plant-specific phosphorylation site predictor. Nucleic Acids Res **36**: D1015–D1021

Hove RM, Bhave M (2011) Plant aquaporins with non-aqua functions: deciphering the signature sequences. Plant Mol Biol **75**: 413–430

Huang F, Zago MK, Abas L, van Marion A, Galván-Ampudia CS, Offringa R (2010) Phosphorylation of conserved PIN motifs directs Arabidopsis PIN1 polarity and auxin transport. Plant Cell **22**: 1129–1142

Ishii T, Matsunaga T (1996) Isolation and characterization of a boron-rhamnogalacturonan-II complex from cell walls of sugar beet pulp. Carbohydr Res **284**: 1–9

Ishii T, Matsunaga T, Pellerin P, O'Neill MA, Darvill A, Albersheim P (1999) The plant cell wall polysaccharide rhamnogalacturonan II self-assembles into a covalently cross-linked dimer. J Biol Chem **274**: 13098–13104

Iwai H, Hokura A, Oishi M, Chida H, Ishii T, Sakai S, Satoh S (2006) The gene responsible for borate cross-linking of pectin Rhamnogalacturonan-II is required for plant reproductive tissue development and fertilization. Proc Natl Acad Sci U S A **103**: 16592–16597

Iwai H, Masaoka N, Ishii T, Satoh S (2002) A pectin glucuronyltransferase gene is essential for intercellular attachment in the plant meristem. Proc Natl Acad Sci U S A **99**: 16319–16324

Kleine-Vehn J, Dhonukshe P, Sauer M, Brewer PB, Wiśniewska J, Paciorek T, Benková E, Friml J (2008) ARF GEF-dependent transcytosis and polar delivery of PIN auxin carriers in Arabidopsis. Curr Biol **18**: 526–531

Kleine-Vehn J, Ding Z, Jones AR, Tasaka M, Morita MT, Friml J (2010) Gravity-induced PIN transcytosis for polarization of auxin fluxes in gravity-sensing root cells. Proc Natl Acad Sci U S A **107**: 22344–22349

Kleine-Vehn J, Wabnik K, Martiniere A, Langowski L, Willig K, Naramoto S, Leitner J, Tanaka H, Jakobs S, Robert S, et al (2011) Recycling, clustering, and endocytosis jointly maintain PIN auxin carrier polarity at the plasma membrane. Mol Syst Biol **7**: 540

Kobae Y, Sekino T, Yoshioka H, Nakagawa T, Martinoia E, Maeshima M (2006) Loss of AtPDR8, a plasma membrane ABC transporter of Arabidopsis thaliana, causes hypersensitive cell death upon pathogen infection. Plant Cell Physiol **47**: 309–318

Kobayashi M, Kouzu N, Inami A, Toyooka K, Konishi Y, Matsuoka K, Matoh T (2011) Characterization of Arabidopsis CTP:3-deoxy-D-manno-2-octulosonate cytidylyltransferase (CMP-KDO synthetase), the enzyme that activates KDO during rhamnogalacturonan II biosynthesis. Plant Cell Physiol **52**: 1832–1843

Kobayashi M, Matoh T, Azuma JI (1996) Two chains of rhamnogalacturonan II are cross-linked by borate-diol ester bonds in higher plant cell walls. Plant Physiol **110**: 1017–1020

Kouchi H, Kumazawa K (1976) Anatomical responses of root tips to boron deficiency: III. Effect of boron deficiency on sub-cellular structure of root tips, particularly on morphology of cell wall and its related organelles. Soil Sci Plant Nutr **22**: 53–71

Křeček P, Skůpa P, Libus J, Naramoto S, Tejos R, Friml J, Zažímalová E (2009) The PIN-FORMED (PIN) protein family of auxin transporters. Genome Biol **10**: 249

Kremer JR, Mastronarde DN, McIntosh JR (1996) Computer visualization of three-dimensional image data using IMOD. J Struct Biol **116**: 71–76

Langowski L, Ruzicka K, Naramoto S, Kleine-Vehn J, Friml J (2010) Trafficking to the outer polar domain defines the root-soil interface. Curr Biol **20**: 904–908

Leonard A, Holloway B, Guo M, Rupe M, Yu G, Beatty M, Zastrow-Hayes G, Meeley R, Llaca V, Butler K, et al (2014) tassel-less1 encodes a boron channel protein required for inflorescence development in maize. Plant Cell Physiol **55**: 1044–1054

Li T, Choi W-G, Wallace IS, Baudry J, Roberts DM (2011) Arabidopsis thaliana NIP7;1: An Anther-Specific Boric Acid Transporter of the Aquaporin Superfamily Regulated by an Unusual Tyrosine in Helix 2 of the Transport Pore. Biochemistry **50**: 6633–6641

Liu Y, Zhang S (2004) Phosphorylation of 1-aminocyclopropane-1-carboxylic acid synthase by MPK6, a stress-responsive mitogen-activated protein kinase, induces ethylene biosynthesis in Arabidopsis. Plant Cell **16**: 3386–3399

Loomis WD, Durst RW (1992) Chemistry and biology of boron. Biofactors **3**: 229

Luschnig C, Vert G (2014) The dynamics of plant plasma membrane proteins: PINs and beyond. Development **141**: 2924–2938

Luu D-T, Martinière A, Sorieul M, Runions J, Maurel C (2012) Fluorescence recovery after photobleaching reveals high cycling dynamics of plasma membrane aquaporins in Arabidopsis roots under salt stress. Plant J **69**: 894–905

Ma JF, Tamai K, Yamaji N, Mitani N, Konishi S, Katsuhara M, Ishiguro M, Murata Y, Yano M (2006) A silicon transporter in rice. Nature **440**: 688–691

Ma JF, Yamaji N, Mitani N, Tamai K, Konishi S, Fujiwara T, Katsuhara M, Yano M (2007) An efflux transporter of silicon in rice. Nature **448**: 209–212

Matoh T, Ishigaki K, Mizutani M, Matsunaga W, Takabe K (1992) Boron nutrition of cultured tobacco BY-2 cells I. Requirement for and intracellular localization of boron and selection of cells that tolerate low levels of boron. Plant cell Physiol **33**: 1135–1141

Matoh T, Ishigaki K, Ohno K, Azuma J (1993) Isolation and characterization of a boron-polysaccharide complex from radish roots. Plant cell Physiol **34**: 639–642

Maurel C (2007) Plant aquaporins: Novel functions and regulation properties. FEBS Lett **581**: 2227–2236

Meusser B, Hirsch C, Jarosch E, Sommer T (2005) ERAD: the long road to destruction. Nat Cell Biol **7**: 766–772

Michniewicz M, Zago MK, Abas L, Weijers D, Schweighofer A, Meskiene I, Heisler MG, Ohno C, Zhang J, Huang F, et al (2007) Antagonistic regulation of PIN phosphorylation by PP2A and PINOID directs auxin flux. Cell **130**: 1044–1056

Mitani-Ueno N, Yamaji N, Zhao FJ, Ma JF (2011) The aromatic/arginine selectivity filter of NIP aquaporins plays a critical role in substrate selectivity for silicon, boron, and arsenic. J Exp Bot **62**: 4391–4398

Mizutani M, Watanabe S, Nakagawa T, Maeshima M (2006) Aquaporin NIP2;1 is mainly localized to the ER membrane and shows root-specific accumulation in Arabidopsis thaliana. Plant Cell Physiol **47**: 1420–1426

Mravec J, Skůpa P, Bailly A, Hoyerová K, Krecek P, Bielach A, Petrásek J, Zhang J, Gaykova V, Stierhof Y-D, et al (2009) Subcellular homeostasis of phytohormone auxin is mediated by the ER-localized PIN5 transporter. Nature **459**: 1136–1140

Nakagawa T, Suzuki T, Murata S, Nakamura S, Hino T, Maeo K, Tabata R, Kawai T, Tanaka K, Niwa Y, et al (2007) Improved Gateway binary vectors: high-performance vectors for

creation of fusion constructs in transgenic analysis of plants. Biosci Biotechnol Biochem **71**: 2095–2100

Naramoto S, Otegui MS, Kutsuna N, de Rycke R, Dainobu T, Karampelias M, Fujimoto M, Feraru E, Miki D, Fukuda H, et al (2014) Insights into the localization and function of the membrane trafficking regulator GNOM ARF-GEF at the Golgi apparatus in Arabidopsis. Plant Cell **26**: 3062–3076

Nelson BK, Cai X, Nebenfuhr A (2007) A multicolored set of in vivo organelle markers for co-localization studies in Arabidopsis and other plants. Plant J **51**: 1126–1136

Noda Y, Sasaki S (2005) Trafficking mechanism of water channel aquaporin-2. Biol Cell **97**: 885–892

Noguchi K, Dannel F, Pfeffer H, R mheld V, Hayashi H, Fujiwara T (2000) Defect in root-shoot translocation of boron in Arabidopsis thaliana mutant bor1-1. J Plant Physiol **156**: 751–755

Nuhse TS, Stensballe A, Jensen ON, Peck SC (2004) Phosphoproteomics of the Arabidopsis plasma membrane and a new phosphorylation site database. Plant Cell **16**: 2394–2405

O'Neill MA, Eberhard S, Albersheim P, Darvill AG (2001) Requirement of borate cross-linking of cell wall rhamnogalacturonan II for Arabidopsis growth. Science (80-) **294**: 846

O'Neill MA, Warrenfeltz D, Kates K, Pellerin P, Doco T, Darvill AG, Albersheim P (1996) Rhamnogalacturonan-II, a Pectic Polysaccharide in the Walls of Growing Plant Cell, Forms a Dimer That Is Covalently Cross-linked by a Borate Ester in vitro conditions for the formation and hydrolysis of the dimer. J Biol Chem **271**: 22923–22930

Offringa R, Huang F (2013) Phosphorylation-dependent trafficking of plasma membrane proteins in animal and plant cells. J Integr Plant Biol **55**: 789–808

Otegui MS, Herder R, Schulze J, Jung R, Staehelin LA (2006) The proteolytic processing of seed storage proteins in Arabidopsis embryo cells starts in the multivesicular bodies. Plant Cell **18**: 2567–2581

Park W, Scheffler BE, Bauer PJ, Campbell BT (2010) Identification of the family of aquaporin genes and their expression in upland cotton (Gossypium hirsutum L.). BMC Plant Biol **10**: 142

Pearson G, Robinson F, Beers Gibson T, Xu BE, Karandikar M, Berman K, Cobb MH (2001) Mitogen-activated protein (MAP) kinase pathways: regulation and physiological functions. Endocr Rev **22**: 153–183

Petruccelli S, Otegui MS, Lareu F, Tran Dinh O, Fitchette AC, Circosta A, Rumbo M, Bardor M, Carcamo R, Gomord V, et al (2006) A KDEL-tagged monoclonal antibody is efficiently retained in the endoplasmic reticulum in leaves, but is both partially secreted and sorted to protein storage vacuoles in seeds. Plant Biotechnol J **4**: 511–527

Pound MP, French AP, Atkinson JA, Wells DM, Bennett MJ, Pridmore T (2013) RootNav: navigating images of complex root architectures. Plant Physiol **162**: 1802–1814

Preston GM, Carroll TP, Guggino WB, Agre P (1992) Appearance of water channels in Xenopus oocytes expressing red cell CHIP28 protein. Science **256**: 385–387

Rahman A, Bannigan A, Sulaman W, Pechter P, Blancaflor EB, Baskin TI (2007) Auxin, actin and growth of the Arabidopsis thaliana primary root. Plant J **50**: 514–528

Reinhardt D, Pesce E-R, Stieger P, Mandel T, Baltensperger K, Bennett M, Traas J, Friml J, Kuhlemeier C (2003) Regulation of phyllotaxis by polar auxin transport. Nature **426**: 255–260

Reiter W-D, Vanzin GF (2001) Molecular genetics of nucleotide sugar interconversion pathways in plants. Plant Cell Walls. Springer, pp 95–113

Rivera-Serrano EE, Rodriguez-Welsh MF, Hicks GR, Rojas-Pierce M (2012) A small molecule inhibitor partitions two distinct pathways for trafficking of tonoplast intrinsic proteins in Arabidopsis. PLoS One **7**: e44735

Robinson DG, Scheuring D, Naramoto S, Friml J (2011) ARF1 localizes to the golgi and the trans-golgi network. Plant Cell **23**: 846–850

Römisch K (2005) Endoplasmic reticulum-associated degradation. Annu Rev Cell Dev Biol **21**: 435–456

Roppolo D, De Rybel B, Tendon VD, Pfister A, Alassimone J, Vermeer JEM, Yamazaki M, Stierhof Y-D, Beeckman T, Geldner N (2011) A novel protein family mediates Casparian strip formation in the endodermis. Nature **473**: 380–383

Rost B, Casadio R, Fariselli P, Sander C (1995) Transmembrane helices predicted at 95% accuracy. Protein Sci **4**: 521–533

Rösti J, Barton CJ, Albrecht S, Dupree P, Pauly M, Findlay K, Roberts K, Seifert GJ (2007) UDP-glucose 4-epimerase isoforms UGE2 and UGE4 cooperate in providing UDP-galactose for cell wall biosynthesis and growth of Arabidopsis thaliana. Plant Cell **19**: 1565–1579

Ruzicka K, Strader LC, Bailly A, Yang H, Blakeslee J, Langowski L, Nejedlá E, Fujita H, Itoh H, Syono K, et al (2010) Arabidopsis PIS1 encodes the ABCG37 transporter of auxinic compounds including the auxin precursor indole-3-butyric acid. Proc Natl Acad Sci U S A **107**: 10749–10753

Ryden P, Sugimoto-Shirasu K, Smith AC, Findlay K, Reiter W-D, McCann MC (2003) Tensile properties of Arabidopsis cell walls depend on both a xyloglucan cross-linked microfibrillar network and rhamnogalacturonan II-borate complexes. Plant Physiol **132**: 1033–1040

Sade N, Vinocur BJ, Diber A, Shatil A, Ronen G, Nissan H, Wallach R, Karchi H, Moshelion M (2009) Improving plant stress tolerance and yield production: is the tonoplast aquaporin SlTIP2; 2 a key to isohydric to anisohydric conversion? New Phytol **181**: 651–661

Schiefelbein J, Somerville C (1990) Genetic Control of Root Hair Development in Arabidopsis thaliana. Plant Cell **2**: 235–243

Seifert GJ, Barber C, Wells B, Dolan L, Roberts K (2002) Galactose Biosynthesis in Arabidopsis: Genetic Evidence for Substrate Channeling from UDP-D-Galactose into Cell Wall Polymers. Curr Biol **12**: 1840–1845

Shelden MC, Howitt SM, Kaiser BN, Tyerman SD (2009) Identification and functional characterisation of aquaporins in the grapevine, Vitis vinifera. Funct Plant Biol **36**: 1065–1078

Shorrocks VM (1997) The occurrence and correction of boron deficiency. Plant Soil **193**: 121–148

Stein M, Dittgen J, Sánchez-Rodríguez C, Hou B-H, Molina A, Schulze-Lefert P, Lipka V, Somerville S (2006) Arabidopsis PEN3/PDR8, an ATP binding cassette transporter, contributes to nonhost resistance to inappropriate pathogens that enter by direct penetration. Plant Cell **18**: 731–746

Steinmann T, Geldner N, Grebe M, Mangold S, Jackson CL, Paris S, Gälweiler L, Palme K, Jürgens G (1999) Coordinated polar localization of auxin efflux carrier PIN1 by GNOM ARF GEF. Science (80-) **286**: 316–318

Stierhof YD, El Kasmi F (2010) Strategies to improve the antigenicity, ultrastructure preservation and visibility of trafficking compartments in Arabidopsis tissue. Eur J Cell Biol **89**: 285–297

Strader LC, Bartel B (2009) The Arabidopsis PLEIOTROPIC DRUG RESISTANCE8/ABCG36 ATP binding cassette transporter modulates sensitivity to the auxin precursor indole-3-butyric acid. Plant Cell **21**: 1992–2007

Sui H, Han B-G, Lee JK, Walian P, Jap BK (2001) Structural basis of water-specific transport through the AQP1 water channel. Nature **414**: 872–878

Takano J, Miwa K, Fujiwara T (2008) Boron transport mechanisms: collaboration of channels and transporters. Trends Plant Sci **13**: 451–457

Takano J, Noguchi K, Yasumori M, Kobayashi M, Gajdos Z, Miwa K, Hayashi H, Yoneyama T, Fujiwara T (2002) Arabidopsis boron transporter for xylem loading. Nature **420**: 337–340

Takano J, Tanaka M, Toyoda A, Miwa K, Kasai K, Fuji K, Onouchi H, Naito S, Fujiwara T (2010) Polar localization and degradation of Arabidopsis boron transporters through distinct trafficking pathways. Proc Natl Acad Sci U S A **107**: 5220–5225

Takano J, Wada M, Ludewig U, Schaaf G, von Wirén N, Fujiwara T (2006) The Arabidopsis major intrinsic protein NIP5;1 is essential for efficient boron uptake and plant development under boron limitation. Plant Cell **18**: 1498–1509

Tamura K, Shimada T, Kondo M, Nishimura M, Hara-Nishimura I (2005) KATAMARI1/MURUS3 Is a novel golgi membrane protein that is required for endomembrane organization in Arabidopsis. Plant Cell **17**: 1764–1776

Tanaka M, Takano J, Chiba Y, Lombardo F, Ogasawara Y, Onouchi H, Naito S, Fujiwara T (2011) Boron-dependent degradation of NIP5;1 mRNA for acclimation to excess boron conditions in Arabidopsis. Plant Cell **23**: 3547–3559

Tanaka M, Wallace IS, Takano J, Roberts DM, Fujiwara T (2008) NIP6;1 is a boric acid channel for preferential transport of boron to growing shoot tissues in Arabidopsis. Plant Cell **20**: 2860–2875

Tejos R, Sauer M, Vanneste S, Palacios-Gomez M, Li H, Heilmann M, van Wijk R, Vermeer JE, Heilmann I, Munnik T, et al (2014) Bipolar Plasma Membrane Distribution of Phosphoinositides and Their Requirement for Auxin-Mediated Cell Polarity and Patterning in Arabidopsis. Plant Cell **26**: 2114–2128

Uehara M, Wang S, Kamiya T, Shigenobu S, Yamaguchi K, Fujiwara T, Naito S, Takano J (2014) Identification and characterization of an arabidopsis mutant with altered localization of NIP5;1, a plasma membrane boric acid channel, reveals the requirement for d-galactose in endomembrane organization. Plant Cell Physiol **55**: 704–714

Uemura T, Kim H, Saito C, Ebine K, Ueda T, Schulze-Lefert P, Nakano A (2012) Qa-SNAREs localized to the trans-Golgi network regulate multiple transport pathways and extracellular disease resistance in plants. Proc Natl Acad Sci **109**: 1784–1789

Uemura T, Ueda T (2014) Plant vacuolar trafficking driven by RAB and SNARE proteins. Curr Opin Plant Biol **22**: 116–121

Verdoucq L, Rodrigues O, Martinière A, Luu DT, Maurel C (2014) Plant aquaporins on the move: reversible phosphorylation, lateral motion and cycling. Curr Opin Plant Biol **22**: 101–107

Viotti C, Bubeck J, Stierhof Y-D, Krebs M, Langhans M, van den Berg W, van Dongen W, Richter S, Geldner N, Takano J, et al (2010) Endocytic and secretory traffic in Arabidopsis merge in the trans-Golgi network/early endosome, an independent and highly dynamic organelle. Plant Cell **22**: 1344–1357

Voxeur A, Fry SC (2014) Glycosylinositol phosphorylceramides from Rosa cell cultures are boron-bridged in the plasma membrane and form complexes with rhamnogalacturonan II. Plant J **79**: 139–149

Wallace IS, Choi W-G, Roberts DM (2006) The structure, function and regulation of the nodulin 26-like intrinsic protein family of plant aquaglyceroporins. Biochim Biophys Acta - Biomembr **1758**: 1165–1175

Wallace IS, Roberts DM (2005) Distinct transport selectivity of two structural subclasses of the nodulin-like intrinsic protein family of plant aquaglyceroporin channels. Biochemistry **44**: 16826–16834

Yin Y, Huang J, Gu X, Bar-Peled M, Xu Y (2011) Evolution of plant nucleotide-sugar interconversion enzymes. PLoS One **6**: e27995

Zelazny E, Miecielica U, Borst JW, Hemminga MA, Chaumont F (2009) An N-terminal diacidic motif is required for the trafficking of maize aquaporins ZmPIP2;4 and ZmPIP2;5 to the plasma membrane. Plant J **57**: 346–355

Zulawski M, Braginets R, Schulze WX (2013) PhosPhAt goes kinases--searchable protein kinase target information in the plant phosphorylation site database PhosPhAt. Nucleic Acids Res **41**: D1176–D1184

Figures

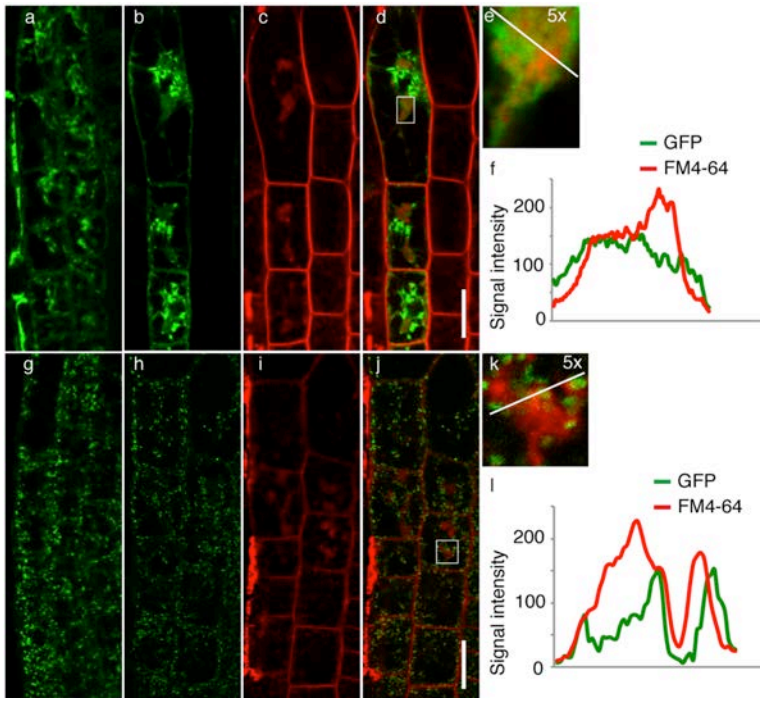

Figure 1.1 Localization of an endoplasmic reticulum marker and Golgi marker in root epidermal cells of the *uge4* mutant. ER-GFP (**a-f**) and YFP-Got1p homolog (**g-l**) in the wild-type (**a, g**) and *uge4* mutant (**b-e, h-k**) cells were imaged. Plant roots were stained with FM4-64 for 30-40 min (**c, i**). Merged GFP and FM4-64 images are shown (**d, e, j, k**). White rectangles in **d** and **j** are five-fold enlargements (**e and k)** and were used for the correlation coefficient analysis (PSC coefficients shown in text). Lines in **e** and **k** were used for the plot profile analysis (**f and l**). Scale bars = 20 μm. Enlarged images in a-d and g-j are shown in Fig. S1 a-d and e-h, respectively.

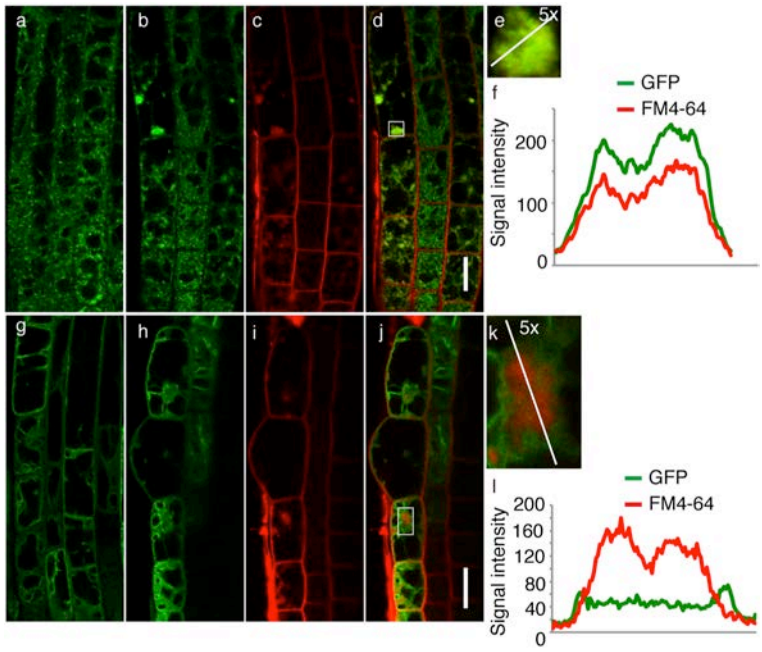

Figure 1.2 Localization of the MVB/LEs marker and the vacuolar membrane marker in *uge4* mutant root epidermal cells. GFP-VAMP727 (**a-f**) and γ-TIP-GFP (**g-l**) in wild-type (**a, g**) and *uge4* mutant cells (**b-e, h-k**) were imaged. Plant roots were stained with FM4-64 for 30-40 min (**c, i**). Merged images of GFP and FM4-64 are shown (**d, e, j, k**). White rectangles in **d** and **j** are five-fold enlargements (**e and k)** and used for correlation coefficient analysis (PSC coefficients shown in text). Lines in e and k are used for plot profile analysis (**f and l**). Scale bars = 20 μm. Enlarged images in a-d and g-j are shown in Fig. S1 i-l and m-p, respectively.

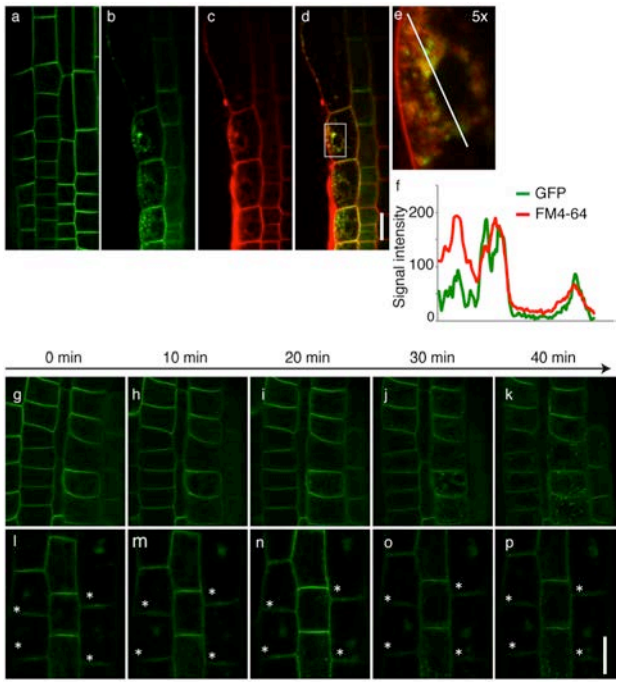

Figure 1.3 Localization and vacuolar trafficking of BOR1-GFP in root epidermal cells of the *uge4* mutant. BOR1-GFP localization under low-boron (3 μM B) conditions in the wild-type (**a**) and *uge4* mutant (**b-e**). Intracellular aggregates containing BOR1-GFP were observed in the *uge4* mutant (**b-d**). Plant roots were stained with FM4-64 for 30-40 min (**c-e**). White rectangles in **d** are fivefold enlargements (**e)** and used for correlation coefficient analysis (PSC coefficients shown in text). A line in **e** is used for plot profile analysis (**f**). Trafficking of BOR1-GFP after shifting from a low B condition (0.6 μM) to a high B condition (500 μM) in the wild-type (g-k) and *uge4* mutant (l-p). Asterisks indicate cells with aggregates. Scale bars = 20 μm. Enlarged images in a-d are shown in Fig. S1 q-t.

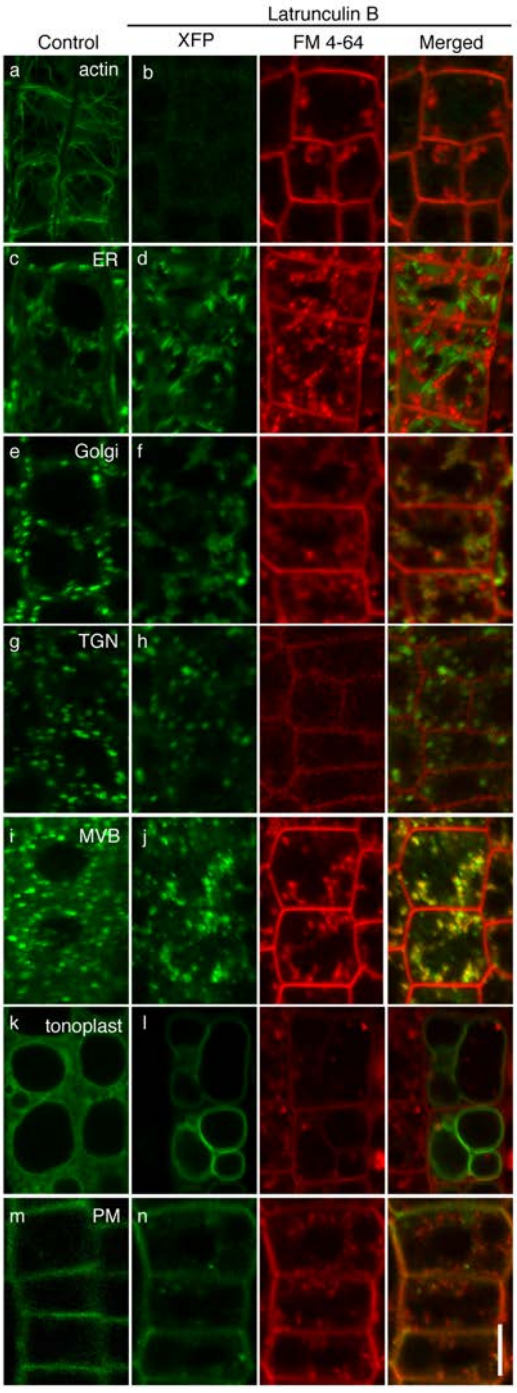

Figure 1.4 Effects of disruption of actin polymerization on the localization of endomembrane markers. Endomembrane markers in the wild-type background were imaged after treatment with 10 μM of latrunculin B. DMSO (0.1 %) was used as a control. FM 4-64 was employed to label intracellular aggregates. Lifeact-Venus (**a, b**), ER-GFP (**c, d**), YFP-Got1p homolog (**e, f**), YFP-VTl12 (**g, h**), GFP-VAMP727 (**i, j**), γ-TIP-GFP (**k, l**), and BOR1-GFP (**m, n**) were used. Scale bar = 20 μm.

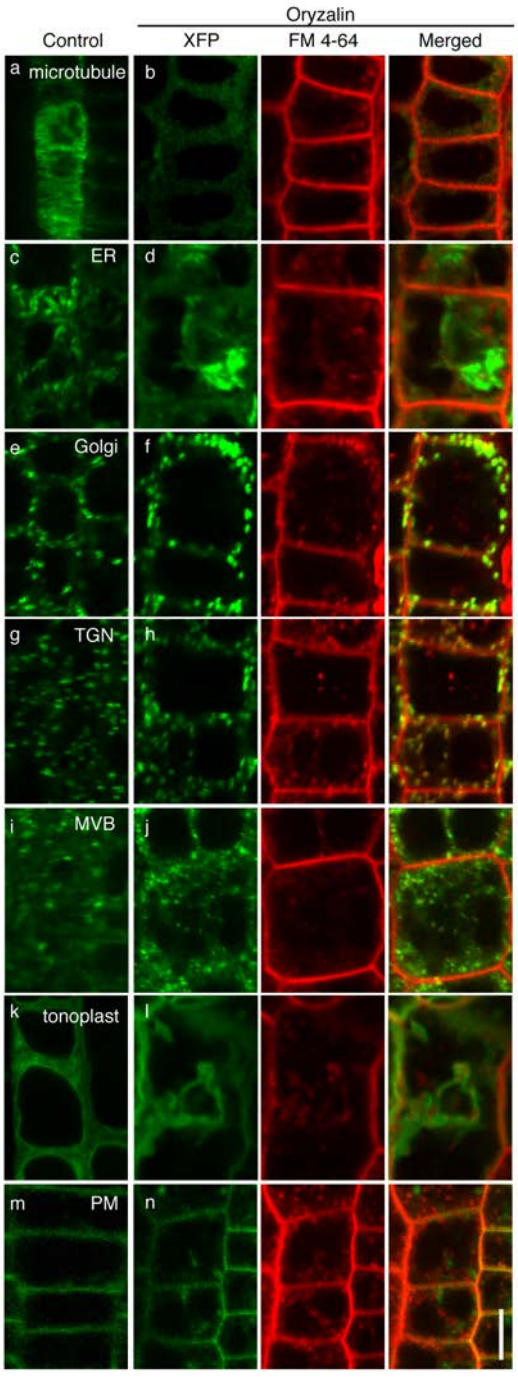

Figure 1.5 Effects of disrupting microtubule polymerization on localization of endomembrane markers. Endomembrane markers in the wild-type background were imaged after treatment with 10 µM oryzalin. DMSO (0.1%) was used as a control. FM 4-64 was employed to label intracellular aggregates. GFP-TUB (**a, b**), ER-GFP (**c, d**), YFP-Got1p homolog (**e, f**), YFP-VTl12 (**g, h**), GFP-VAMP727 (**i, j**), g-TIP-GFP (**k, l**) and BOR1-GFP (**m, n**) were used. Scale bar = 20 µm.

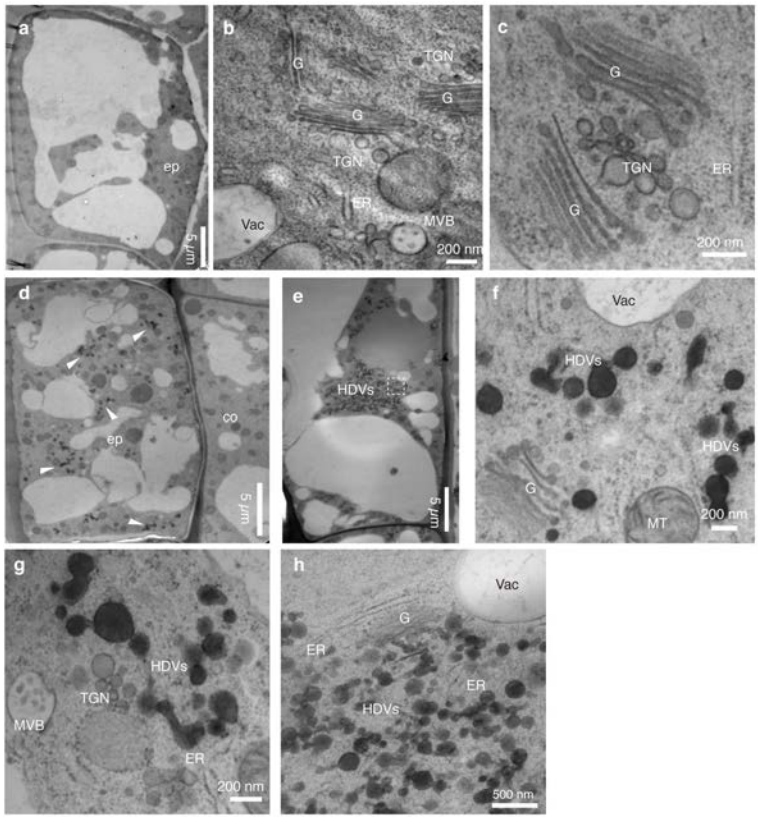

Figure 1.6 Ultrastructure analysis of elongating epidermal cells of the *uge4* mutant. Electron micrographs of elongating epidermal cells of the wild-type (**a-c**) and the *uge4* mutant roots (**d-h**). The cells of the *uge4* mutant develop abnormal high-electron-density vesicles (HDVs) in the cytoplasm (d and e, white arrowhead in **d**). HDVs are closely located to TGN/EEs (**g, h**). An enlarged image of the region indicated by a rectangle (e) is shown in (h). G: Golgi; TGN: *trans*-Golgi network; ER: endoplasmic reticulum; MT: mitochondrion; MVB: multivesicle body; Vac: vacuole; HDVs: high-electron-density vesicles; co: cortex cells; ep: epidermal cells.

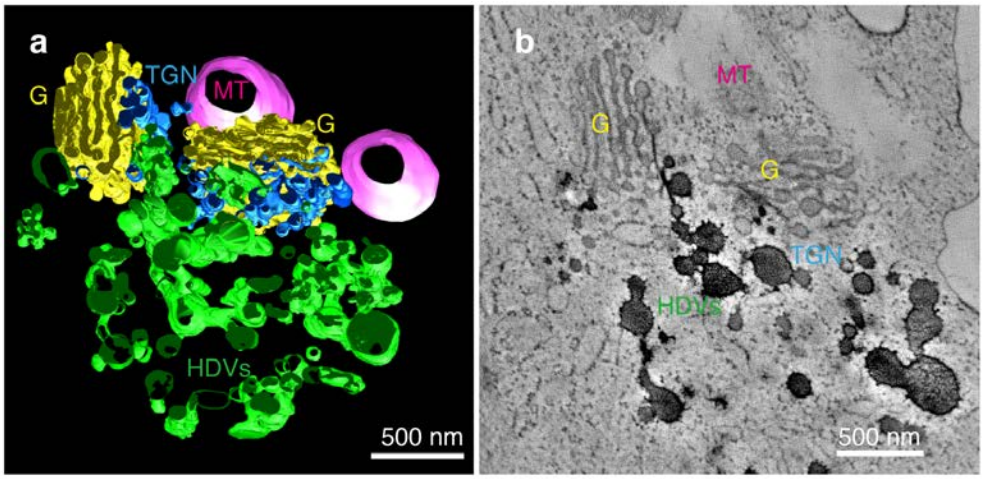

Figure 1.7 Electron tomography analysis of high-electron-density vesicles in root epidermal cells of the *uge4* mutant. An ultrathin section (~300 nm thickness) was imaged at 10,000× from +60.0° to −60.0° at 1.0° intervals. A 3D-model processed by IMOD software (**a**) and a tomographic slice (**b**) were selected to represent the spatial interconnection of the high-density vesicles (HDVs). Sequential images are shown in a Supplemental movie. G: Golgi; TGN: *trans*-Golgi network; MT: mitochondrion; HDVs: high-electron-density vesicles.

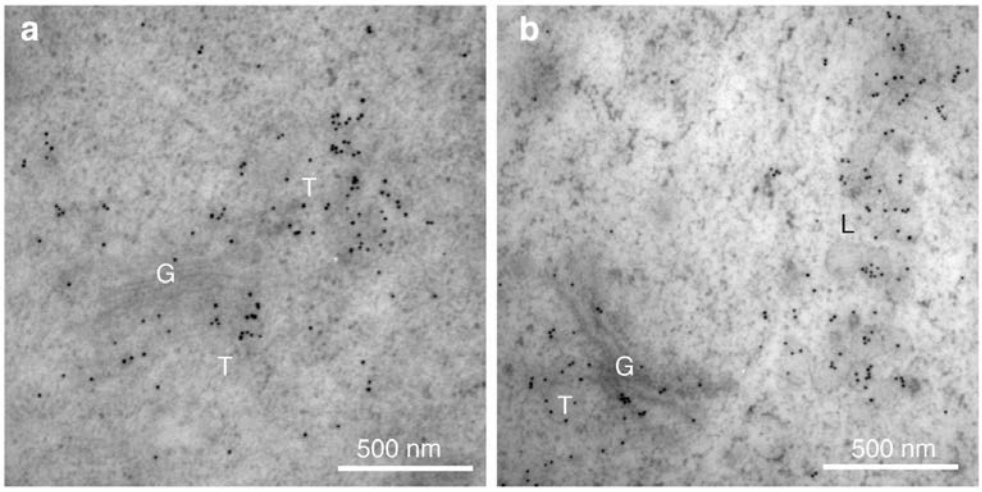

Figure 1.8 Immuno-electron microscopy of the ARF1 protein in *uge4* mutant root epidermal cells. An anti-ARF1 antibody and 10-nm gold-conjugated secondary antibody were used for the immunogold analysis. The Golgi stacks and the TGNs in wild-type cells were labeled with 10-nm gold particles (**a**). Besides the Golgi and the TGN, large vesicles were also labeled in the *uge4* mutant (**b**). T: *trans*-Golgi network; G: Golgi; L: large vesicles.

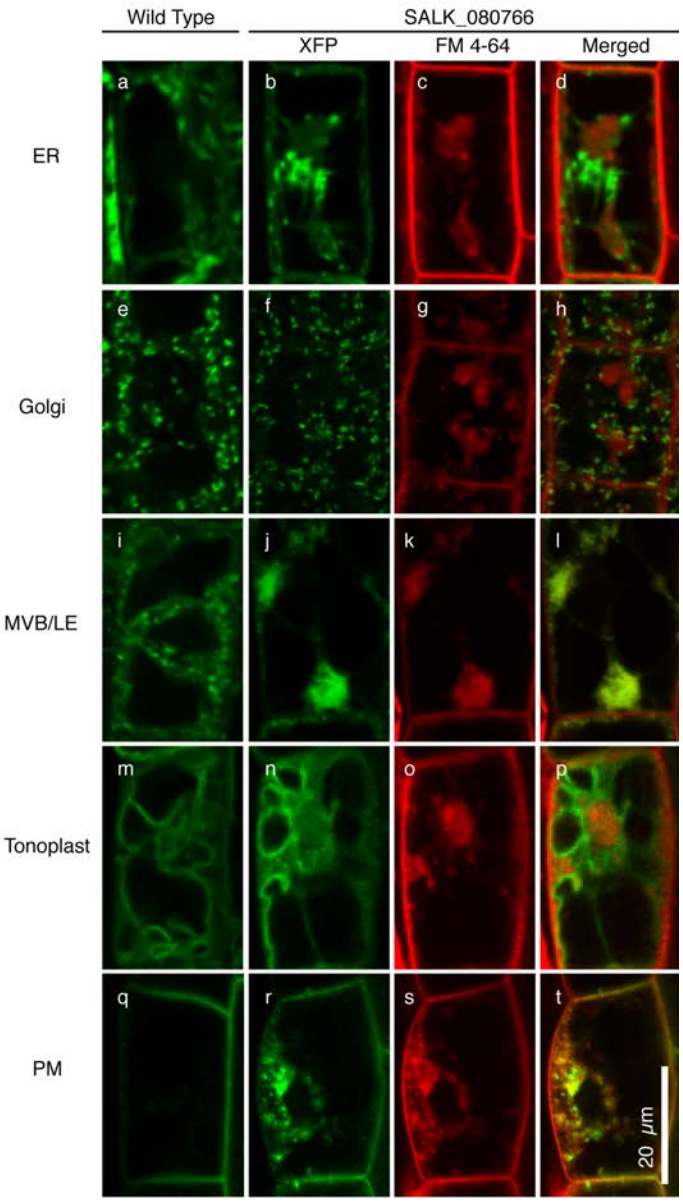

Figure S1 Localization of various markers in root epidermal cells of the *uge4* mutant. ER-GFP in the wild-type (**a**) and *uge4* mutant (**b-d**), YFP-Got1p homolog in the wild-type (**e**) and *uge4* mutant (**f-h**), GFP-VAMP727 in the wild-type (**i**) and *uge4* mutant (**j-l**), g-TIP-GFP in the wild-type (**m**) and *uge4* mutant (**n-p**), and BOR1-GFP in the wild-type (**q**) and *uge4* mutant (**r-t**). Plant roots were stained with FM4-64 for 30-40 min prior to image with confocal microscopy.

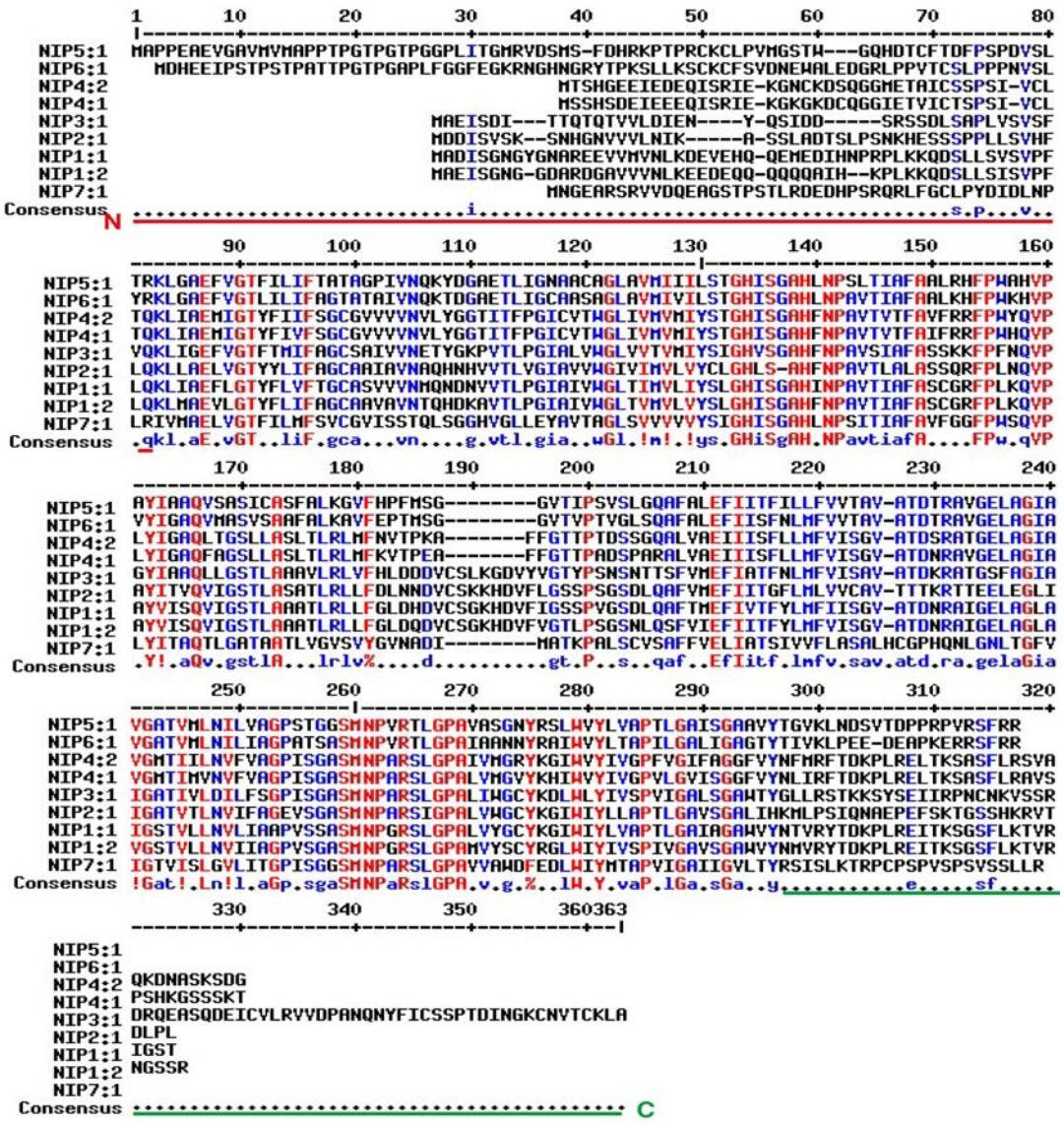

Figure 2.1 Alignment of amino acid sequences of NIPs. The alignment was performed using ClustalW2 (http://www.ebi.ac.uk/Tools/msa/clustalw2/). The N- and C-terminal regions were indicated by the red and green lines at the bottom of sequences, respectively.

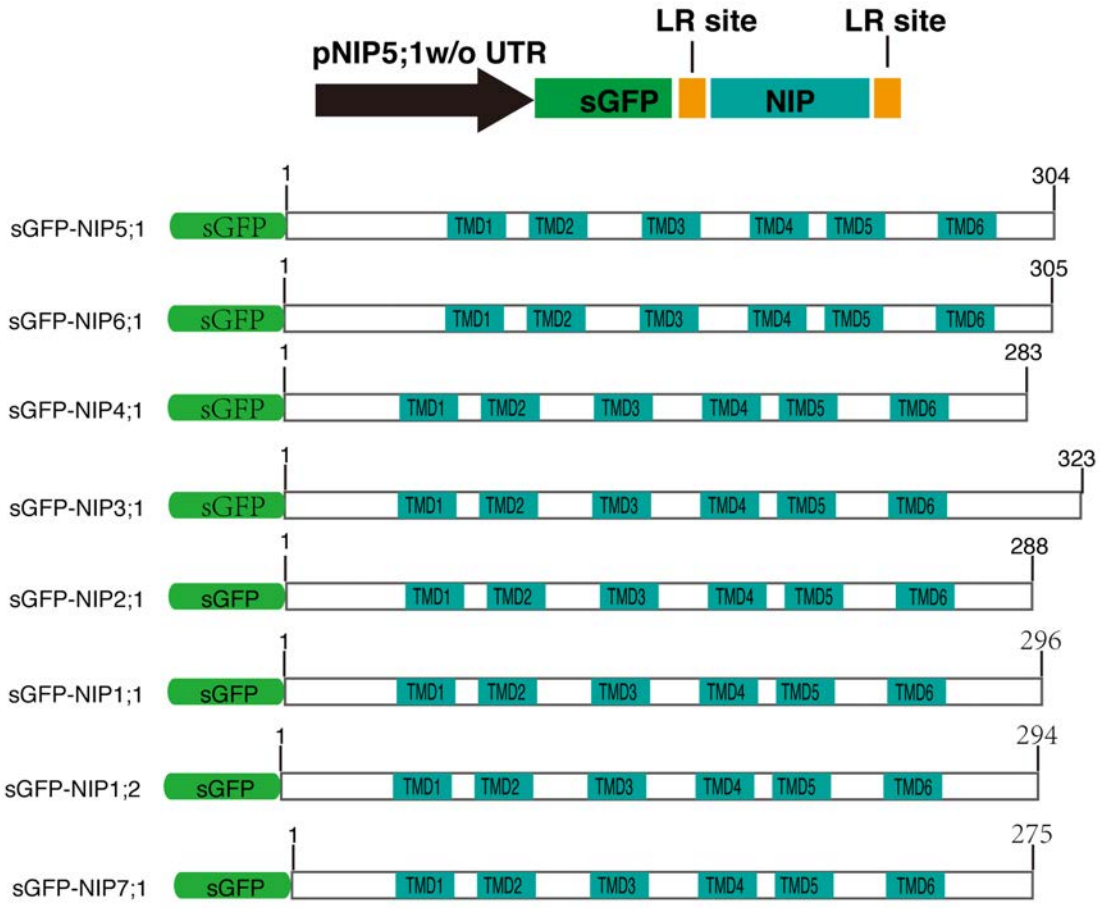

Figure 2.2 Expression vector and structure of NIPs. Eight NIP sequences were subcloned into a Gateway destination vector pShw18, which contains sGFP to fuse N-terminus of NIPs. sGFP-fused NIPs were expressed under the control of NIP5;1 promoter without the 5' UTR.

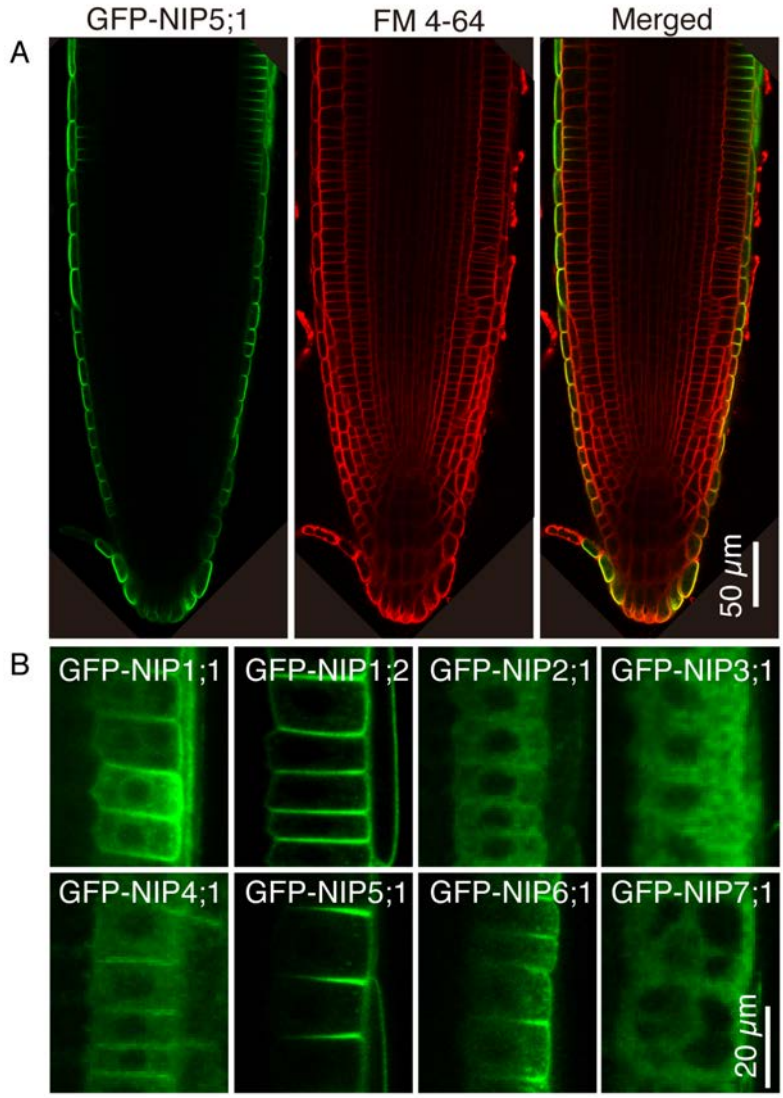

Figure 2.3 Localization of NIPs in root epidermal cells of Arabidopsis. sGFP-fused NIPs were expressed under the control of *NIP5;1* promoter without 5'UTR. Root tips were stained with 4 μM FM4-64 for 30 min before observation. Longitudinal view of roots tip region (A) and epidermal cells at the transition zone (B) of 3-5 days old plants are shown.

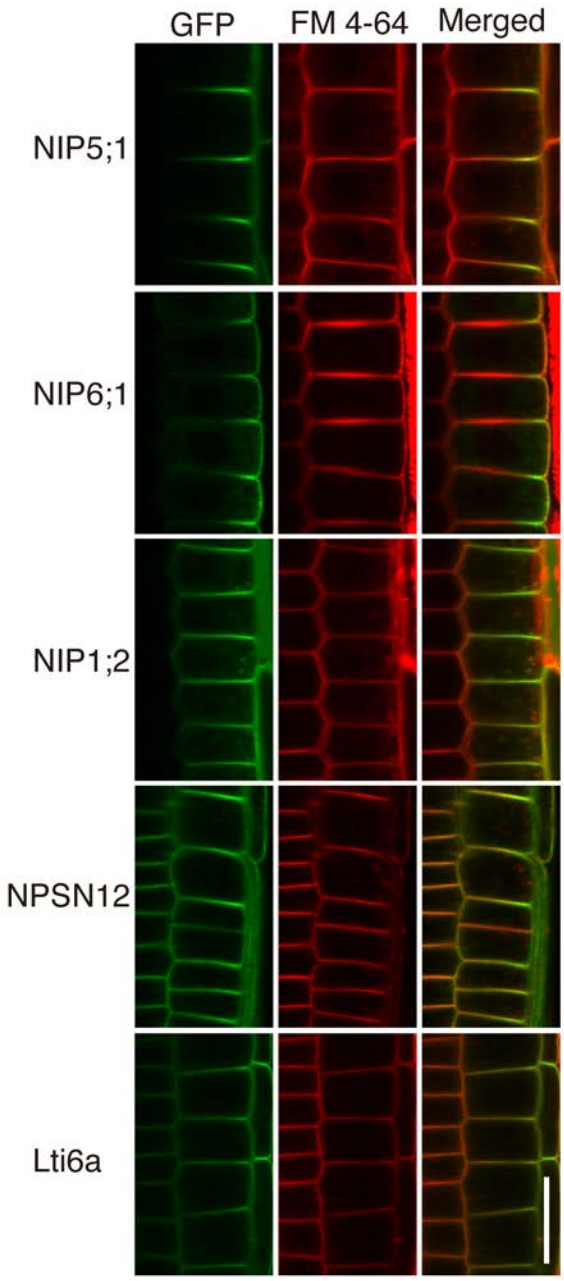

Figure 2.4 Identification of NIP1;2 as a non-polar localized NIP. Root tips were stained with 4 μM FM4-64 for 30 min before imaging. Longitudinal view of the root epidermal cells in the transition zone are shown. EYFP-NPSN12 and EGFP-Lti6a were used as PM non-polar controls in epidermal cells. Scale bar = 20 μm.

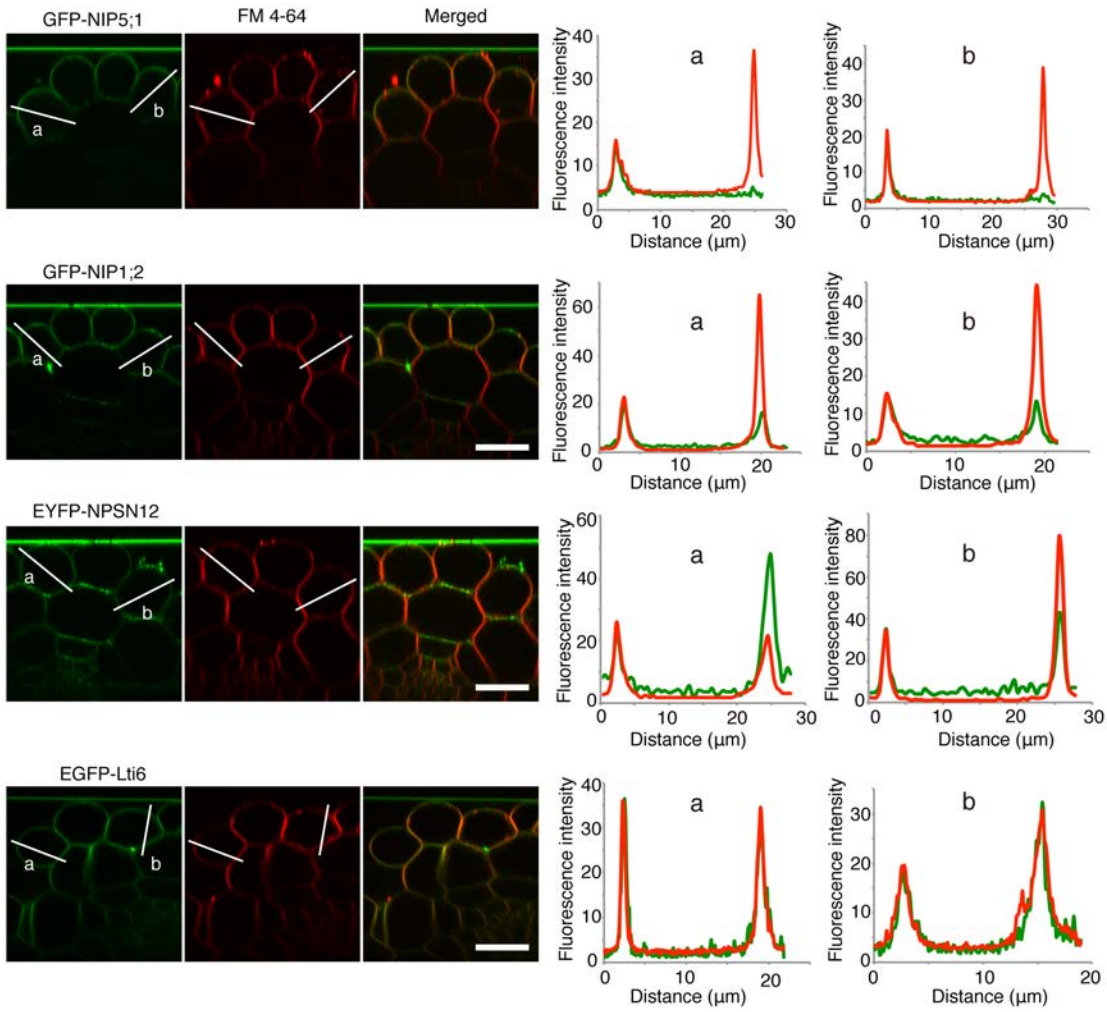

Figure 2.5 Cross-sectional view and plot profile analysis of GFP fusions in epidermal cells. Confocal imaging was performed on root elongation zone with the xzy scanning mode using galvanometric driven z-stage (SuperZ, Leica). FM4-64 was used to stain plasma membrane 30 minutes prior to imaging. Plot profiles indicate the distribution of fluorescence intensity of GFP (green) and FM 4-64 (red) along lines from soil-side to stele-side indicated (white lines). Scale bars = 20 μm.

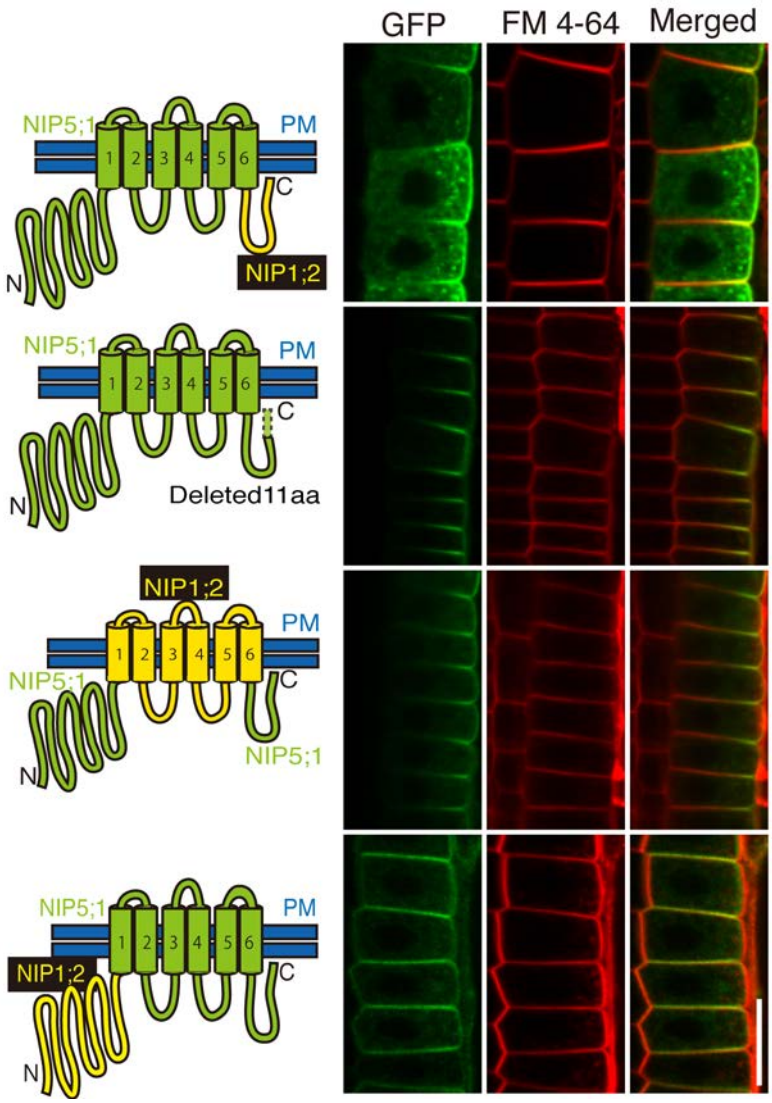

Figure 2.6 N-terminal region of NIP5;1 is required for its polar localization. Chimera constructs (illustrations) were generated by swapping corresponding sequence between *NIP1;2* and *NIP5;1* and expressed as GFP fusions in root epidermal cells. FM 4-64 was used to stain the PM in a uniform way. Scale bar = 20 μm.

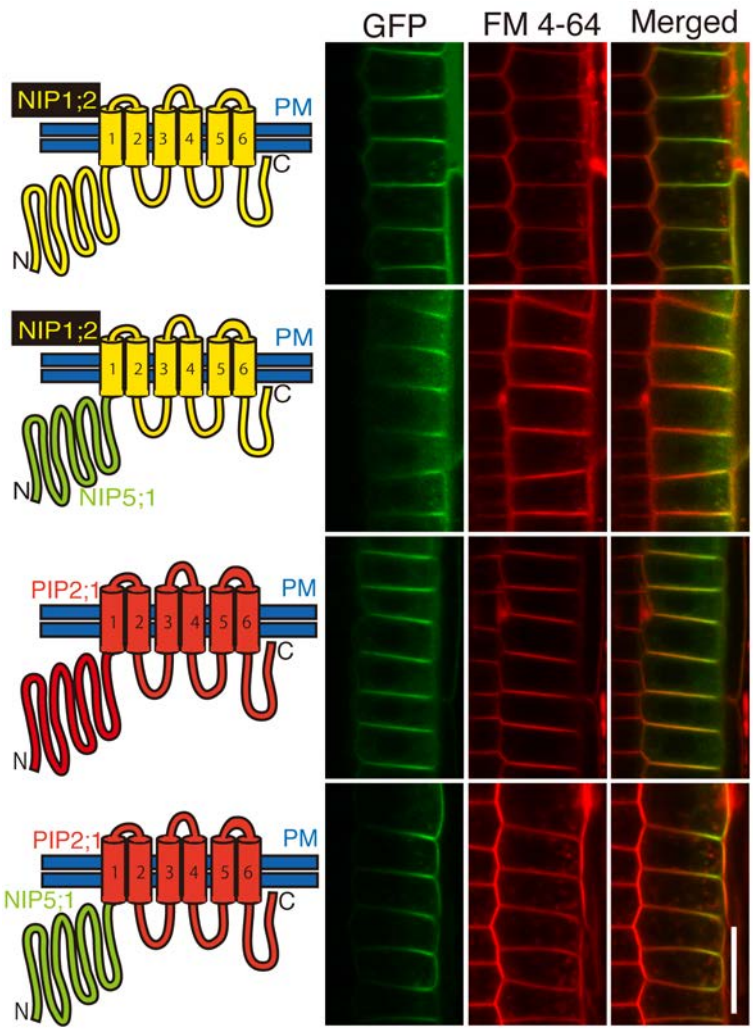

Figure 2.7 N-terminal region of NIP5;1 directs polar localization of aquaporins. Chimera constructs (illustrations) were generated by swapping corresponding sequence between NIP1;2 or PIP2;1 and NIP5;1 and expressed as GFP fusions in root epidermal cells. The sGFP-fused wild-type NIP1;2 and PIP2;1 were used as control. FM 4-64 was used to stain the PM in a uniform way. Scale bar = 20 μm.

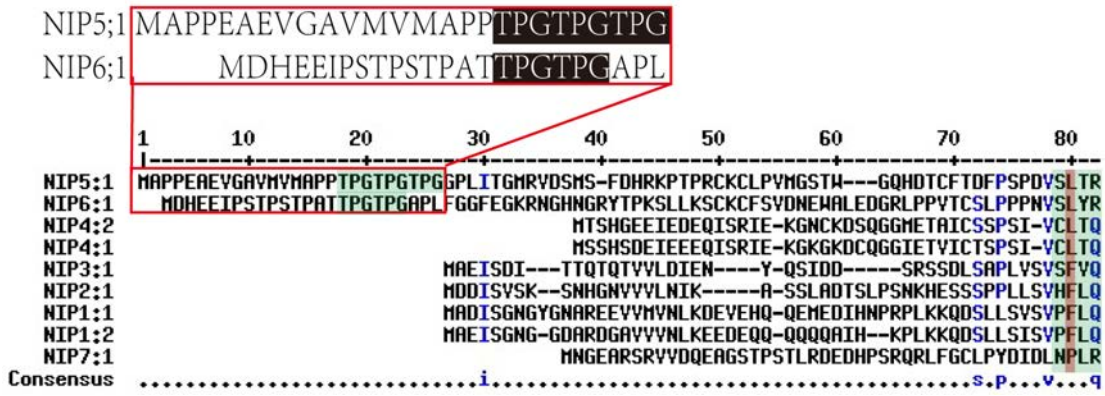

Figure 2.8 Alignment of the N-terminal regions of NIPs. The alignment was performed using ClustalW2 (http://www.ebi.ac.uk/Tools/msa/clustalw2/). "TPG" repeats are conserved in NIP5;1 and NIP6;1 but not in other NIPs. Except NIP7;1, a leucine/phenylalanine residue is conserved at the end of N-terminal regions (shaded by red color).

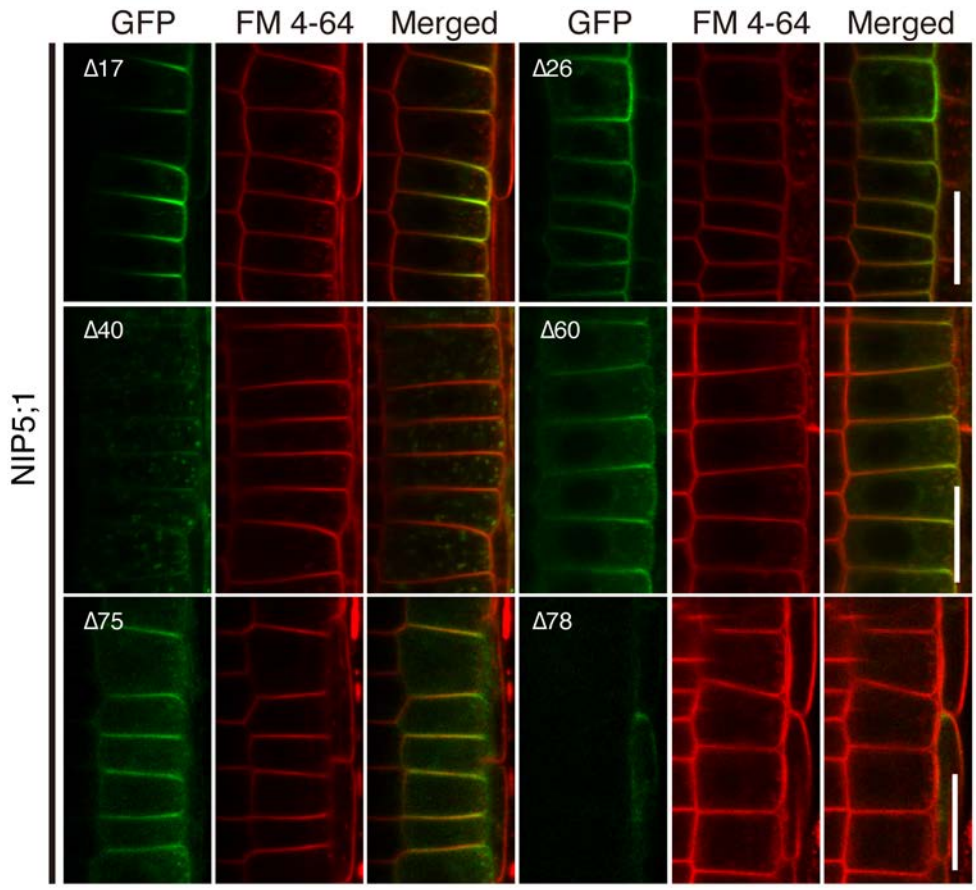

Figure 2.9 Deletion of the N-terminal region of NIP5;1 affected the polar localization of sGPF-NIP5;1. Truncated NIP5;1 (ΔN17, ΔN26, ΔN40, ΔN60, ΔN75 and ΔN78) fused at N-terminus with sGFP were expressed in root epidermal cells. FM 4-64 at 4 μM was used to stain the PM in a uniform way. Scale bars = 20 μm.

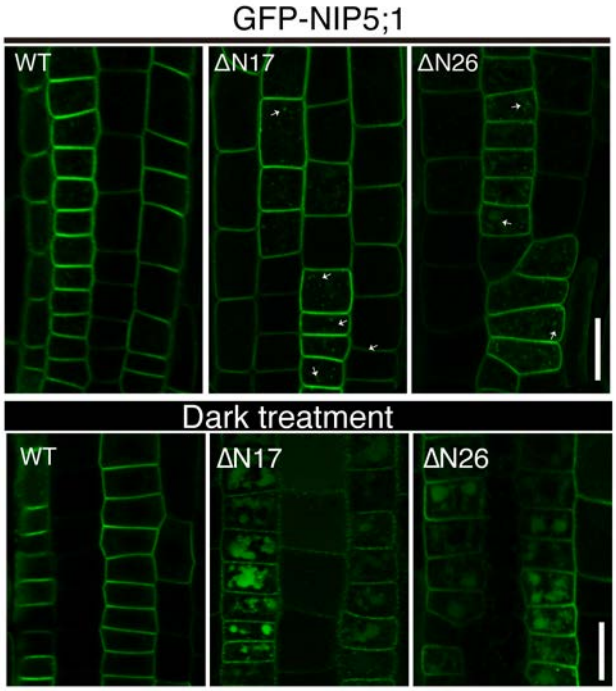

Figure 2.10 Deletion of the N-terminal region of NIP5;1 induced vacuolar trafficking. Localization of GFP-NIP5;1 wild-type and truncated mutants in root epidermal cells of plants grown under a light condition (up) and after 8 hours dark treatment (down). Scale bars = 20 μm.

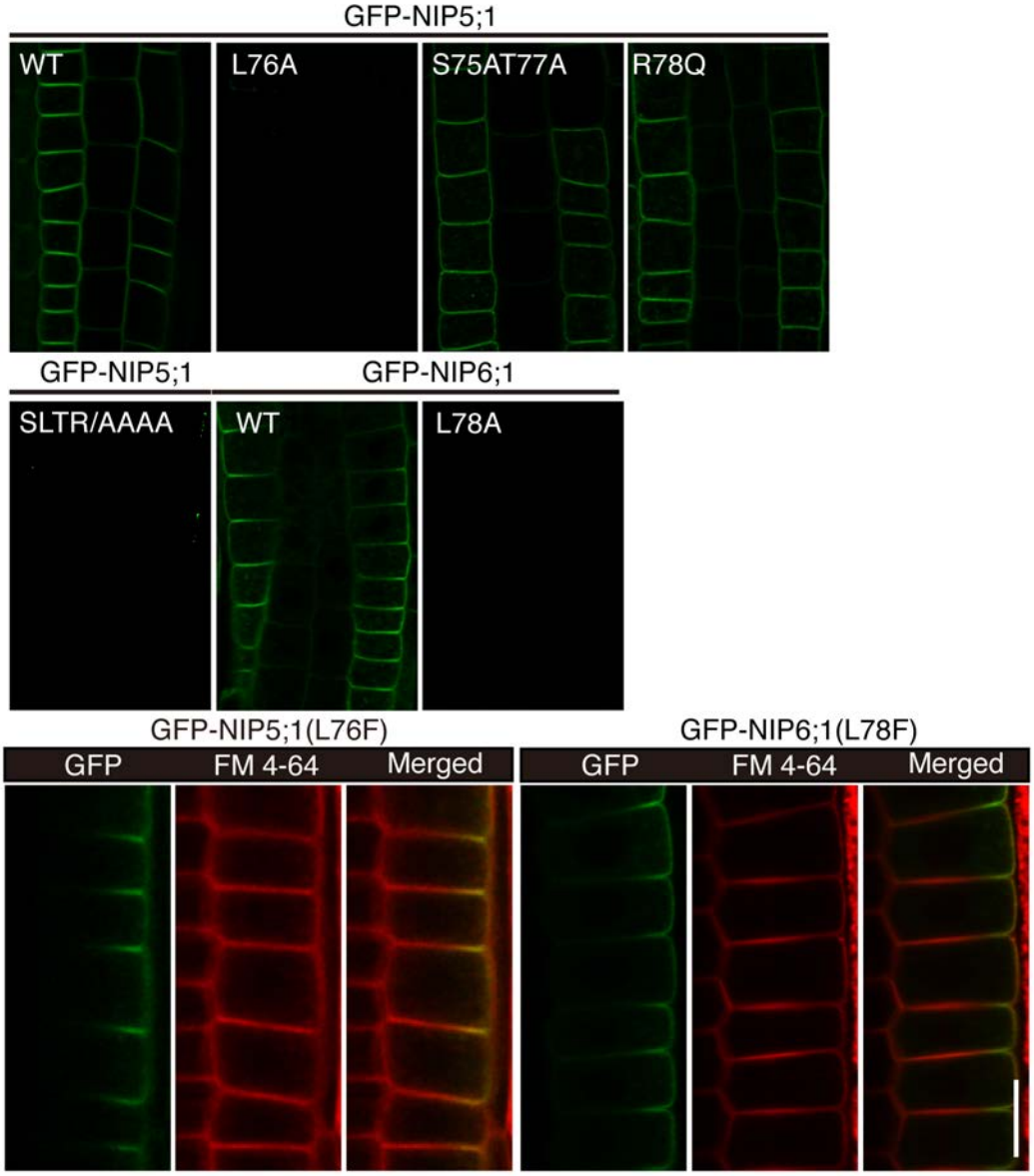

Figure 2.11 Mutational analysis identified a conserved leucine residue for the PM localization of NIP5;1 and NIP6;1. Localization and expression levels of GFP-NIP5;1/NIP6;1 amino-acid substituted mutants were compared by confocal microscopy at same setting in epidermal cells. FM 4-64 was used to stain PM in a uniform way. Scale bar = 20 μm.

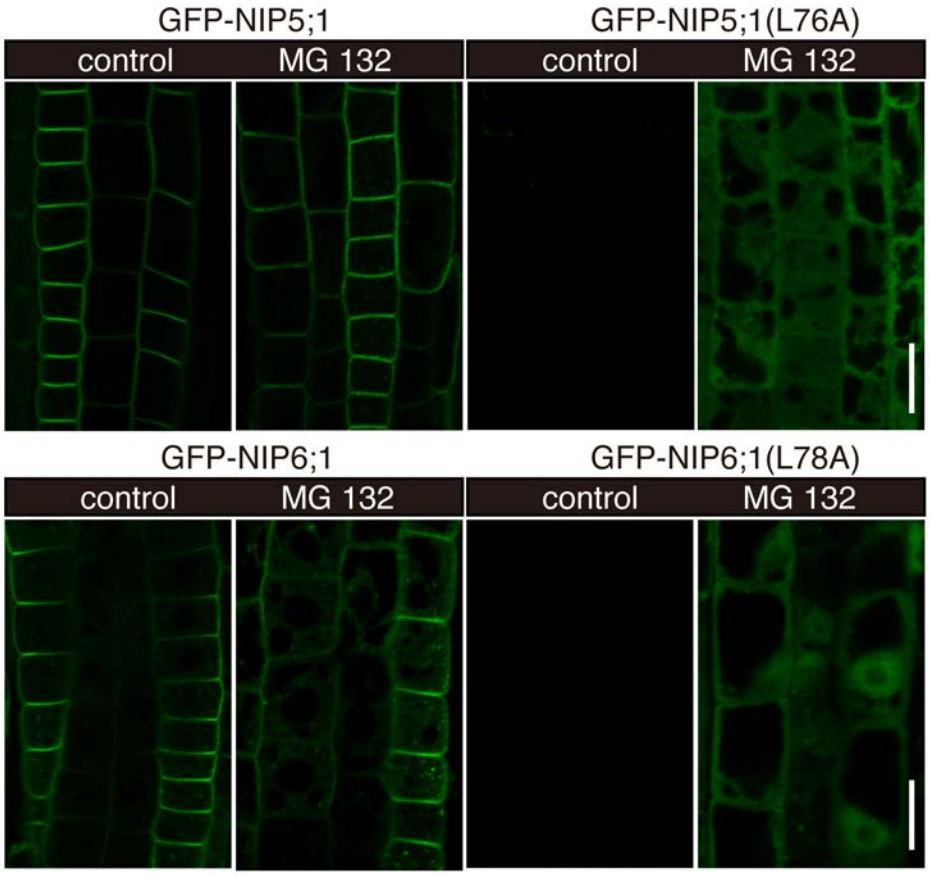

Figure 2.12 Alanine substitution of the conserved leucine induced ER-associated protein degradation (ERAD) of NIP5;1 and NIP6;1. Both GFP-NIP5;1 L76A and GFP-NIP6;1 L78A were undetectable under a control condition, while incubation with 50 μM MG 132, a inhibitor of 26S proteasome, for 5 h caused cytosolic GFP accumulation. Control treatments were performed with 0.2% DMSO. Scale bars = 20 μm.

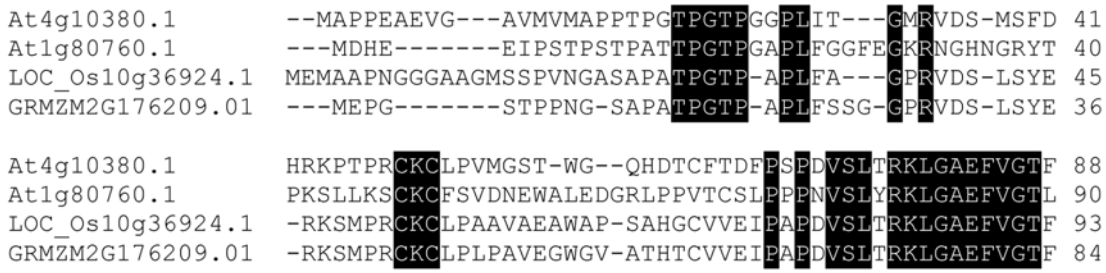

Figure 2.13 Alignment of the N-terminal regions of boric acid channels from Arabidopsis, rice and maize. Arabidopsis boric acid channels (At4g10380.1 encodes NIP5;1; At1g80760.1 encodes NIP6;1), rice boric acid channel (LOC_Os10g36924.1 encodes OsNIP3;1) and maize boric acid channel (GRMZM2G176209.01 encodes ZmNIP3;1) have evolutionarily conserved "TPG" repeats in their N-terminal regions.

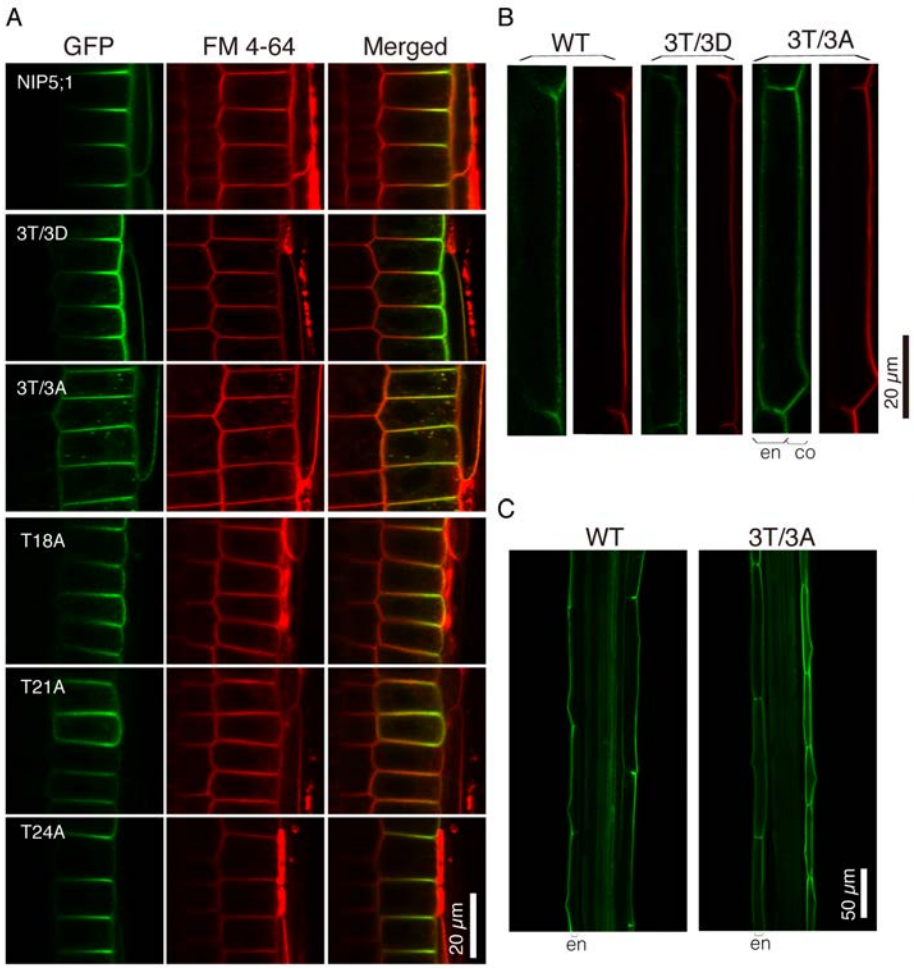

Figure 2.14 Conserved threonine residues are important for the polar localization of NIP5;1 in epidermal cells and endodermal cells. Triple amino-acid substituted mutants GFP-NIP5;1 (T18D/T21D/T24D) and GFP-NIP5;1 (T18A/T21A/T24A), and single amino acid substituted mutants were expressed in epidermal cells (A) and endodermal cells (B) under control of the *NIP5;1* promoter without 5' UTR. Triple amino-acid substituted mutants GFP-NIP5;1 (T18A/T21A/T24A) was expressed in endodermal cells (C) under control of the *CASP1* promoter. FM 4-64 was used to stain PM in a uniform way. En: endodermal cells, co: cortical cells.

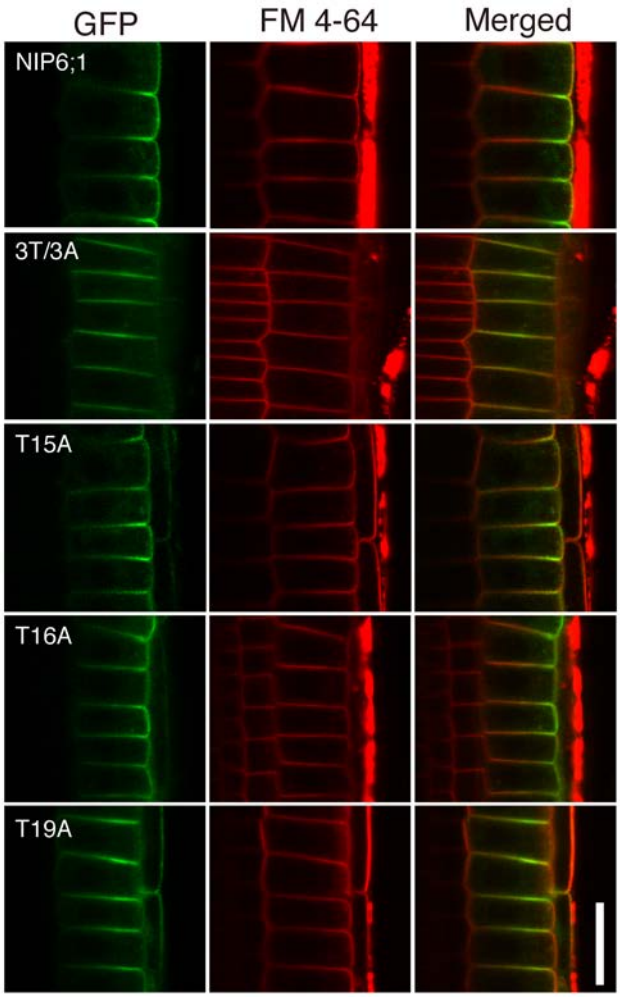

Figure 2.15 Conserved threonine residues are important for the polar localization of NIP6;1 in epidermal cells. Triple amino acid substituted mutant GFP-NIP6;1 (T15A/T16A/T19A) and three single amino acid substituted mutants were expressed in epidermal cells under control of the *NIP5;1* promoter without 5' UTR. FM 4-64 was used to stain PM in a uniform way. Scale bar = 20 μm

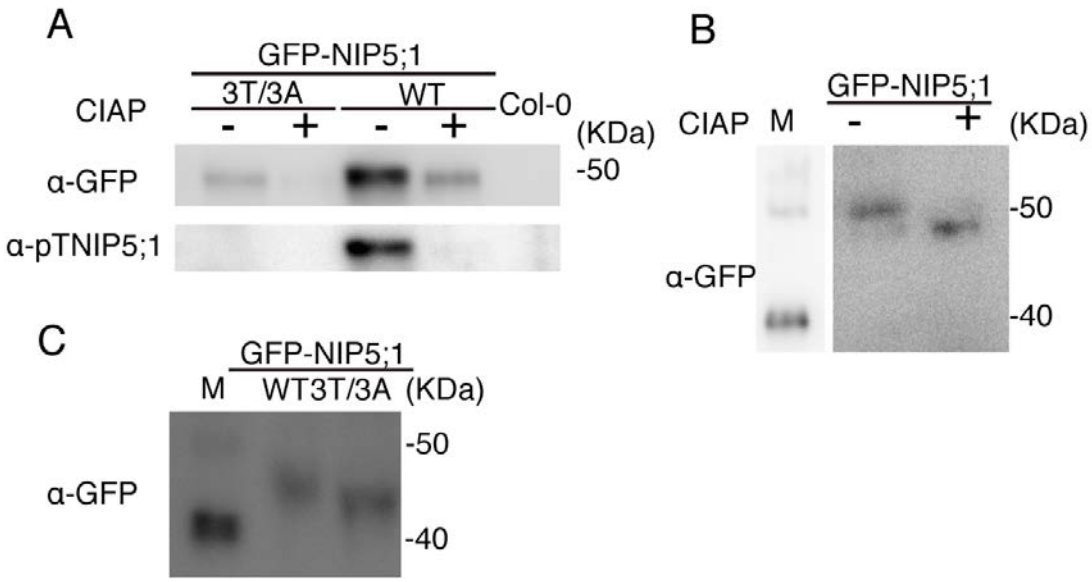

Figure 2.16 NIP5;1 is phosphorylated *in vivo* at the conserved threonine residues. (A) Immunoprecipitated samples of GFP-NIP5;1 wild-type and 3T/3A mutant treated with/without Calf intestinal alkaline phosphatase (CIAP) were run on NuPAGE gel. PVDF membrane with transferred proteins were immuno-blotted with an anti-GFP and an anti-pTNIP5;1 antibody. Col-0 was used as a negative control. (B) Membrane fractions containing GFP-NIP5;1 were treated with/without CIAP and run on Phos-tag gel. Transferred proteins were immuno-blotted with an anti-GFP antibody. (C) Immuno-blotting analysis of GFP-NIP5;1 wild-type and 3T/3A mutant in membrane fractions using Phos-tag gel.

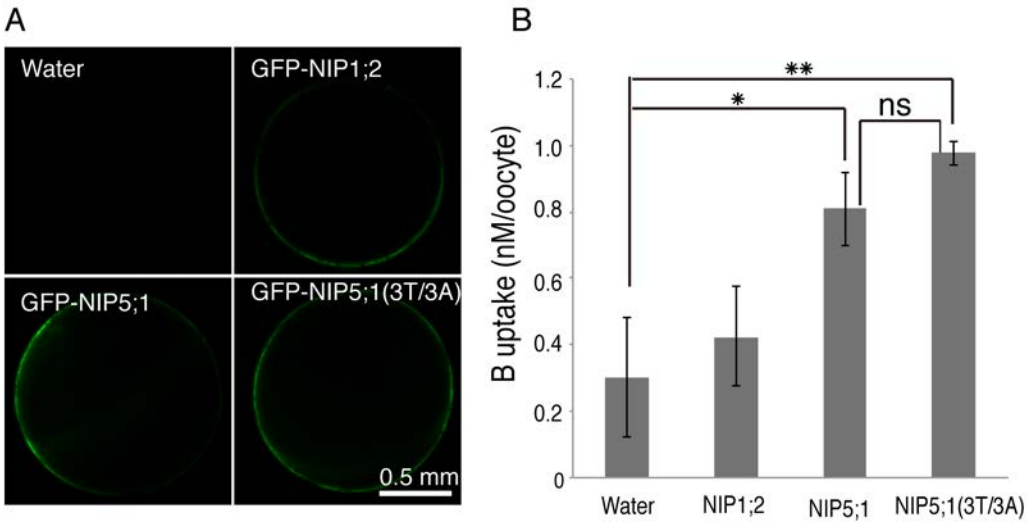

Figure 2.17 Boric acid uptake assay in oocytes. Equivalent amount (~ 50 ng) of cRNA of *GFP-NIP1;2*, *GFP-NIP5;1,* and *GFP-NIP5;1 T18AT21AT24A* were injected into oocytes, and water was injected as a negative control (A). The oocytes were incubated with 5 mM boric acid for 30 min and boron concentration in oocytes were measured by ICP-MS. Five GFP-positive oocytes (A) were used as a sample and 4 samples were collected for each construct (B). Scale bar = 0.5 mm, error bars indicate ± SD. Student's *t*-test (*: $p < 0.05$; **: $p < 0.01$; n s: no significant difference).

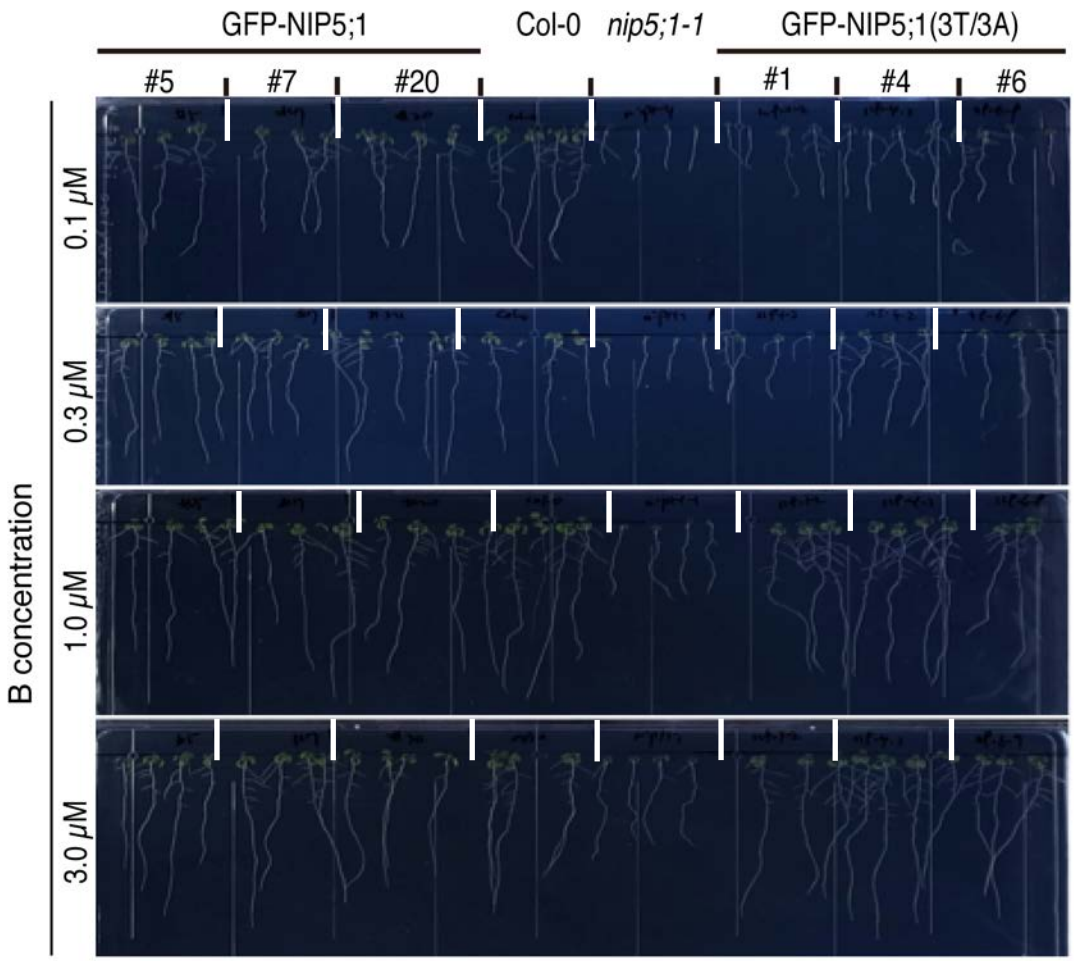

Figure 2.18 Phenotype comparison of GFP-NIP5;1 wild-type and 3T/3A mutant expressing *nip5;1-1* lines under low boron conditions. Transgenic T3 homozygous lines harboring GFP-NIP5;1 wild-type and 3T/3A mutant in *nip5;1-1* background, *nip5;1-1* mutant, and Col-0 (wild-type) plants were grown under low boron conditions. After 2 days treatment at 4 °C, the plates were vertically placed in a growth chamber at 22 °C for 7 days under a light/dark cycle of 16 h/8 h.

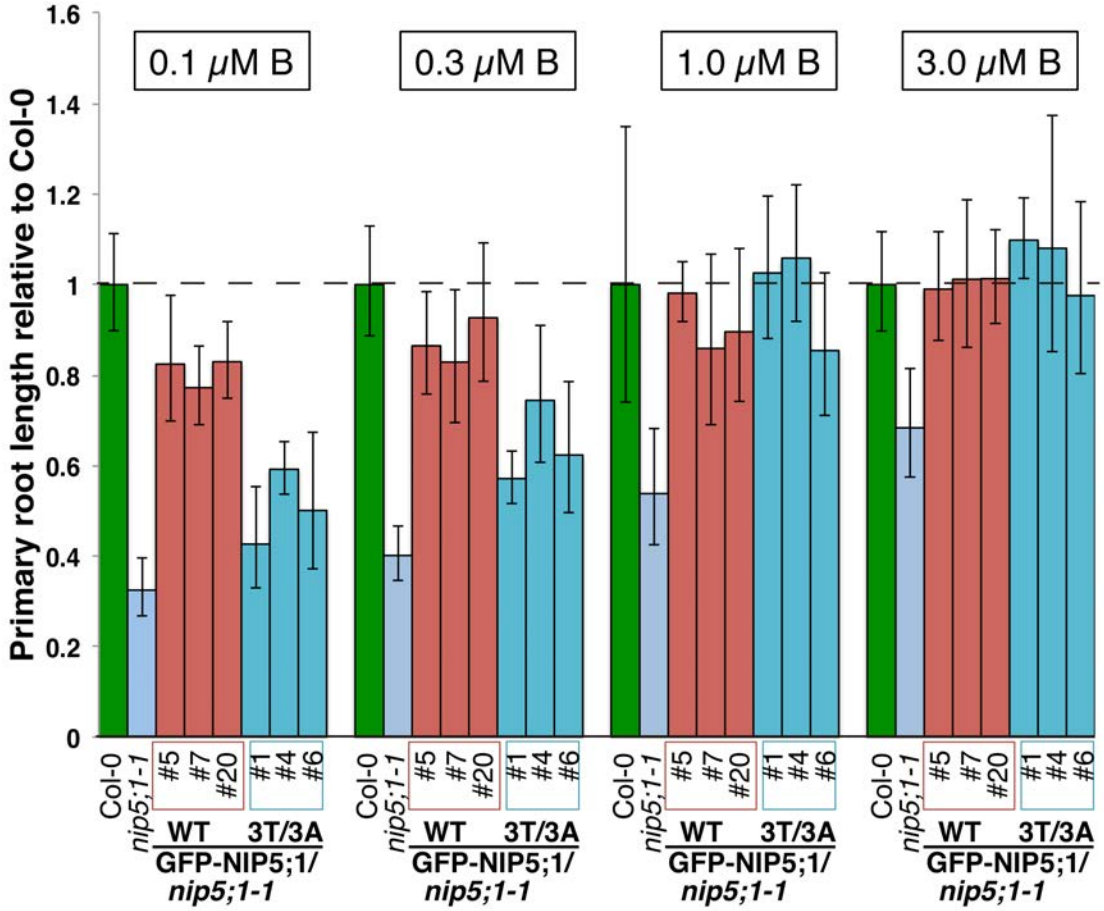

Figure 2.19 Relative length of primary roots of *nip5;1-1* mutant, GFP-NIP5;1 wild-type lines (#5, 7, 20 in *nip5;1-1* background), and 3T/3A mutant lines (#1, 4, 6 in *nip5;1-1* background) compared to Col-0 (wild-type) under low boron conditions. Primary root lengths were measured by the RootNav software. n = 8-16. Error bars indicate ± SD.

Table 1. Primers used in this study.

1	NIP1;1		F	CACCATGGCGGATATCTCGGGAAAC
			R	TCAAGTGCTACCGATTCTCACGGTC
2	NIP1;2		F	CACCATGGCGGAGATCTCGGGAAA
			R	TTAACGAGAGCTACCGTTTCGCAC
3	NIP2;1		F	CACCATGGATGACATATCAGTGAG
			R	TCACAGAGGAAGATCGGTAACTC
4	NIP31		F	CACCATGGCTGAGATTTCTGATATTACTAC
			R	TCACGCCAACTTACATGTAACATTACATTTG
5	NIP4;1		F	CACCATGTCTTCGCATAGTGATGAAAT
			R	TTAAGTCTTAGAACTAGAACCCTTGTG
6	NIP5;1		F	CACCATGGCTCCACCGGAGGCT
			R	TTAACGACGAAAGCTCCTAACCGGACG
7	NIP6;1		F	CACCATGGATCATGAGGAAATTCC
			R	TCATCTTCTGAAGCTCCTCCTCTC
8	NIP7;1		F	CACCATGAATGGTGAGGCACGGT
			R	TTAACGTAAAAGTGAAGAAACGGAAGGG
9	pNIP5;1		F	CACCAAGCTTCGAAAGCAAGCATTC
			R	GTCTAGAGGGCTTTGAAAGATTTTT
10	PIP2;1		F	CACCATGGCAAAGGATGTGGAAGC
			R	TTAGACGTTGGCAGCACTTCTG
11	Nter1;2-NIP5;1	NIP1;2Nter	R	CTCGGCTCCAAGCTTTTGTAAGAAAGGGACAGAGATAGAGAG
		NIP5;1TMD	F	GTCCCTTTCTTACAAAAGCTTGGAGCCGAGTTCG
12	Nter5;1-NIP1;2	NIP5;1Nter	R	CTCCGCCATCAACTTGCGAGTGAGGGAGACATCAG
		NIP1;2TMD	F	GTCTCCCTCACTCGCAAGTTGATGGCGGAGGTTTTG
13	Nter5;1-TMD1;2-Nter5;1	NIP5;1Nter	R	
		NIP1;2TMD	F	
		NIP1;2TMD	R	AAGCTTAACACCTGTATAAACCCACGCACCCGAAAC
		NIP5;1Cter	F	GGTGCGTGGGTTTATACAGGTGTTAAGCTTAACGATAGCG
14	NIP5;1-Cter1;2	NIP5;1TMD	R	GTCCCTTTCTTACAAAAGCTTGGAGCCGAGTTCG

		NIP1;2C	F	GGTGCAGCGGTCTACAACATGGTTCGATATACTGATAAGCC
		NIP5;1Nter	R	CTCTGCGATAACTGCGCGAGTGAGGGAGACATCAG
15	Nter5;1-PIP2;1	PIP2;1TMD	F	GCAGTTATCGCCGAGTTCGTAG
16	NIP5;1ΔC11		R	TTAAGTCACGCTATCGTTAAGCTTAACACC
17	NIP5;1ΔN17		F	GACGAGCTGTACAAGACGCCGGGGACACCGGGAAC
18	NIP5;1ΔN26		F	GACGAGCTGTACAAGGGACCGTTGATCACGGGGATG
19	NIP5;1ΔN40		F	CACCGATCATCGGAAACCAACGCC
20	NIP5;1ΔN60		F	CACCCAACATGACACATGCTTCACCG
21	NIP5;1ΔN75		F	CACCCTCACTCGCAAGCTTGGAG
22	NIP5;1ΔN78		F	CACCAAGCTTGGAGCCGAGTTC
23	NIP5;1 L76A		F	CTCCTGATGTCTCCGCCACTCGCAAGCTTGGAG
			R	CTCCAAGCTTGCGAGTGGCGGAGACATCAGGAG
24	NIP5;1 S75AT77A		F	CTCTCCTGATGTCGCCCTCGCTCGCAAGCTTGGAG
			R	CTCCAAGCTTGCGAGCGAGGGCGACATCAGGAGAG
25	NIP5;1 R78Q		F	GATGTCTCCCTCACTCAGAAGCTTGGAGCCGAG
			R	CTCGGCTCCAAGCTTCTGAGTGAGGGAGACATC
26	NIP5;1 SLTR/AAAA		F	GTCGCCGCAGCTGCAAAGCTTGGAGCCGAGTTCGTG
			R	TGCAGCTGCGGCGACATCAGGAGAGGGAAA
27	NIP5;1 L76F		F	CTCCTGATGTCTCCTTCACTCGCAAGCTTG
			R	CAAGCTTGCGAGTGAAGGAGACATCAGGAG
28	NIP6;1L78A		F	CCTCCCCCTAACGTTTCCGCCTACCGCAAGTTGGGAGC
			R	GCTCCCAACTTGCGGTAGGCGGAAACGTTAGGGGGAGG
29	NIP6;1L78F		F	CCTCCCCCTAACGTTTCCTTCTACCGCAAGTTGGGAG
			R	CTCCCAACTTGCGGTAGAAGGAAACGTTAGGGGGAGG
30	NIP5;1 3T/3A		F	CCGGGGGCACCGGGAGCACCGGGAGGACCGTTGATC
			R	TCCCGGTGCCCCCGGCGCTGGAGGAGCCATCACCATTAC

31	NIP5;1 3T/3D	F	CCGGGGGATCCGGGAGATCCGGGAGGACCGTTGATCAC
		R	TCCCGGATCCCCCGGATCTGGAGGAGCCATCACCATTAC
32	NIP5;1 T18A	F	TCCTCCAGCGCCGGGGACACCGGGAACAC
		R	CCCGGCGCTGGAGGAGCCATCACCATTAC
33	NIP5;1 T21A	F	GCCGGGGGCACCGGGAACACCGGGAGGAC
		R	CCCGGTGCCCCCGGCGTTGGAGGAGCCATC
34	NIP5;1 T24A	F	ACCGGGAGCACCGGGAGGACCGTTGATC
		R	CCCGGTGCTCCCGGTGTCCCCGGCGTTG
35	NIP6;1 3T/3A	F	GCAGCACCGGGGGCTCCAGGAGCGCCGCTCTTTGG
		R	AGCCCCCGGTGCTGCCGCCGGCGTTGAGGGCGTGG
36	NIP6;1 T16A	F	GGCGACAGCCCCGGGGACTCCAGGAGCG
		R	CCCGGGGCTGTCGCCGGCGTTGAGGGCG
37	NIP6;1 T19A	F	CCCGGGGGCTCCAGGAGCGCCGCTCTTTG
		R	CCTGGAGCCCCCGGGGTTGTCGCCGGCG
38	sGFP-NIP5;1 for oocyte assay	F	CACCGGATCC ATGGTGAGCAAGG
		R	GGATCC TTAACGACGAAAGCTCCTAAC
39	sGFP-NIP5;1 3T/3A for oocyte assay	F	CACCGGATCC ATGGTGAGCAAGG
		R	GGATCC TTAACGACGAAAGCTCCTAAC
40	sGFP-NIP1;2 for oocyte assay	F	CACCGGATCC ATGGTGAGCAAGG
		R	GGATCC TTAACGAGAGCTACCGTTTCG
41	Promoter *CASP1*	F	GACTCTAGAGGATCCTTAATCTGCATAAAAGTGAGT
		R	GCCCTTGCTCACCATTTTCTCTTGCAATTGGGGTT

Acknowledgements

First and foremost, I wish to thank my advisor, assistant professor Junpei Takano notably for his encouragement, patience and passion in my work, all of which helped me. I joined his research group in October 2011 with little understanding in cell biology. He always showed confidence in me and taught me step by step.

I sincerely appreciate Mr Uehara for establishing plants materials that are indispensible in my doctoral thesis, and Mr Toshiaki Ito (Hokkaido University) for teaching me electron microscopy.

Numerous advices from Professor Satoshi Naito and Associate Professor Hitoshi Onouchi expanded my ability of experimental design and techniques, those are required for my academic development. I would like to thank professor Satoshi Naito and Associate professor Hitoshi Onouchi for their time and patience to teach me so much.

I am thankful to current and former members of molecular biology laboratory, particularly Mrs Kayo Konishi and Mrs Tomoko Shimizu, who helped me construct plasmids and grow plants; Mr Hiroaki Koyama for providing RNA material; Dr. Shiji Wakuta and Mr Akira Yoshinari for valuable discussion on my experiments and data analysis.

I want to thank Professor Jianfeng Ma and Mrs Namiki. Mitani-Ueno (Okayama University) for kind helps in my oocyte assay experiment; Associate Professor Yoichiro Fukao (Ritsumeikan University) for MS analysis although the data was not included n the thesis; Mr Niko Geldner (University of Lausanne), Mr Takashi Ueda (University of Tokyo), and ABRC for providing materials.

Finally, I must thank my family, who always supported me and believed in my abilities and encouraged me to try my best. Especially, my wife, Aping Xu, continually contributes to my life and work during my graduate study.

I could not carry out the research without all assistance above.